UNIVERSITEIT VAN PRETORIA
UNIVERSITY OF PRETORIA
YUNIBESITHI YA PRETORIA

HEAT TRANSFER AND PRESSURE DROP CHARACTERISTICS IN THE TRANSITIONAL FLOW REGIME WITH TWISTED TAPE INSERTS

by

Sogo Mayokun Abolarin

Submitted in partial fulfilment of the requirements for the degree

Doctor of Philosophy (PhD)
in Engineering

Department of Mechanical and Aeronautical Engineering

University of Pretoria, South Africa

May 2019

Supervisor: Prof JP Meyer

Co-supervisor: Dr M Everts

Abstract

Title: Heat transfer and pressure drop characteristics in the transitional flow regime with twisted tape inserts

Supervisor: Prof JP Meyer

Co-supervisor: Dr M Everts

Department: Mechanical and Aeronautical Engineering

Degree: PhD (Mechanical Engineering)

Studies on heat transfer and pressure drop characteristics in a tube with twisted tape inserts have been receiving research attention in the laminar and turbulent flow regimes since 1921. However, several gaps exist in the transitional flow regime. The purpose of this study was to experimentally investigate the heat transfer and pressure drop characteristics in a smooth circular copper tube with conventional twisted tape (CTT) inserts, alternating clockwise and counter clockwise twisted tape (CCCTT) inserts and peripheral u-cut twisted tape (PUCTT) inserts without and with ring (PUCTTR) inserts.

An experimental set-up was designed and constructed in this study. The set-up was validated by comparing the results of the heat transfer and pressure drop characteristics in a smooth tube (without twisted tape inserts) with literature. The smooth circular copper tube had a wall thickness, an inner diameter, and a length of 1.5 mm, 19 mm, and 5.27 m respectively. The twisted tape inserts considered in this study were fabricated from 1 mm thick and 18 mm wide copper strips. The strips used for the CTT inserts were twisted to form tapes with twist ratios of 3, 4 and 5. A total of five 900 mm long CTT inserts were connected longitudinally to an additional 770 mm insert to form a tape with overall length of 5.27 m. The strips used for CCCTT inserts were twisted to obtain a twist ratio of 5 and 12 tapes were joined longitudinally so that a clockwise direction twisted tape insert was connected to a counter clockwise direction twisted tape insert. The assembling was at connection angles of 0°, 30° and 60°, to form CCCTT inserts with an overall length of 5.27 m. For the PUCTT inserts, the peripheries of the strips were cut to achieve depth ratios of 0.105 and 0.216. The strips were twisted to form tapes with a twist ratio of 5 and ring inserts were soldered on the PUCTT inserts to form PUCTTR inserts with ring space ratios of 1.25, 2.5 and 5. A total of five 900 mm long PUCTT inserts were connected longitudinally to an additional 770 mm insert to form a tape with overall length of 5.27 m.

Water was circulated as test fluid and experiments were conducted at constant heat flux boundary condition, at Reynolds numbers of 300 – 11 404. This Reynolds number range covered the transitional flow regime, as well as sufficient parts of the laminar and turbulent flow regimes. This study focused on the identification of the transitional flow regime with the

CTT, CCCTT, PUCTT and PUCTTR inserts. With the CTT inserts, it was the influence of twist ratio and heat flux on the transitional flow regime. For the CCCTT inserts, it was the influence of connection angle and heat flux on the transitional flow regime. Modified Grashof number which is a function of heat flux was used to describe free convection effects in the CTT and CCCTT inserts. The PUCTT and PUCTTR inserts it was the influence of depth ratio as well as ring space ratio on the transitional flow regime.

When twist ratios and heat fluxes of the CTT inserts were compared, a reduction in twist ratio and heat flux caused the transitional flow regime to occur earlier. When the CCCTT inserts were compared it was found that both the start and end of the transitional flow regime were influenced by the connection angle and heat flux. When different connection angles of the CCCTT inserts were compared it was found that an increase in connection angle enhanced the heat transfer in the transitional flow regime. An increase in heat flux significantly enhanced the heat transfer in the laminar flow regime and delayed transition. When depth ratios of the PUCTT inserts were compared, an increase in depth ratio caused the transitional flow regime to occur earlier. Furthermore, the transitional flow regime occurred earlier with PUCTTR inserts than with PUCTT inserts and transition occurred even earlier as the ring space ratio was reduced. An increase in depth ratio and reduction in ring space ratio significantly enhanced heat transfer in the transitional flow regime. It can be concluded that when the CTT, CCCTT and PUCTT inserts were compared, transition first occurred with the CCCTT inserts and delayed the most with the CTT inserts.

Heat transfer and pressure drop correlations were developed to predict the experimental data in the laminar, transitional and turbulent flow regimes. Where applicable the correlations were developed as a function of Reynolds number, twist ratio, modified Grashof number, connection angle, depth ratio and ring space ratio.

Publications

The journal articles published and conference papers presented at international conferences in the course of this study are provided below:

Journal articles

1. J.P. Meyer, **S.M. Abolarin**, Heat transfer and pressure drop in the transitional flow regime for a smooth circular tube with twisted tape inserts and a square-edged inlet, International Journal of Heat and Mass Transfer, 117 (2018) 11-29.
2. **S.M. Abolarin**, M. Everts, J.P. Meyer, Heat transfer and pressure drop characteristics of alternating clockwise and counter clockwise twisted tape inserts in the transitional flow regime, International Journal of Heat and Mass Transfer, 133 (2019) 203-217.
3. **S.M. Abolarin**, M. Everts, J.P. Meyer, The influence of peripheral u-cut twisted tapes and ring inserts on the heat transfer and pressure drop characteristics in the transitional flow regime. International Journal of Heat and Mass Transfer, 132 (2019) 970-984.

Conference papers

1. **S.M. Abolarin** M. Everts and J.P. Meyer, Pressure drop characteristics of transitional flow regime through a smooth tube with peripheral u-cut twisted tape inserts. 14th International Conference of Heat Transfer, Fluid Mechanics and Thermodynamics, 22 - 24 July 2019, Wicklow, Ireland.

2. **S.M. Abolarin** and J.P. Meyer, Heat transfer and pressure drop characteristics in the transitional flow regime of twisted tape insert in a circular tube with re-entrant inlet. Proceedings of the 16th International Heat Transfer Conference, pp. 4567-4574, IHTC16-23213, 10-15 August 2018, Beijing, China.

3. **S.M. Abolarin** and J.P. Meyer, Colburn *j*-factor in the transitional flow regime in a plain circular tube with twisted tape insert and square-edge entry. 13th International Conference of Heat Transfer, Fluid Mechanics and Thermodynamics pp. 972-977, 17th - 19th July 2017, Slovenia.

4. **S.M. Abolarin** and J.P. Meyer, Area goodness factor of flow in a plain circular tube with twisted tape insert and square-edge entry in the transitional flow regime. 13th International Conference of Heat Transfer, Fluid Mechanics and Thermodynamics, pp. 978-983 17th - 19th July 2017, Slovenia.

5. **S.M. Abolarin** and J.P. Meyer, Pressure drop in the transitional flow regime inside smooth tubes with twisted tape inserts, 12th International Conference on Heat Transfer, Fluid Mechanics and Thermodynamics, pp. 505-510, 11 – 13 July 2016, Malaga, Spain.

6. **S.M. Abolarin** and J.P. Meyer, Heat transfer in the transitional flow regime inside smooth tubes with twisted tape inserts, 12th International Conference on Heat Transfer, Fluid Mechanics and Thermodynamics, pp. 1135-1140, 11 – 13 July 2016, Malaga, Spain.

Dedication

This thesis is dedicated to Almighty GOD, who gave me the wisdom, knowledge and understanding to successfully complete this study. To Him be all the glory, honor and adoration forever and ever in Jesus name. Amen.

Acknowledgements

I appreciate the following individuals for their firm support during the course of this study:

- Prof JP Meyer and Dr M Everts, for their supervision of the study, the skills imparted in me and the resources provided;
- Mr D Gouws, Mr C Moon, Mr P Kruger, Mr E Mohale and Mr KJ Mthombeni, for their technical assistance during the fabrication and testing of the experimental set-up and Ms T Evans, Mrs I Meyer and Ms K Kunene for all their administrative support;
- Mrs OO Abolarin (my lovely wife and the Queen of my heart) and Mr ME Abolarin (Son) for their love, patience, continuous support, encouragement and prayers;
- Mr EB and Mrs RA Abolarin, Engr AO and Mrs Abolarin, Mr SB and Mrs MS Abolarin and Mr D and Mrs R Oyinloye for their love and for bringing me up in the nature, admonition and to the glory of God, their constant prayers, encouragement, moral and financial supports;
- Engr JO and Mrs T Abolarin, Mr and Mrs S Opatola, Dr AA and Mrs TT Abolarin, Mr S and Mrs IO Kolawole, Mr E and Mrs OO Adeoye and Miss OG Abolarin and cousins, nieces and nephews for the love, support and encouragement;
- Mrs OA Ayoola, Mr OA and Mrs B Ayoola, Mr O and Mrs R Olaore, Mr AO and Mrs A Ayoola, Mr DB Ayoola for their love and prayers;
- Mr SE and Mrs CA Bamgbose, Mr J Adaramaja, Mr OO and Mrs TO Shonibare, Mr L and Mrs L Aboudou, Mrs B Afolabi for their love and encouragement;
- Prof EJ Bala, Prof AS Sambo, Prof O Adegbenro, Prof AJ Kehinde, Prof SJ Ojolo, Prof O Ogundipe, Prof K Craig, Prof J Dirker, Dr NDL Burger, Dr EOB Ogedengbe, Dr OT Olakoyejo, Dr KA Adelaja, Dr S Adio, Dr O Adewunmi and Dr O Noah for their leadership and support;
- Dr SB and Mrs O Owolabi, Mr O and Mrs M Fatokun, Mr T and Mrs R Ademola, Mr J and Mrs B Olawoyin, Mr P and Mrs G Akinwale, Mr S and Mrs Bamgbose, Mr MM and Mrs L Ajose, Mrs S Isong, Engr J and Mrs F Ogbemhe, Engr DRE and Mrs Z Ewim, Engr AI and Mrs Bashir, Engr O and Mrs T Olatunji, Engr SA and Mrs A Aasa, Engr A Shote, and Engr S Giwa for their support and encouragement.

I appreciate the following organizations for their financial support:

- Department of Science and Technology (DST);
- National Research Foundation (NRF);
- University of Pretoria.

I appreciate the love and prayers of the members of the:

- Church of Christ, Ashley Gardens, Pretoria, South Africa;
- Church of Christ, Rietfontein, Pretoria, South Africa;
- Church of Christ, Ado-Odo, Ogun State, Nigeria;

- Church of Christ, Egbeda, Lagos State, Nigeria.

I appreciate the primary, secondary and tertiary education received as well as innovative, science and engineering skills acquired from the following institutions and members of staff:

- Methodist Central School I, Ado-Odo, Ogun State, Nigeria;
- St. Stephen's Comprehensive High School, Ado-Odo, Ogun State, Nigeria;
- Department of Mechanical Engineering, University of Lagos, Nigeria.

I am grateful for the study-leave opportunity given to me and the support of the leadership, governing board and members of staff of the:

- Energy Commission of Nigeria (ECN);
- National Centre for Energy Efficiency and Conservation, (NCEEC), Nigeria.

May God continue to bless you all in Jesus name. Amen.

Table of contents

List of figures

List of tables

Nomenclature

a	axis intercept of the linear equations of the CTT	
A	area	m^2
b	constant	
c	slope of the linear equations	
Cp	specific heat capacity at constant pressure	J/kg.K
d	y-axis intercept of the linear equations in the smooth tube or cut distance of PUCTT and PUCTTR inserts	mm
D	test section diameter	m
d_{cut}	cut depth	m
D_r	ring diameter	m
D_t	cutting tool diameter	m
D_w	wire diameter	m
eb	energy balance error	
f	friction factor	
f_r	frequency	Hz
g	acceleration due to gravity	m/s^2
Gr	Grashof number	
Gr^*	modified Grashof number	
h	heat transfer coefficient	$W/m^2.°C$
H	pitch of the twisted tape; axial distance for a 180° rotation in twist	m
I	current	A
j	Colburn j-factor	
k	thermal conductivity of the fluid	W/m.K
L	length/laminar flow regime	m
L_{cut}	cut length	m
$L_{\Delta P}$	pressure drop length	m
L_{th}	thermal entrance length	m
$\dot{m}$	mass flow rate	kg/s
Nu	Nusselt number	
P	pressure	Pa
Pr	Prandtl number	
p_r	ring insert pitch	m
$\dot{q}$	heat flux	W/m^2
$\dot{Q}$	heat transfer rate	W
Re	Reynolds number	
ΔRe	width of the transitional flow regime	
R_d	depth ratio (d_{cut}/W)	
R_r	ring space ratio (p_r/W)	
t	time	s
T	temperature	°C
V	voltage	V
W	tape width	m
x	axial position measured from tube inlet	m
y	twist ratio (H/W)	

Greek symbols

β	thermal expansion coefficient	m^2/s
δ	thickness of the twisted tape insert	m
μ	dynamic viscosity	kg/m.s
ρ	density	kg/m^3
σ	standard deviation	
θ	connection angle	°
v	kinematic viscosity	m^2/s

Subscripts

1,2,3,…,n	measuring station number from station $n = 1$ to station $n = 21$
b	bulk
c	cross-sectional
cr	critical
e	exit, electrical
h	heated length
i	inlet, inner
L	laminar
m	mean
P	pressure
qt	end of transitional flow regime
R	transition
s	surface
T	turbulent
th	thermal

Abbreviations

CTT	conventional twisted tape
CCCTT	clockwise and counter clockwise twisted tape
PUCTT	peripheral u-cut twisted tape
PUCTTR	peripheral u-cut twisted tape with ring

1. Introduction

1.1 Background

Increase in population and industrialization have led to the continuous rise in consumption and cost of limited available energy resources. Productivity has been reduced or grounded in some industries as a result of the high energy consumption and cost associated with production processes. A practical examination, investigation and re-evaluation of industrial practices, processes and procedures influencing this energy consumption rise are vital towards the achievement of energy savings and productivity improvement. Improvement of production processes in the industries is hinged on the adoption and implementation of various energy management measures in order to reduce energy consumption and cost on energy consuming equipment.

One of the very important energy consuming equipment in engineering application is the heat exchanger. Heat exchangers are found in domestic applications [1], industrial processes such as manufacturing, and food processing [2, 3], chemical and petrol-chemical industries [4-6], power stations that use fossil, nuclear or renewable energy sources [7-11], internal combustion engines–radiator [12, 13], etc. In these applications heat exchangers play important roles in meeting our heat transfer needs for example heat transfer from one medium to another (hot to cold or cold to hot) and heat conversion and recovery.

In these applications the two major variables generally investigated in heat exchanger design, operation and efficiency evaluation are heat transfer and pressure drop. The study of these two variables have over the years being restricted to two of the three flow regimes which are the laminar flow regime and the turbulent flow regime. In practice, heat exchangers are often found unknowingly operating in the third flow regime between the laminar and turbulent regimes. This regime is known as the transitional flow regime. In general, the transitional flow regime has been avoided or received the least research attention compared to the other two flow regimes.

There are specifically two groups of researchers that have dedicated attention to experimental investigations in the transitional flow regime. The first groundbreaking work was performed by Prof Afshin Ghajar and co-workers [14-21] from the Oklahoma State University and the second by Prof Josua P. Meyer and co-workers [22-25] at the University of Pretoria. They have studied the effects of inlet sections on the transitional flow regime in smooth tubes. Ghajar and his co-workers investigated three different types of inlets at constant heat flux boundary conditions in smooth tubes (macro and micro). Their most important finding was that the inlet geometry influenced transition characteristics inside tubes.

Prof Meyer and co-workers found in general the same dependency of inlet geometry on transitional characteristics. However, they generated results for cooling experiments with constant wall temperature [26] and their tubes had internally spiraled fins. They also conducted experiments in the transitional flow regime using nanofluids [22, 27], micro

channels [28], developing and fully developed flow region [29-31] and inlet spacing and protrusion of multiple tubes [32].

Both Prof Ghajar and Prof Meyer not only conducted their experiments with different types of inlets, but also installed calming sections upstream of the different types of inlet geometries, to dampen out upstream flow disturbances. The geometry of the calming sections used by Prof Meyer were based on the design of Prof Ghajar's calming section.

Meyer [33] in a comprehensive review presented the state-of-the-art, latest work, gaps and opportunities on the thermo-hydraulic characterization in tubes in the transitional flow regime. The most recent research work on the transitional flow regime was divided into five parts namely conventional convective heat transfer and friction factors in smooth tubes, the work of Ghajar and Tam, the work of Meyer, low-Reynolds-number end and other related work. The review emphasized the important need for more research work in the transitional flow regime. These included (1) increasing vital understanding of the mechanism and effects on heat transfer, (2) obtaining a generalized equation particularly for the design industry that adequately describes all the flow regimes, (3) considering nanofluids instead of conventional fluids and (4) investigating augmentation techniques in enhanced tubes. In more specific, the review identified thirteen foci for further studies and thus suggested that more studies are needed in the transitional flow regime particularly in enhanced tubes.

Consequent to the recommendation of Meyer [33] for a comprehensive research in the transitional flow regime in enhanced tubes, this present study seeks to fill this gap by conducting an experimental heat transfer and pressure drop investigation on the influence of twisted tape inserts placed in a smooth circular tube on transitional flow regime using water as test fluid.

1.2 Problem statement

Heat transfer and pressure drop investigations with the use of twisted tape inserts only focused on heat transfer enhancement and not specifically on the identification of the three flow regimes (laminar, transitional and turbulent). Furthermore, experimental research work with the use of the twisted tapes inserts has received tremendous attention in the laminar and turbulent flow regimes [34-39]. The recent comprehensive reviews of experimental investigations by Liu and Sakr [3], Maradiya et al. [40], Hasanpour et al. [41, 42], Varun et al. [43] and Zhang et al. [44] of using different twisted tape inserts were, however, limited to the laminar and the turbulent flow regimes with no attention paid to the transitional flow regime. Numerical studies with the use of twisted tapes inserts have been reported for fully developed flow in the laminar flow regime by Date [45] and Hata et al. [46, 47] for constant heat flux boundary condition and Du Plessis and Kröger [48] for constant wall temperature boundary condition.

The laminar and turbulent flow regimes that have been investigated have their own characteristics. The laminar flow regime is characterised with low heat transfer coefficient and low pressure drop, while the turbulent flow regime is associated with high heat transfer coefficient and pressure drop. This means that there is a need for research in the transitional

flow regime where there could be a compromise between the laminar (low heat transfer and pressure) and turbulent (high heat transfer and pressure drop) [33].

In open literature, the use of a calming section and inlet geometries (re-entrant, square-edge and bellmouth) that have been found to influence the transitional flow regime in smooth tube have not been previously investigated with the use of twisted tape inserts. Therefore, comprehensive data in the transitional flow regime in an enhanced tube with different inlet geometries are still scarce.

Therefore, despite the enormous research investigations available in the laminar and turbulent flow regimes, research gaps exist in the transitional flow regime. Hence there is a need to investigate and scientifically correlate the heat transfer and pressure drop of heat exchanger equipped with twisted tape inserts in all the flow regimes, with particular focus on the identification of the transitional flow regime. The availability of data for transitional flow regime would help in the improvement and efficiency of heat exchangers [24].

1.3 Aim

The purpose of this study was to experimentally investigate the heat transfer and pressure drop characteristics of twisted tape inserts with different modifications in the transitional flow regime, and at different constant heat flux boundary conditions. The sole aim of the study was on the identification of the transitional flow regime with the twisted tape inserts. As the transitional flow regime "connects" the laminar and turbulent flow regimes; the results of these two flow regimes are also given. Three twisted tape inserts were considered in this study. The first were conventional twisted tape (CTT) inserts with twist ratios of 3, 4 and 5. The second were clockwise and counter clockwise twisted tape (CCCTT) inserts with connection angles of 0°, 30° and 60° and the twist ratio of 5. The third were peripherally u-cut twisted tape (PUCTT) inserts without ring and with ring (PUCTTR) inserts with the twist ratio of 5. The PUCTT and PUCTTR were cut on the periphery to achieve depth ratios of 0.105 and 0.216. The rings were inserted to form tapes with ring space ratios of 1.25, 2.5 and 5. As the inlet geometry significantly affects transition [14, 15, 18, 20], a square-edged inlet was used.

1.4 Objectives

The specific objectives of this study were to:

- design, fabricate, install and commission an experimental set-up for the investigation of heat transfer and pressure drop characteristics in a smooth tube with twisted tape inserts;
- experimentally determine the temperatures (inlet bulk fluid, test section surface and exit bulk fluid) and pressure drop data along a smooth circular copper tube. The tube inner diameter was 19 mm with an outer diameter of 22 mm and a length of 5.27 m. The Reynolds number range was 300 to 11 404 covering the laminar, transitional and turbulent flow regimes using water as test fluid;

- process the data using appropriate data reduction methods, obtain convective heat transfer in terms of Colburn *j*-factor and the pressure drop in terms of friction factors, where relevant as a function of Reynolds number, twist ratio, heat flux, connection angle, depth ratio and ring space ratio;
- determine the influence of twist ratios, connection angles, heat fluxes, depth ratios and ring space ratios on the Colburn *j*-factor and friction factors with particular emphasis on the identification of the start, end and width of transitional flow regime;
- develop and compare correlations with the experimental data in the transitional flow regime as well as in the laminar and turbulent flow regimes for smooth tube and tube fitted with twisted tape inserts.

1.5 Scope of work

The scope of this research work was to investigate the transitional flow regime in a smooth hard-drawn circular copper tube with an inner diameter of 19 mm, a wall thickness of 1.5 mm and a length of 5.27 m. Four categories of experiments were conducted. The first category was the smooth tube experiments (without any twisted tape and ring inserts). The second category was when the CTT inserts of twist ratios 3, 4 and 5 were placed in the smooth tube and the experiments were conducted at heat fluxes of 2, 3 and 4 kW/m^2. The third category was when the CCCTT inserts with the connection angles of 0°, 30° and 60° and twist ratio of 5 were placed in the smooth tube and the experiments were conducted at heat fluxes of 1.35, 2, 3 and 4 kW/m^2. The fourth category was when the PUCTT inserts with width ratios of 0.105 and 0.106 without rings and with rings (PUCTTR) of ring space ratios of 1.25, 25 and 5 were placed in the smooth tube and the experiments were conducted at heat fluxes of 1.35 and 2 kW/m^2. Water was used as test fluid at an inlet temperature of 20 °C. The Reynolds number range varied from 300 to 11 404, this range covered all the three flow regimes (laminar, transitional and turbulent).

1.6 Original outcomes

The outcomes of this study were published as part of this thesis in three articles. The original contributions and highlights of the three articles with relevant chapters are as follows:

Chapter 5, Meyer and Abolarin [49]

- Colburn *j*-factors and friction factors can be divided into three different flow regimes (laminar, transitional and turbulent);
- Start and end of transitional flow regime of the CTT inserts occurred earlier than smooth tubes;
- The transitional flow regime occurred earlier as the twist ratio reduced;
- The transitional flow regime occurred earlier as the heat flux reduced;
- Heat transfer was enhanced as the twist ratio reduced in the transitional flow regime;
- Correlations were developed to predict the Colburn *j*-factors and friction factor experimental data in the three flow regimes (laminar, transitional and turbulent) for both the smooth tube and tube with twisted tape insert.

Chapter 6, Abolarin et al. [50]

- Colburn *j*-factors and friction factors can be divided into three different flow regimes (laminar, transitional and turbulent);
- Start and end of transitional flow regime of the CCCTT inserts occurred earlier than CTT and PUCTT inserts;
- The transitional flow regime occurred earlier as the connection angle increased;
- The transitional flow regime occurred earlier as the heat flux reduced;
- Increased connection angle enhanced heat transfer in the transitional flow regime;
- Correlations were developed firstly, to predict the start and end of the transitional flow regime and secondly, to predict the Colburn *j*-factor and friction factor experimental data in the three flow regimes (laminar, transitional and turbulent) as a function of Reynolds number, connection angle and modified Grashof number.

Chapter 7, Abolarin et al. [51]

- Colburn *j*-factors and friction factors can be divided into three different flow regimes (laminar, transitional and turbulent);
- Start and end of transitional flow regime of the PUCTT inserts occurred earlier than CTT inserts and was delayed compared with CCCTT inserts;
- Start and end of transitional flow regime of the PUCTTR inserts occurred earlier than PUCTT inserts;
- The transitional flow regime occurred earlier as the depth ratio increased;
- The transitional flow regime occurred earlier as the ring space ratio reduced;
- Heat transfer was enhanced in the transitional flow regime as the depth ratio increased and ring space ratio reduced;
- Correlation were developed to predict the Colburn *j*-factor and friction factor experimental data in the three flow regimes (laminar, transitional and turbulent) as a function of Reynolds number, depth ratio and ring space ratio.

1.7 Overview of thesis

Chapter 1 covered the introduction and background, problem statement, aim, specific objectives, scope, original outcomes and the thesis overview. Chapter 2 detailed the comprehensive literature survey and gaps in literature as regards transitional flow regime with the use of twisted tape inserts. Chapter 3 contained the experimental set-up, procedure, data reduction, calibration of Pt100 probes, thermocouples, and pressure transducers and uncertainty analysis. Chapter 4 focused on validation of the heat transfer and friction factor experimental data with literature. Chapter 5 [49] covered the heat transfer and pressure drop in the transitional flow regime for a smooth circular tube with conventional twisted tape inserts. Chapter 6 [50] contained the details of the heat transfer and pressure drop characteristics of alternating clockwise and counter clockwise twisted tape inserts in the transitional flow regime. Chapter 7 [51] focused on the influence of peripheral u-cut twisted tapes and ring inserts on the heat transfer and pressure drop characteristics in the transitional flow regime. Chapter 8 provided the summary, conclusions of the thesis and recommendations for future work.

2. Literature survey

2.1 Introduction

The purpose of this chapter is to summarize the state-of-the-art of heat transfer and pressure drop in the laminar, transitional and turbulent flow regimes in enhanced tubes. It discusses enhancement techniques generally and then focused on twisted tape inserts in the three flow regimes. Furthermore, previous studies were presented related to the different types of twisted tape inserts, flow regimes and gaps that exist for study in the transitional flow regime when twisted tape inserts were placed in smooth tube heat exchangers.

2.2 Enhancement techniques

Heat exchangers are found in many residential-, commercial- and industrial applications because of the important roles they play in meeting our heat transfer needs and the growing concerns for energy as a grand challenge. For example, heat conversion and heat recovery in energy or power generation systems; which include power stations (nuclear, fossil or renewable energy production systems) [7], manufacturing processes [2, 40], aircraft and transport industries [13, 52, 53], etc. The heat exchangers found in these applications are either with smooth or enhanced surfaces.

Literature shows that simple enhancement techniques can improve the heat transfer performance and thus lead to higher efficiencies [40, 54-72]. This is because heat exchanger enhancement provides the benefits of compactness through thermal resistance reduction. This could be achieved by either reduction in effective heat transfer area or generation of swirl on the inside of the tube or channel passage. Other benefits of heat exchanger enhancement are improved overall performance, higher efficiencies, reduced materials and operating costs etc. [40, 73].

Generally, the enhancement techniques are categorized into active, passive, or a combination of both active and passive heat transfer enhancement techniques [74-77]. Active techniques such as vibration of a fluid surface, jet impingement, fluid injection and suction, electrostatic fields [13], etc., require additional external power to successfully improve the heat transfer. Passive techniques do not require external power and consist of geometrical modifications to the tube geometry and/or inserts or additional devices that disturb or alter the flow path [71]. As fluid flowed in a tube/channel passage with passive enhancement techniques (inserts) flow blockage, partitioning, redevelopment, disturbance and recirculation occur. The inserts cause reduction in hydraulic diameter and thermal boundary layer as well as increased flow velocities, flow path, fluid mixing and flow turbulence [78, 79]. These flow patterns created by the insertion of any of the passive techniques lead to heat transfer enhancement.

A number of passive techniques have been suggested, fabricated and incorporated in heat exchangers. Some of these include coatings and/or roughness on the inner surface of the tube/channel passage [80-82], corrugated tubes [2, 4, 41, 54, 59, 62, 63, 83-91], dimpled tubes [92, 93], wire ring inserts [13, 71, 94], circular rings with wire net inserts [79], metal

foam [95], conical ring inserts [96-101], wire coils [58, 60, 86, 102-110], anchor shaped inserts [111], winglet vortex generators [112, 113], wavy delta winglets [114], perforated hollow circular cylinder inserts [115], perforated vortex generator inserts [116], outer grooved cylinder and inner rotating cylinder [117, 118], helical and eccentric helical screw tape inserts [119-122] and twisted tape inserts with different modifications [8, 38, 55, 62, 63, 69, 78, 123-142]. In all of these, twisted tape inserts have been regarded as one of the simplest, because they can be fabricated at low cost, can easily be installed and have low maintenance [3, 143-145].

2.3 Twisted tape inserts

Twisted tape inserts (Fig. 2.1) are fabricated by twisting metallic strips with tape thickness, δ, tape width, W, to form a desired pitch, H, with a 180° rotation in twist. They are placed inside a tube/channel through which a fluid is flowing in order to improve the heat transfer. The twisted tapes are generally differentiated by their twist ratio. The twist ratio denoted by, y, is defined as the ratio of the twist pitch, H, to the tape width, W, as, $y = H/W$. This twist ratio has been found to be one of the major factors that influence heat transfer [73]. Whenever the tape width is equal to the inner diameter of the tube ($W = D_i$), then the inner diameter of the tube is used when determining the twist ratio, otherwise the tape width is used.

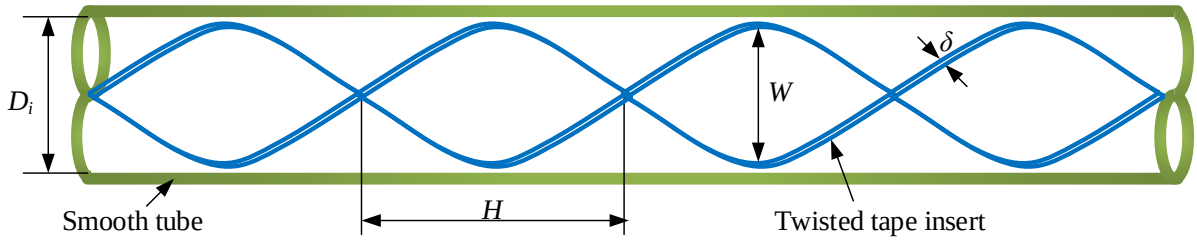

Fig. 2.1. Schematic of a conventional twisted tape (CTT) insert showing the tape pitch, H, width, W, and thickness, δ, placed inside a smooth tube with an inner diameter, D_i.

The twisted tape insert as a flow turbulator has been found in many cases to increase heat transfer performance [146-148], particularly at lower Reynolds numbers. The extent of the heat transfer enhancement depends in most cases on the manner in which the tape is twisted, modified, the tape materials and on the application. Manglik and Bergles [78, 135, 149] and Bartwal et al. [79] attributed the increased heat transfer when twisted tape inserts are placed in tube to (1) reduction in hydraulic diameter, (2) partition and blockage of the tube cross section, which caused flow velocity to increase, (3) increase in flow path due to the helical configuration of the tape; this caused increased wetted perimeter, reduced flow cross-sectional area and increased length at which the fluid flow, (4) influence of secondary flow caused by the twist and (5) the metallic (material) conductivity of the tape insert, which makes them to behave as fins particularly when they are in contact with the inner surface of the tube/channel. This therefore increased the effective heat transfer area.

The twisted tape inserts' modifications could be in different forms. It could be fabricated to rotate in different directions, it could be short or full length, loose or tight fit [150, 151], tapered [152, 153], smooth or cut on the periphery as well as with perforation [137, 154-159].

The tape could be fitted in a tube as single, double or triple [69, 137, 160, 161] depending on the applications. The modification of the twisted tape insert was for the sole purpose of improving heat transfer and thermal efficiency compared to smooth tubes (without twisted tape inserts). The advantages of using a twisted tape insert over a smooth tube include a higher heat transfer rate, improved mixing of the test fluid across the tube cross-section [70, 137, 162] and a thinner boundary layer thickness [160, 163]. However, the helical rotating pattern of twisted tape insert gives rise to a centrifugal force which is greater than the longitudinal force, and thus imposes secondary motion [135]. The overall effect of these forces makes the flow with twisted tape inserts to be accompanied with higher pressure drop [157, 164]. This has led to increased research investigations to improve the thermal efficiency of heat exchangers. In an attempt to reduce the pressure drop, experiments have also been conducted using shorter lengths of twisted tape insert [165-167].

The first person to have probably considered twisted tape insert was Royds [168]. The purposes of the investigation were for the heat transfer and pressure drop measurements and identification of the potential benefits of heat transfer enhancement. This study was followed by the semi-analytical study of Smithberg and Landis [169], where fully developed turbulent flow in tubes with respect to velocity distribution, friction losses and heat transfer were studied. They considered conventional twisted tape (CTT) inserts with twist ratios ranging from 3.62 – 22 using air and water as test fluids over the Reynolds numbers range of 5 000 – 50 000.

Subsequently, most heat transfer and pressure drop investigations with twisted tape inserts only focused on heat transfer enhancements. They focused on either the laminar flow regime for Reynolds numbers between 13 and 3 000 [6, 38, 48, 75, 132, 133, 135, 167, 170-190] or the turbulent flow regime for Reynolds numbers greater than 3 000 [13, 35, 58, 129, 143, 162, 164, 191-199] and not specifically on the transitional flow regime.

2.4 Laminar flow regime

The use of twisted tape insert as a passive enhancement technique using experimental constant heat flux boundary conditions was first investigated by Hong and Bergles [38]. The study considered CTT inserts with twist ratios of 2.45 and 5.08. The experimental investigation was conducted in the laminar flow regime over a Reynolds number range from 13 - 2 260, water and ethylene glycol were used as the test fluids. This Reynolds number range was reported as being laminar without any references to a transitional flow regime. The heat transfer and pressure drop were reported in terms of Nusselt number and friction factor respectively. Nusselt number and friction factor correlations developed in the study were said to be applicable to forced convection heat transfer. In the concluding remarks, the study recommended experimental investigation in the transitional flow regime, as this would serve as a basis of providing an all-encompassing correlation for the laminar, transitional and turbulent flow regimes.

In an attempt to identify the free convection effect in laminar flow regime with twisted tape inserts, Bandyopadhyay et al. [75] conducted heat transfer experiments using servotherm oil

as test fluid. The twist ratios of the twisted tape considered varied from 3.9 – 8.1 and the experiments were performed over the Reynolds number range of 35 – 1 756. Two test sections were used with inner diameters of 22.8 mm and 31.7 mm, they both had the same length of 2 m. In their work they first established whether their results were fully developed or not. Fully developed flow was said to have been assumed when the averaged axial temperature distribution (at each measuring station) on the surfaces of the two test sections and the averaged bulk temperature of the fluid increased linearly in the direction of flow. It then followed that the flow was said to have been fully developed from the second measuring station (axial tube length-to-diameter ratio, $x/D_i \geq 22$) from the test section inlet. Following the determination that their work was fully developed, they proceeded to identify the influence of free convection. In order to identify the free convection effect, they compared their experimental fully developed Nusselt number with the forced convection Nusselt number determined using the correlation developed by Hong and Bergles [38]. In their report they concluded that (1) swirl effect dominated free convection effect wherever the ratio of their fully developed Nusselt number to the forced convection Nusselt number of Hong and Bergles [38] was less than 1.2, (2) the effect of swirl balanced that of free convection when the ratio is between 1.2 and 2 and, (3) the free convection effects dominated the swirl effects of the tape whenever the ratio was greater than 2.

Experiments performed with short-lengths, regularly-spaced and full-lengths as well as smoothly varying pitch twisted tape inserts, were conducted by Saha et al. [167, 174, 188] at constant heat flux over a laminar range of Reynolds numbers from 45 - 1 150 with servotherm oil as the working fluid. They considered tapes with twist ratios of 2.5 – 10 and space ratios (distance between tapes to tube inner diameter) from 0 to 5. They found that the heat transfer and friction factor characteristics were a function of Reynolds number, Prandtl number, twist ratio, space ratio, tape length and pitch smoothness. The short-length tapes caused the lowest friction factor and Nusselt number and were found to be better than full-length tapes. A similar remark was made by Klaczak [200] and Lokanath [201], who compared the performance of half-length to full-length twisted tape inserts. Saha and Dutta [167] reported that an approximate of 15% reduction in friction factor and Nusselt number were obtained when smooth swirl tape was compared with gradually decreasing pitch tape.

Wongcharee and Eiamsa-ard [132] reported heat transfer and friction factor characteristics in laminar swirl flow conditions with twisted tape inserts that alternated between clockwise and counter clockwise (CCCTT) inserts (Fig. 2.2) for Reynolds numbers from 830 - 1 990. The test section in which the experiments were conducted was a smooth copper tube with an inner diameter, an outer diameter and a length of 18 mm, 22 mm and 1 m respectively. The twisted tape inserts used in the study were made from aluminum strips with a thickness and a width of 1 mm and 18 mm respectively. The tapes were twisted to form twist ratios of 3, 4 and 5 in a 180° rotation. Each CCCTT insert was cut at a desired length on both sides to a depth of 4 mm and then twisted to an angle of 90° to produce a tape with an opposing direction. A calming section with an inner diameter and a length of 18 mm (equal to the inner diameter of the test section) and 3.6 m respectively were connected upstream of the test section in order to reduce entrance effects. The study compared the performance of CTT inserts with the

CCCTT inserts. When the results were compared, the heat transfer, friction factor and thermal performance factor of the alternating CCCTT inserts were higher than CTT inserts. When the twist ratios were compared, the tape with the twist ratio, $y = 3$, was found to be most efficient with respect to heat transfer enhancement. The study obtained a maximum heat transfer improvement of 5% at a Reynolds number of 830.

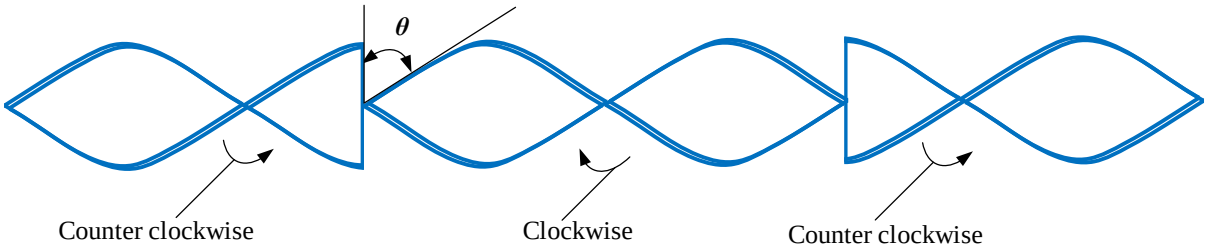

Fig. 2.2. Schematic of the clockwise and counter clockwise twisted tape (CCCTT) inserts showing the connection angle, θ, and the rotation of the tape insert.

Other laminar experimental studies on twisted tape inserts are the works of Watanabe et al. [68], which used air as the test fluid, and Bandyopadhyay et al. [75], which used oil as the test fluid. Computational investigations in the laminar flow regime include the works of Date [45] and Date and Gaitonde [202]. They discovered that the laminar friction factor increased as the twist ratio reduced and that regardless of the twist ratios laminar friction factors tend to converge as the Reynolds numbers reduced. Similarly, the laminar Nusselt numbers increased as the twist ratios were decreased, the increased Nusselt numbers were obvious at higher laminar Reynolds numbers. As the Reynolds numbers reduced the Nusselt numbers were reported to be a function of both Reynolds number and Prandtl number. Du Plessis and Kröger [48], later on reported that the laminar Nusselt number depends on Prandtl number, Reynolds number, dimensionless axial distance, tape thickness and fin.

However, in general in all these studies, the transitional flow regime was not identified and/or discussed, or very little attention was given to it, as it was not the primary focus or purpose of their studies. Liu and Sakr [3] found out that twisted tape inserts produced better performance in laminar regime than turbulent regime, while other passive techniques gave better performance in turbulent than in the laminar flow.

2.5 Turbulent flow regime

In the turbulent flow regime, several studies investigated the use of twisted tape inserts using a constant heat flux boundary condition and Reynolds number from 3 000 and above. Both Bas and Ozceyhan [145] and Eiamsa-ard et al. [203] used air as the test fluid, while Seemawute and Eiamsa-ard [143] used water as the test fluid. These studies were only carried out for the purpose of characterising the heat transfer enhancement of twisted tapes over smooth tubes, and not for the establishment of the boundaries of the three flow regimes (laminar, transitional and turbulent).

The effect of clearance between CTT inserts width and the inner diameter of a tube on pressure drop in turbulent flow with water as test fluid was reported in Ayub and Al-Fahed

[148]. The experimental study was carried out when CTT inserts of twist ratio of 3.6, 5.5 and 7.3 were separately placed in a smooth copper tube. The tube had an outer diameter of 15.9 mm and wall thickness of 1.05 mm. The experiments were conducted using constant wall temperature boundary condition and Reynolds number range of 8 000 - 35 000. The results showed a decreasing friction factor for increasing Reynolds numbers and increasing pressure drop with tape width. An increase and decrease pressure drop were reported in the case of twist ratio of 3.6 with clearance of 0.89 mm, this undulation was attributed to secondary flow. For the tapes with other twist ratio, the pressure drop decreased with increase in tape width.

Similarly, in the work of Gunes and Karakaya [151] where loose-fit perforated twisted tape inserts with twist ratios of 2, 2.5 and 3 and diameter ratios of 0.0714, 0.107 and 0.143 were considered. The experiments were conducted over a Reynolds number range of 4 860 – 24 130 at constant heat flux in a tube with an inner diameter of 56 mm. Increase in Nusselt number, friction factor and thermal performance factor was found as both the twist ratios and hole diameter ratios were decreased. It was concluded that the tape with the twist ratio of 2 and hole diameter of 0.0714 produced the highest thermal performance factor of about 1.3.

An experimental study was carried out by Chang et al. [35] on the investigation of heat transfer and pressure drop enhancement with three tape inserts. A tube of inner diameter of 15 mm was used and the three tape inserts were plain tapes (without twist), CTT inserts and serrated twisted tape inserts. The width of the tapes was 15 mm and with twist ratios of 1.58, 1.88 and 2.81. Dry air was used as the test fluid in the turbulent regime of Reynolds number range 5 000 - 25 000 and at constant heat flux boundary condition. It was found that the Nusselt number and the friction factor increased as the twist ratio decreased. When the results of the serrated twisted tapes were compared with smooth tubes (without inserts), the heat transfer results of the serrated twisted tapes increased by 250%-480%, also the heat transfer enhancement achieved with serrated twisted tapes was 1.3 to 2% times that of CTT inserts [35, 69].

Eiamsa-ard et al. [203] experimentally investigated the thermal characteristics of heat transfer and pressure drop in a smooth copper tube with an outer and an inner diameters of 50 mm and 47 mm respectively. This tube was fitted with single and dual CTT inserts of twist ratios 3, 4 and 5. Air was used as test fluid and the experiments were performed at constant heat flux boundary condition over a Reynolds number range of 4 000 - 19 000. The heat transfer enhancement in the dual CTT inserts was approximately 12% to 29% higher than the single CTT inserts. However, the friction factor of the dual twisted tape is 23% higher than the single twisted tape. The friction factor was also observed to decrease with increased Reynolds numbers and twist ratios.

The influence of tapered twisted tape inserts on heat transfer and pressure drop were investigated in the work of Piriyarungrod et al. [152]. The CTT inserts were made from aluminium sheets and were of twist ratios of 3.5, 4 and 4.5. Each tape was then tapered at the angles of 0°, 0.3°, 0.6° and 0.9°. The tapered inserts were fabricated by gradual reduction (trimming) of the width of the straight inserts in the direction of flow. The experiments were

preformed over the Reynolds number range of 6 000 – 20 000. It was found that the decreasing twist ratios and increasing taper angle enhanced the heat transfer and friction factor.

Promvonge [204] conducted an experimental study on the influence of the combination of CTT inserts with twist ratios of 4 and 6 with wire coil inserts of pitch ratios of 4, 6 and 8. The test section consisted of a copper tube of length 1.5 m, wall thickness of 1.5 mm and inner diameter of 47 mm. The experiments were performed at a constant heat flux boundary condition using air as test fluid over a range of Reynolds number of 3 000 - 18 000. When the Nusselt numbers of the CTT inserts were compared with a smooth tube, it was found that the CTT inserts alone was 20 to 50% higher than smooth tubes. The friction factors were higher by 5-times when the CTT inserts were compared with smooth tubes. It also followed that the friction factors of the wire alone were found to be twice that of CTT inserts.

Eiamsa-ard and Promvonge [205] presented the performance assessment of alternating CCCTT inserts in the turbulent flow regime. The test section in which the CCCTT inserts were placed was made from copper tube with an inner diameter, a thickness and a length of 19 mm, 1.5 mm and 1 m. The CCCTT inserts (of thickness of 1 mm, width of 18 mm and length of 1 m) considered were fabricated from straight aluminum strips which were twisted along the longitudinal axis to twist ratios of 3, 4 and 5. Each tape twist was connected longitudinally at three angles of 30°, 60° and 90°. The authors referred to these angles at which the tapes were connected as twist angles. The experiments were conducted over a Reynolds number range of 3 000 – 27 000 at a constant heat flux with water used as test fluid. When the CCCTT inserts were compared, twist ratios and angles were found to influence the heat transfer and pressure drop. When the CCCTT inserts were compared with CTT inserts at the same twist ratio, it was found that the heat transfer coefficients were higher by 13 – 42%. When the twist angles were compared the CCCTT inserts performed better than the CTT inserts by 27 – 91%. The tape with the twist angle of 90° and twist ratio of $y = 3$ produced the maximum heat transfer enhancement. As the twist angle was increased on the CCCTT inserts, the fluid larger portions were directed in the opposite direction where the tapes were connected. This was found to lead to a stronger collision and mixing when the fluid recombined as well as more disturbance that inhibited boundary layer development.

Eiamsa-ard et al. [206] modified CTT inserts to form delta-winglet twisted tape inserts. They investigated the influence of delta-winglet twisted tape insert on heat transfer and pressure drop by using water as the test fluid. Two modifications of the tape inserts were considered, the first was the straight delta-winglet and the second was oblique delta-winglet. The inserts were fabricated to form three twist ratios of 3, 4 and 5, wing cut ratios of 0.11, 0.21 and 0.32 and were placed in a tube with an inner diameter and a length of 19.5 mm and 1 m respectively. Experiments were conducted in the turbulent Reynolds number range of 3 000 - 27 000. It was found that the decrease in twist ratios and increase in wing cut ratio led to the Nusselt number and friction factor enhancement of about 1.1 – 1.6 compared with a smooth tube. When the oblique and straight delta-winglet twisted tapes were compared, it was found that the oblique inserts were more effective; producing higher heat transfer coefficients than

the straight delta winglet insert. Similar enhancement observation was reported with increased Nusselt numbers with the use of twin delta winglet, serrated, broken, ribbed, spiky and multiple twisted tape inserts have also been reported [35, 160, 196, 207-210]. All these studies have demonstrated various passive techniques using twisted tape inserts to achieve heat transfer enhancement in tubes.

Seemawute and Eiamsa-ard [143] conducted experiments with peripherally cut twisted tape with alternate axis in a smooth circular tube with an inner diameter of 19 mm at constant heat flux boundary condition. Water was used as test fluid and the range of Reynolds number was 5 000 - 20 000. It was found that the Nusselt numbers of the alternate axis tape were higher by 184% compared with that of the smooth tube. The peripherally cut tape had an enhancement of 102%, while the CTT inserts produced an enhancement of 57% over smooth tube.

Eiamsa-ard et al. [190] reported the influences of peripherally-cut twisted tape inserts with depth ratios of 0.11, 0.22 and 0.33, width ratios of 0.11, 0.22 and 0.33 and twist ratio of 3. The experimental study was conducted over the Reynolds number range of 1 000 – 20 000, using water as the test fluid. It was found that higher turbulence of the test fluid in the vicinity of the tube resulted in the increase of heat transfer coefficient. The results showed that the heat transfer performance increased as the depth ratio was increased and the width ratio decreased. In the lower Reynolds number ranges close to 1 000, the maximum increase in the Nusselt number was 12.8-times, while in the higher Reynolds numbers range the maximum increase in the Nusselt number was 2.6-times that of a smooth tube. The thermal performance in the lower Reynolds number range was 5, while in the higher Reynolds number range, it was 1.3. Though the study covered a wide range of Reynolds numbers up to 1 000, no transitional flow characteristics were obtained in the investigation.

Eiamsa-ard and Promvonge [211], modified the CTT insert to form a tape with serrated edges. The experiments conducted on the serrated tape was over the Reynolds number range of 4 000 to 20 000. The purpose was to determine the heat transfer and pressure drop of the serrated tape. It was found that, as the depth ratio increased and width ratio reduced, the Nusselt number increased. When compared with a smooth tube, the Nusselt number of the serrated tape increased by 72%, while it was 27% higher than the Nusselt number of the CTT inserts. A similar result of heat transfer coefficient increase as the depth ratio was increased and the width ratio was reduced was also obtained in the work of Murugesan et al. [134, 212] where the heat transfer and pressure drop with V-cut twisted tape insert in the turbulent flow regime were experimentally investigated. The Reynolds number of the study was over the range of 2 000 - 12 000 and water was used as the test fluid. The performance of the V-cut tape was compared with that of the CTT inserts with twist ratios of 2, 4.4 and 6. It follows that the V-cut tape induced additional flow disturbance and secondary flow close to the inner surface of the tube compared to the CTT inserts. The maximum increase in the Nusselt number as a result of the V-cut was 1.1, while that of the friction factor was 1.3. The overall thermal performance was found to be 1.1 higher than that of the CTT inserts.

Hasanpour et al. [41] reported the heat transfer and pressure drop investigation of a corrugated tube with CTT inserts, perforated and peripheral 'U-' and 'V-cut' twisted tape inserts. The twist ratios of the tapes were 3, 5 and 7. The hole ratios of the perforation were 0.11 and 0.33, while the depth ratios of the peripheral cuts were 0.3 - 0.6. The tapes were tested in the turbulent flow regime over the Reynolds number range of 5 000 – 15 000. The combination of these parameters led to more than 350 experiments that were conducted. The heat transfer and pressure drop of the peripheral-cut tapes were found to be higher than the CTT inserts, however the perforated tapes produced the least heat transfer and friction factor results.

Eiamsa-ard et al. [13], reported the investigation of the influence of CTT inserts combined with circular ring inserts on the heat transfer and pressure drops as well as thermal performance in a smooth tube. The tube had an inner diameter and a length of 64 mm and 1.5 m respectively. The twisted tape inserts that were placed in the tube had twist ratios of 3, 4 and 5, while the rings of each tape were spaced at a pitch ratio of 1, 1.5 and 2. The experiments were conducted over the Reynolds number range of 6 000 to 20 000 using air as test fluid and at a constant heat flux boundary condition. When the combined effects of the tape and rings were compared with the singular effect of the rings, it was found that the combined effect made the heat transfer, friction factor and thermal performance factor to be higher by 26%, 83% and 6% respectively than the individual effect of the two inserts separately. The tape with the least twist ratio and ring pitch ratio produced the highest performance factor.

In general, the literature indicates that previous studies reviewed above were for the singular purpose of enhancement. They are limited to the laminar and turbulent flow regimes and not transitional flow regime.

2.6 Transitional flow regime

The transitional flow regime, in general was avoided in most studies because of unreliable predictions [213], inadequate understandings [214], complex behaviours [215], unclear transition mechanisms [216] and because it is considered as a metastable regime with different transport phenomena [217]. However, Meyer [33] reported that the transitional regime could be a good compromise between the laminar (low heat transfer and pressure drop) and turbulent (high heat transfer and pressure drop) flow regimes. Meyer [33] therefore, suggested that more research should be conducted in the transitional flow regime and particularly in enhanced tubes.

Therefore, in the following review on previous work done using twisted tape inserts and other passive enhancement techniques, cases occurred where experiments were most probably in the transitional flow regime. However, no specific attention was given to this regime, and it was either reported as part of the laminar or turbulent flow regimes, or as part of both regimes. The geometry effects of the inlets which had been found to influence the transitional flow regime in smooth tubes by the work performed by Prof Afshin Ghajar and his co-workers from Oklahoma State University [15, 17, 19, 21, 218], and the second by

Prof Josua Meyer and his co-workers at the University of Pretoria [1, 22, 26, 28, 33, 219] were not considered in the studies with twisted tape inserts and in some cases, a tube length with the same diameter as the test section, was considered as a calming section. This ensured hydrodynamic fully developed flow since there was no contraction ratio between the calming section and the test section.

That the inlet geometry will influence the critical Reynolds number as well as the transitional results for not only smooth tubes but also for enhanced tubes, has been illustrated for not only the friction factors by Tam et al. [220], but also the heat transfer by Tam et al. [221]. This has been independently verified by Meyer and Olivier [24, 222, 223]. In Tam et al. [221] for example, the effect on heat transfer in the transitional flow regime of three different types of inlet geometries on micro-fin tubes were experimentally studied. The different types of inlets were square-edged, re-entrant, and bellmouth inlet. Meyer and Olivier [24, 223] also included in their studies a long enough tube length (calming section) to ensure hydrodynamically fully developed flow. This type of inlet corresponds to the type of inlet used by Manglik and Bergles [135], Saha and Dutta [167] and Bharadwaj et al. [37], however, it was longer (160D as recommended by Durst et al. [224]) to ensure hydrodynamically fully developed flow at the test section inlet. Tam et al. [221] showed that the transitional flow regime started and ended at Reynolds numbers of 1 946 – 8 105, 2 144 – 8 254 and 3 015 – 8 092, respectively for the re-entrant, square-edged and bellmouth type of inlet geometries. It was therefore concluded by them that the geometry of the inlet influenced the start and end of transition.

Manglik and Bergles [149] experimentally investigated over a Reynolds number range of 300 - 30 000, twisted tape inserts using a uniform wall temperature boundary condition. They concluded that the progression from transition to turbulent was usually characterised with instabilities in flow and fluctuations in velocity. That centrifugal forces from the twisted tape inserts suppress these instabilities and fluctuations, and that secondary flows dampened the turbulent pulsations and thus delayed transition [135]. Based on flow regime maps, Manglik and Bergles [135] stated that flow rates with Reynolds numbers less than 10 000 fall within the transitional flow regime and higher flow rates could be regarded as fully developed turbulent flow. In some cases, turbulent flow may be achieved at lower Reynolds numbers, depending on the twist ratios of the twisted tape inserts used. Furthermore, for the purpose of designing heat exchangers, the study recommended curve fittings of experimental data from the laminar to the turbulent flow regimes, in order to quantify heat transfer coefficients and friction factors in the transitional flow regime.

A delayed transition to turbulent flow with the use of twisted tape inserts has also been reported in Watanabe et al. [68], Donevski and Kulesza [225] and Nair [192]. The critical Reynolds number, that indicates the start of transitional flow regime, of 6 360 reported by Watanabe et al. [68], was in total disagreement with the critical Reynolds number of 30 430 which was provided by Donevski and Kulesza [225]. In these two papers, these critical Reynolds numbers were chosen as the point of intersection between the laminar and the turbulent flow regimes. There was no range of Reynolds numbers clearly defining and differentiating the transition region from laminar to turbulent flow. Date and Jagad [226],

however, stated that the delay in fully turbulent flow was possibly associated with the strong swirl induced by the tape inserts.

Bharadwaj et al. [37] experimentally investigated the heat transfer and pressure drop in a spirally grooved tube with twisted tape inserts. Laminar to fully turbulent Reynolds numbers from approximately 300 to 25 000 were considered. The three most important observations made were: (1) It appeared that transition-like characteristics for a grooved tube without a twisted tape insert started at approximately a Reynolds number of 3 000 and continued up to a Reynolds number of 7 000. (2) There was no abrupt change in the friction factor in the transitional flow regime with a twisted tape insert. (3) A transition-like abrupt change in the Nusselt number with the twisted tape insert was observed at a Reynolds number of 7 000. They have also developed friction factors and Nusselt numbers correlations in the three flow regimes of laminar, transitional and turbulent. However, this was for a grooved tube with a twisted tape insert, not for a smooth tube with a twisted tape (as in this study).

Limited considerations/details were also given to the possible effects of the connection of the test section to the calming section to ensure limited boundary layer disturbances effects. Also, it appears as if the calming section length will not ensure a fully hydrodynamically developed velocity distribution at the test section inlet (based on $L_{th} = 0.05ReD$, at a transition Reynolds number of 3 000 and a diameter of 12.5 mm, it will take approximately 1.9 m for the flow to get fully developed, while the calming section length was 1.2 m). The inlet velocity distribution is an important factor to take into consideration as was shown by Ghajar and co-workers [15, 18, 20, 218] as well as Meyer and co-workers [1, 24-26]. They showed that another calming section length and/or geometry will influence the critical Reynolds number as well as the characteristics of the friction factors and heat transfer coefficients in the transitional flow regime. It is conceded, that as enhancement techniques such as both grooved tubes and twisted tapes were used in the study of Bharadwaj et al. [37], that the effects might be less significant than for smooth tubes.

Ji et al. [73] presented a review article of experimental studies on heat transfer and performance enhancements conducted in the laminar, transitional and turbulent flow regimes for four passive enhancement techniques. The enhancement techniques considered were integral-fins, twisted tape inserts, corrugated tubes and dimple tubes. It was found that specifically twisted tapes were very effective in the laminar and transitional flow regimes and that they may be more suitable for fluids with high viscosities.

Bhadouriya et al. [227] conducted an experimental and numerical investigation of friction factors and heat transfer characteristics of air flowing through a twisted square duct. The twist ratios of the ducts were 11.5 and 16.5 and experiments were conducted for Reynolds number range of 600 - 70 000. The Reynolds number range for the numerical study varied between 100 to 100 000 and the twist ratios were 2.5, 5, 10, and 20. The start of transition was observed during the experimental study at a Reynolds number of 2 900 for the duct with a twist ratio of 11.5, and at a Reynold number of 3 000 for the duct with a twist ratio of 16.5. The transition to turbulent was assumed to have commenced when there was a sudden change in the slope of both the friction factor and heat transfer data in the laminar flow regime.

In general, not only did Tam et al. [220, 221] illustrate that transition from laminar flow regime to turbulent flow regime is not sudden but smooth, they also demonstrated that enhanced tubes caused transition to start earlier compare with smooth tube. Other researchers such as Meyer and Olivier [26, 223] and Garcia et al. [228] reported a similar phenomenon. Meyer and Olivier [26, 223] on their work, when they enhanced tubes with a fin of helix angles of 18° and 27°, found that transitional flow regime started at a Reynolds number of 1 900 and 2 000 respectively as the helix angle increased.

Garcia et al. [228], who experimentally investigated a smooth tube with wire coils of different geometries reported a transition occurrence at the Reynolds numbers of 500 – 2 000. The earliest transition (Re = 500) occurred when the wire coil with the highest disturbance was used. The start and end of transition were found to be a function of the wire geometry. They also found that for the lowest pitch-to-wire diameter the heat transfer coefficient increased up to 200% in the transitional flow regime compared with a smooth tube. This then illustrates that unlike studies that the start of transitional Reynolds numbers were greater than those of smooth tube ($2\,300 \leq Re \leq 4\,000$), that (1) the start of the transitional flow regime occurred earlier in enhanced tube because of flow disturbance introduced by the enhancer, (2) the more the disturbance caused by the enhancer, the earlier the transition occurred (3) the heat transfer enhancement in the transitional flow regime could outweigh not only that of a smooth tube but also other flow regimes. (4) unlike the smooth tube with unpredictable behavior, the transitional flow regime in enhanced tubes have predictable patterns. Garcia et al. [228], in their concluding remarks referred to the transitional flow regime as the best flow regime.

2.7 Summary and conclusions

A review of the heat transfer and pressure drop literature on the transitional flow regime in enhanced tubes has been presented in this chapter. The enhancement techniques could be in the form of active, passive or both. Attention was given to the passive techniques as their benefits outweigh those of the active techniques. Among the passive techniques, specific focus was given to twisted tape inserts. Two important conclusions could be made of the literature on twisted tape inserts in the transitional flow regime.

Firstly, most of the work done in literature was limited to either the laminar or turbulent flow regime and thus little work has been conducted on heat transfer in the transitional flow regime. Some studies included experimental work in the transitional flow regime, but did not concentrate specifically on the transitional flow regime.

Secondly, when transitional flow experiments are conducted, it is essential that the inlet geometry, and calming section are taken into consideration and documented as part of the study. This was not done in previous work on twisted tape inserts in tubes in the transitional flow regime.

Therefore, the purpose of this study was to experimentally investigate the heat transfer and pressure drop characteristics in the transitional flow regime with conventional twisted tape

inserts, clockwise and counter clockwise twisted tape inserts and peripheral u-cut twisted tape inserts placed inside smooth tubes with a square-edged inlet. Specific attention was given to the identification of the transitional flow regime with the twisted tape inserts and the influence of twist ratio, heat flux, connection angle, depth ratio and ring space ratio on the transitional flow regime. The inlet geometry of a square-edged was used, as it is the type of geometry that is simple to be replicated and manufactured by other laboratories, and to be used as an inlet boundary condition for numerical simulations. It is also the type of geometry found in many heat exchangers such as shell-and-tube heat exchangers, where the flow inlet through each tube is from a common header.

3. Experimental set-up and data reduction

3.1 Introduction

This chapter discussed the experimental set-up used in this study to conduct the heat transfer and pressure drop experiments as a function of mass flow rates in both the smooth circular tube and tube with twisted tape inserts. A comprehensive detail of experimental set-up which include the components of the circulation loop, materials used for the calming section, inlet section and test section as well as the equipment and instrumentation used is provided. The data reduction method, experimental procedure as well as test matrix and uncertainty analysis are given.

3.2 Experimental set-up

Fig. 1 shows the schematic diagram of the experimental set-up that was used to conduct the heat transfer and pressure experiments as a function of mass flow rates. The facility was a close loop system, with the major components labelled and described from (1) - (14).

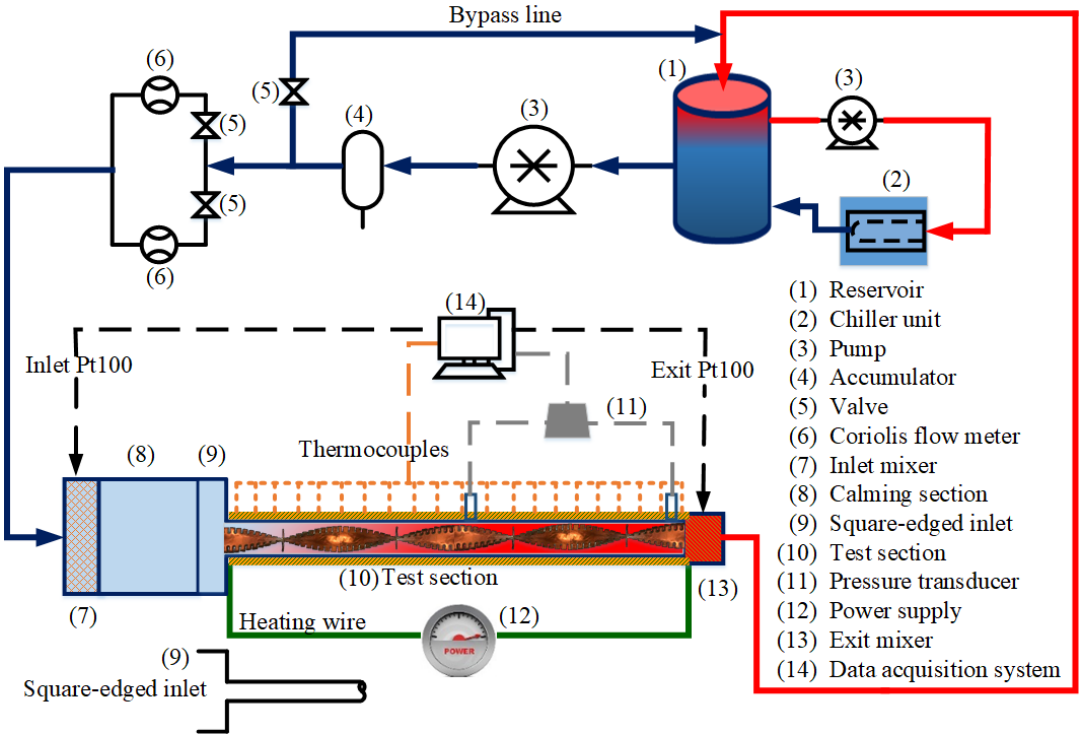

Fig. 3.1. Schematic of the experimental set-up.

3.2.1 Components of circulation loop

The water that was heated in the test section was cooled and maintained at a constant temperature in a reservoir (1) that was connected to a chiller unit (2). The water was pumped (3) through a water loop in which there was an accumulator (4), valves (5) used to

operate the bypass line and/or bank of flow meters (6), an inlet mixer (7), a calming section (8), a square-edged inlet (9), test section (10), pressure transducer (11), a power supply (12), an exit mixer (13) and a data acquisition system (14).

Water was circulated from a 5 000 ℓ reservoir (1) through a test section. The reservoir and the experimental set-up were in a non-airconditioned laboratory in which the ambient air temperatures varied from approximately 15 – 25 °C. The temperature of the water in the reservoir was thermostatically-controlled and continuously maintained at 20 °C with an external chiller unit (2) with a capacity of 15 kW. The water was circulated using an electronically-controlled positive displacement pump (3) with variable speed drive and could pump the water through the circulation loop at volume flow rates varying from 6 – 1 344ℓ/h.

An accumulator (4) was installed after the pump to dampen the flow pulsations associated with the positive displacement pump [24, 229]. The accumulator was of the Hydac bladder type with a diameter, a height and a volume of 173 mm, 419 mm and 4 ℓ respectively. It was charged with nitrogen to an operating pressure of 3.3 MPa and the maximum operating mass flow rate was 10 kg/s.

After the accumulator followed a bypass line that was used when lower mass flow rates were required in the test section. A bypass valve (5) and two valves in parallel, followed after the accumulator, upstream of two Coriolis flow meters (6), each with its own range and accuracies. The valves were installed to make it possible to switch between the Coriolis mass flow meters, as well as to allow water to flow back into the reservoir. In general, it was found that the mass flow fluctuations increased as the pump speed decreased, and the flow fluctuations were the smallest at the highest pump speed [219]. Therefore, the pump was always operated at the highest possible pump speed, and lower mass flow rates (with low mass flow fluctuations) were achieved by controlling the flow opening of the valve in the bypass line.

The Coriolis flow meters (6) were used to control mass flow rates during the experiments. The Coriolis flow meter with a range of 4 – 108 ℓ/h was used for the mass flow rate measurements in the laminar and transitional flow regimes. While the Coriolis flow meter with the flow range of 54 - 2 180 ℓ/h was used for higher mass flow rates, particularly in the turbulent flow regime. The measurement errors of both flow meters, when operated in their prescribed ranges were 0.05% of full scale. After leaving either of the two Coriolis flow meters, the water flowed through a calming section.

3.2.2 Calming section

The calming section (Fig. 3.2) used was in general similar to the design of Ghajar and co-workers [15, 20] except for the following notable differences:

- The inlet mixer was integrated to be part of the inlet of the calming section by increasing the length of the cylindrical geometry of the calming section.
- The material used was not acrylic plastic, but stainless steel (the “straws”, screens and meshes were also manufactured from stainless steel), to ensure that the calming section

could withstand higher pressures than acrylic plastic for other experiments that were planned with propylene glycol as the test fluid.

- The calming section's inner diameter was 200 mm, which gave a larger contraction ratio of about 10.5, compared to Ghajar and Tam [15] and Tam et al. [18], who used a 146 mm inner diameter acrylic tube and a contraction ratio of 9.24.
- The connection of the square-edged to the test section was simpler and different.

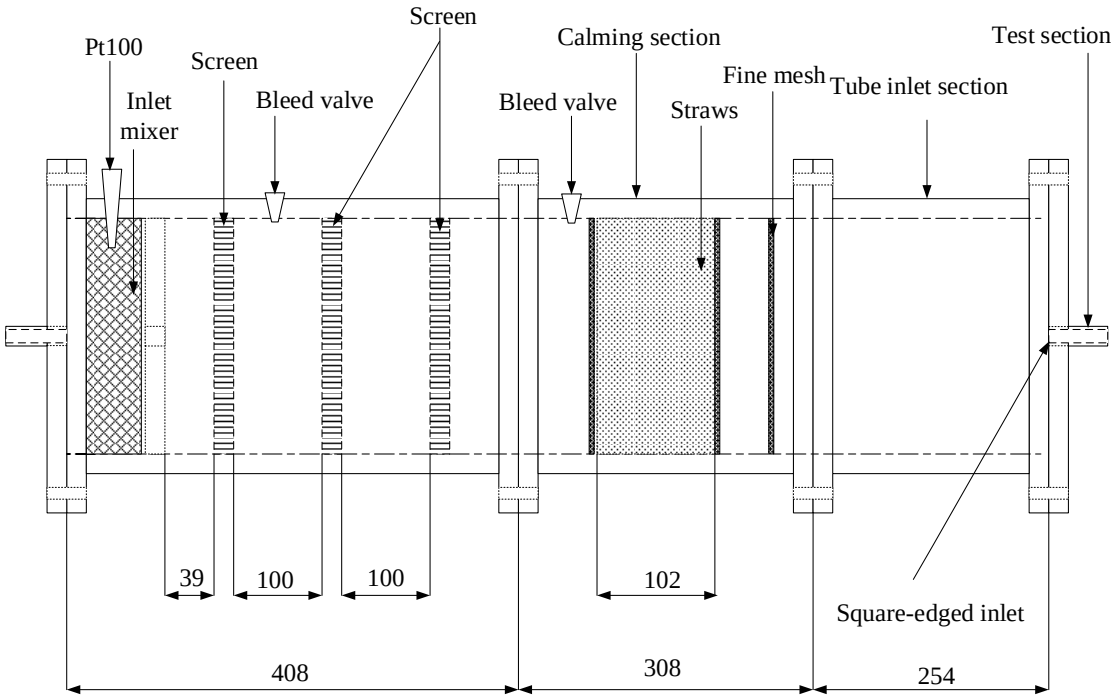

Fig. 3.2. Schematic of the calming section with square-edged inlet configuration based on the calming section of Tam et al. [18].

The calming section (Fig. 3.2) was installed upstream of the test section and comprised of three parts; the inlet mixer (7), the calming section (8) and the square-edged inlet (9). The inlet mixer contained stainless-steel shavings, which ensured good mixing of the water and prevented possible temperature gradients that could develop as the water flowed into the calming section. A Pt100 probe was installed in the inlet mixer to measure the bulk inlet water temperature. The functions of the calming sections were (1) to ensure a uniform velocity distribution of the water flowing into the test section and (2) to accommodate the square-edged inlet, previously considered to influence the transitional flow regime.

Three perforated stainless-steel plates of thickness 10 mm with an open area ratio of 0.31 comprising of 73 holes each one with a diameter of 11 mm were installed after the inlet mixer. This was followed by a total of 1 567 units of stainless-steel straws with an inner diameter of 6 mm, length of 102 mm and open area ratio of 0.92 tightly packed between two meshes on each side of the straws. These meshes were made of stainless steel with wire diameter of 0.55 mm, mesh width of 1.3 mm and open area ratio of 0.55. A fine stainless-steel mesh with a mesh width of 1.5 mm, wire diameter of 0.32 mm and open area ratio of 0.5 was installed before the end of the calming section. The water flowed through this fine mesh before leaving the calming section.

After leaving the calming section, the water flowed into the inlet section cylinder of an inner diameter of 200 mm, an outer diameter of 219 mm and a total length of 254 mm before entering the test section. Fastened on this inlet cylinder is the square-edged inlet to provide a sudden contraction to the water as it flowed into the test section. The square-edged inlet was connected after the calming section and then to the test section. Two bleed valves, one located immediately after the inlet mixer and another located before the straws, were used to bleed out entrained air to avoid bubbles entering the test section. Components (11) - (14) were part of the test section and are discussed in Section 3.2.3.

3.2.3 Test section

The test section (10) accommodated four categories of experiments. The first category used a smooth tube experiments without any twisted tape and ring inserts and the results were compared with literature to validate the experimental set-up and data reduction method. The experimental operating conditions as summarized in Table 3.1. The smooth tube had an inner diameter and a length of 19 mm and 5.27 m respectively and was also used for the experiments in the other three categories.

In the second category of experiments, CTT inserts were placed inside the smooth tube as illustrated in Fig. 3.3(a). The CTT inserts were fabricated from a plain copper sheet with a thickness, δ, of 1 mm, which were cut with a guillotine into strips with a tape width, W, of 18 mm. The two ends of the strips were clamped, one into the jaw chuck and the other on the tool post of a lathe. The tool post was held stationary, while the jaw chuck was rotated manually to achieve the desired pitch, H, and twist ratio, $y = H/W$. The pitch, H, was defined as the axial distance required to complete a 180° rotation in a twisted tape insert. Three twist ratios of y = 3, 4 and 5 were considered. The ends of five 900 mm long CTT inserts as well as an additional 770 mm, were soldered together to form a total length of 5.27 m before they were placed in the smooth tube test section. The parametric values of the CTT insert experimental set-up are summarized in Table 3.1.

Table 3.1. Parametric values of the CTT insert experimental set-up.

Parameters	Symbols	Values
Thickness of twisted tape inserts	δ	1 mm
Outer diameter of test section	D_o	22.0 mm
Inner diameter of test section	D_i	19.0 mm
Pitches of the twisted tape inserts	H	54, 72, 90 mm
Length of twisted tape/test section	L	5.27 m
Heat transfer length	L_h	4.8 m
Pressure drop length	$L_{\Delta P}$	2.45 m
Prandtl numbers	Pr	2.9 – 6.7
Heat fluxes	$\dot{q}$	2, 3, 4 kW/m^2
Reynolds numbers	Re	400 – 11 404
Inlet temperature of the working fluid	T_i	20 °C
Width of twisted tape insert	W	18 mm
Twist ratios	y	3, 4, 5

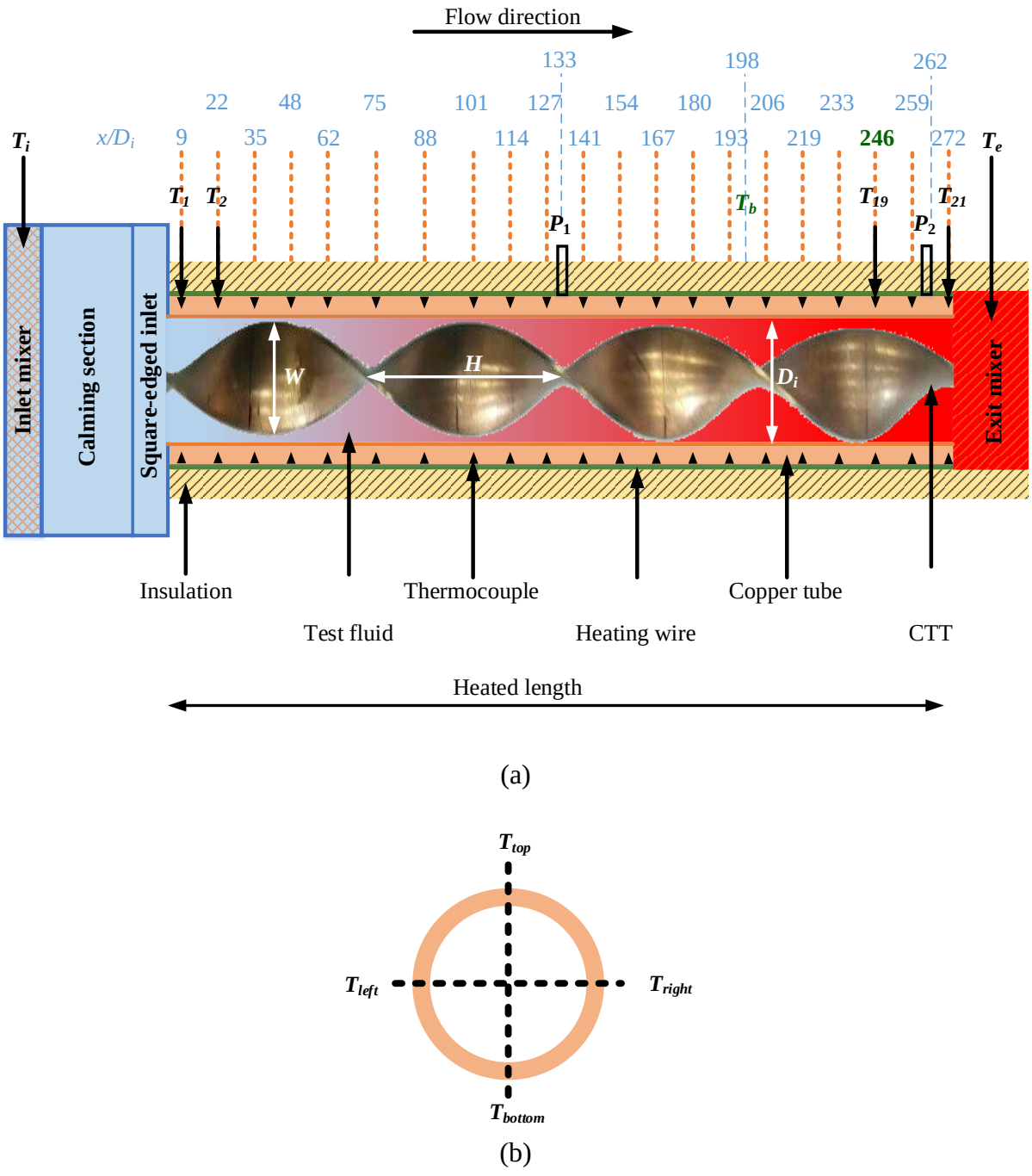

Fig. 3.3. Schematic diagram (not to scale) showing the (a) test section with CTT inserts, the 21 measuring stations (T_1 –T_{21}), station used for bulk temperatures and corresponding bulk Reynolds number, as well as the two pressure taps (P_1 and P_2) and the x/D_i values of each measuring station and (b) cross-sectional view of the test section with the four thermocouple positions on the periphery of the tube.

The third category of experiments was conducted when CCCTT inserts were placed inside the smooth tube (Fig. 3.4). The CCCTT inserts had a thickness, δ, of 1 mm, width, W, of 18 mm and a pitch, H, of 90 mm. The CCCTT inserts consisted of copper plate strips with lengths of 450 mm and a twist ratio, $y = H/W$, of 5. This length ensured five full twists of 180° (or 2.5 twists of 360°) of the tapes. The ends of 12 alternating strips were soldered to each other to form one CCCTT insert. To obtain a total length of 5.27 m, which was the length of the smooth copper test section, the 12th strip had a shorter length of 370 mm. As

indicated in Fig. 3.5, three CCCTT inserts were fabricated, each connected at different connection angles (θ = 0°, 30° and 60°). Fig. 3.5 contains both schematic diagrams and photographs of the CCCTT inserts for different connection angles of 0° (Fig. 3.5(a) and (d)), 30° ((Fig. 3.5(b) and (e)) and 60° ((Fig. 3.5(c) and (f)) respectively. The parametric values of the CCCTT inserts experimental set-up are summarized in Table 3.2.

Table 3.2. Parametric values of the CCCTT inserts experimental set-up.

Parameters	Symbols	Values
Outer diameter of test section	D_o	22.0 mm
Inner diameter of test section	D_i	19.0 mm
Heat transfer length	L_h	4.8 m
Pressure drop length	$L_{\Delta P}$	2.45 m
Thickness of twisted tape inserts	δ	1 mm
Pitch of the twisted tape inserts	H	90 mm
Length of twisted tape/test section	L	5.27 m
Width of twisted tape insert	W	18 mm
Twist ratio	y	5
Connection angles	θ	0°, 30° and 60°
Prandtl numbers	Pr	2.1 – 6.58
Heat fluxes	$\dot{q}$	1.35, 2, 3 and 4 kW/m^2
Reynolds number range for CCCTT	Re	300 – 6 675
Inlet temperature of the test fluid	T_i	20 °C

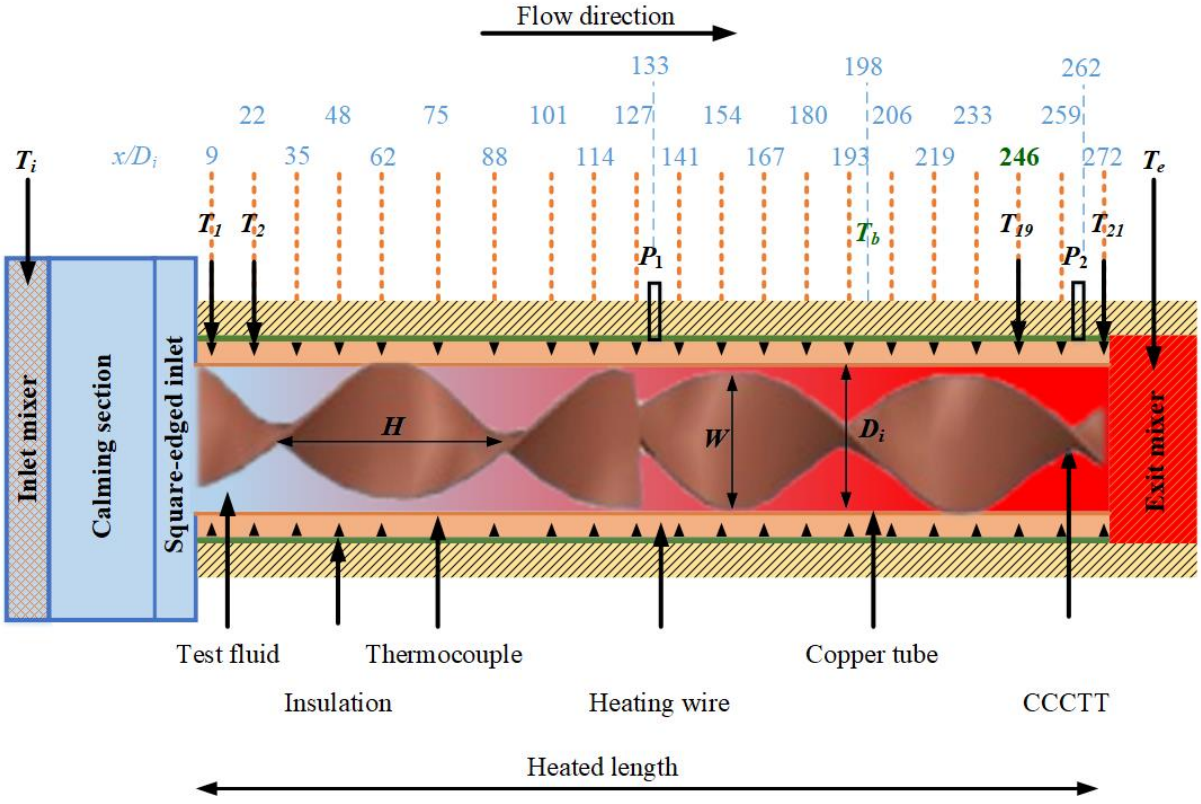

Fig. 3.4. Schematic diagram (not to scale) showing the test section with CCCTT inserts, the 21 measuring stations (T_1 – T_{21}), station used for bulk temperatures and corresponding bulk Reynolds number, as well as the two pressure taps (P_1 and P_2) and the x/D_i values of each measuring station.

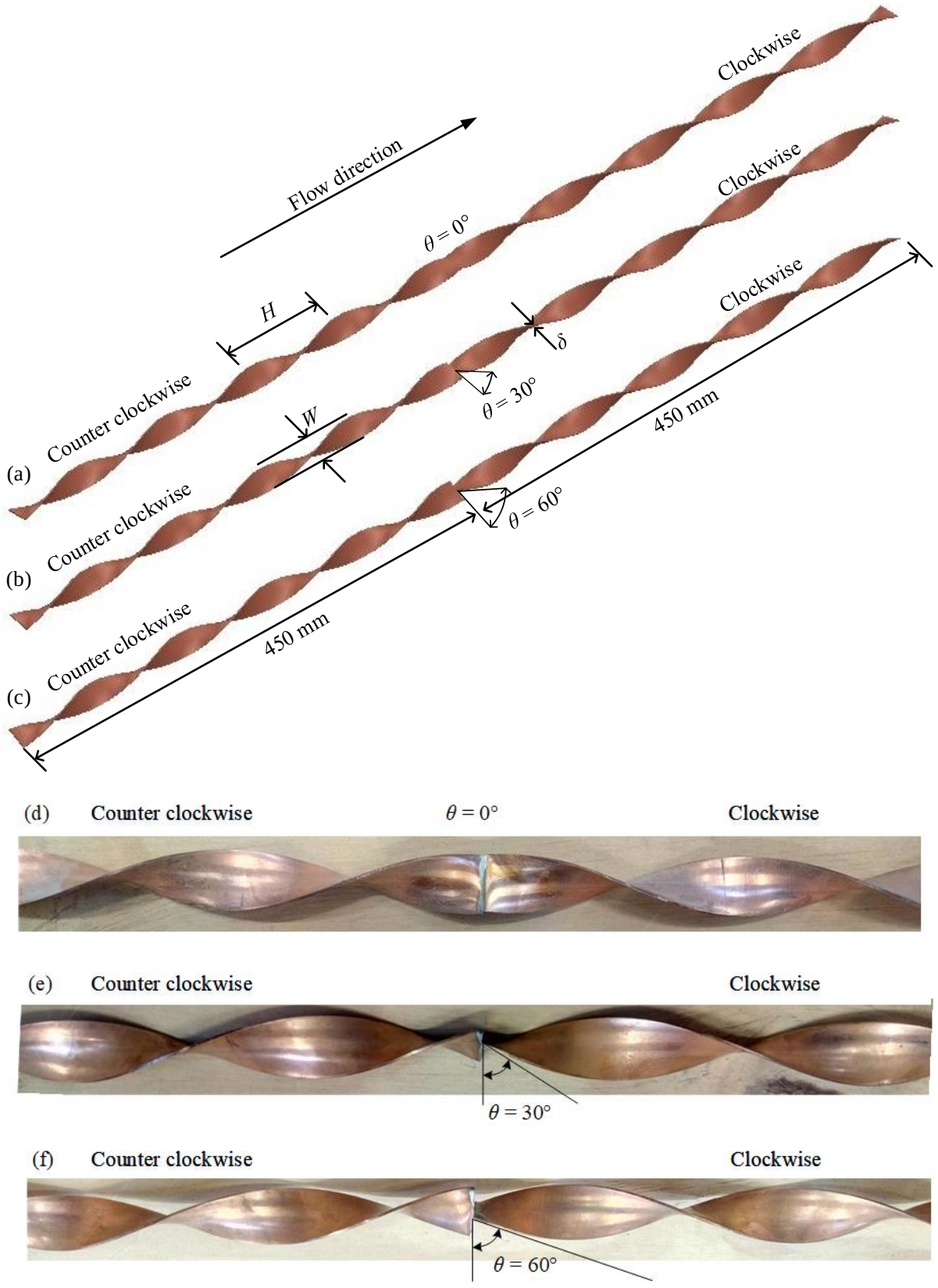

Fig. 3.5. Schematic representation of the CCCTT inserts with connection angles, *θ*, of (a) 0°, (b) 30° and (c) 60°, as well as photographs of the CCCTT inserts with connection angles of (d) 0°, (e) 30° and (f) 60°.

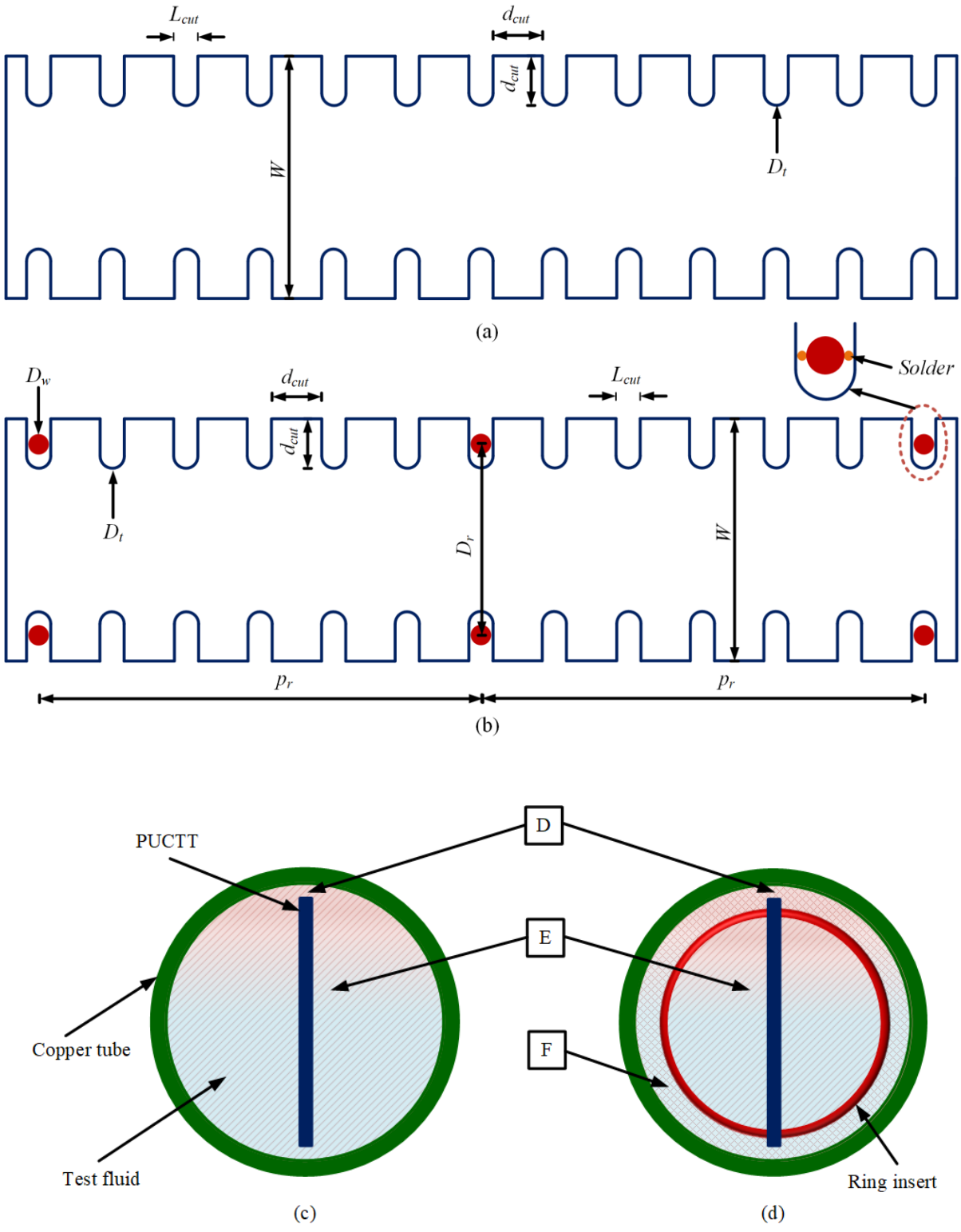

Fig. 3.6. Schematic of (a) PUCTT insert and (b) PUCTTR insert (c) cross-sectional view of PUCTT insert and, (d) cross-sectional view of PUCTTR insert. The additional sketch nomenclature, D, E and F, are discussed in the text.

The fourth category of experiments was conducted in two sets. The first set was when the PUCTT inserts (Fig. 3.6(a)) were placed in the smooth tube (Fig. 3.7). The PUCTT inserts were fabricated from plain soft-drawn copper strips with a tape thickness, δ, of 1 mm and

tape width, W, of 18 mm. The strips were placed in a water-jet cutting machine that carefully cut the desired depths. One strip had a cut depth, d_{cut} = 1.89 mm and the other strip had a cut depth, d_{cut} = 3.89 mm (Fig. 3.6(a)). This translated to depth ratios, $R_d = d_{cut}/W$ = 0.105 and 0.216 respectively. The cutting tool of the water-jet cutting machine had a diameter, D_t, of 1 mm. The strips from the water-jet cutting were then clamped in the jaw chuck and tool post of a lathe. To form the PUCTT insert, the tool post of a lathe was held stationary while the jaw chuck was manually rotated to form the desired tape pitch, H, of 90 mm and twist ratio, $y = H/W$ = 5. The ends of five 900 mm long PUCTT inserts and one 770 mm long PUCTT insert, were soldered together to form a total length of 5.27 m.

Table 3.3. Parametric values of the PUCTT and PUCTTR inserts experimental set-up.

Parameters	Symbols	Values
Thickness of twisted tape insert	δ	1 mm
Cut depth	d_{cut}	1.89 and 3.89 mm
Outer diameter of test section	D_e	22 mm
Inner diameter of test section	D_i	19 mm
Ring insert diameter	D_r	15.9 mm
Pitch of twisted tape insert	H	90 mm
Length of twisted tape/test section	L	5.27 m
Heat transfer length	L_h	4.8 m
Pressure drop length	$L_{\Delta P}$	2.45 m
Ring inserts pitch	p_r	22.5, 45 and 90 mm
Prandtl numbers	Pr	3.32 – 6.58
Heat fluxes	$\dot{q}$	1.35 and 2 kW/m^2
Reynolds numbers range for the PUCTT and PUCTTR inserts	Re	315 – 6 623
Depth ratio	R_d	0.105 and 0.216
Ring space ratio	R_r	1.25, 2.5 and 5
Inlet temperature of the working fluid	T_i	20 °C
Width of twisted tape insert	W	18 mm

For the second set of experiments in the fourth category, PUCTTR inserts (Fig. 3.6(b)) with ring inserts of wire diameter, D_w = 0.84 mm and ring diameter, D_r = 15.9 mm were placed in the smooth tube (Fig. 3.7). Three PUCTTR inserts, with ring insert pitches of p_r = 22.5, 45 and 90 mm respectively, were fabricated for each depth ratio. These were achieved by slotting and soldering a total of 234, 117 and 58 ring inserts, into the cut length, L_{cut} = 1 mm, translating to ring space ratios, $R_r = p_r/W$ = 1.25, 2.5 and 5 respectively. These parameters are summarized in Table 3.3. The parameters in the schematic diagrams of the PUCTT and PUCTTR inserts shown in Fig. 3.6 with dimensions are given in Table 3.4. The acronyms PUCTT1 and PUCTT2 represent the PUCTT inserts with the depth ratios of 0.105 and 0.216 respectively. Furthermore, the acronyms PUCTTR11, PUCTTR12 and PUCTTR13 represent the PUCTT inserts of depth ratio, R_d = 0.105 with ring space ratios, R_r = 1.25, 2.5 and 5 respectively. The acronyms PUCTTR21, PUCTTR22, and PUCTTR23 represent the PUCTT insert of depth ratio, R_d = 0.216 with ring space ratios, R_r = 1.25, 2.5 and 5 respectively.

Table 3.4. Summary of the PUCTT and PUCTTR inserts parameters.

Insert	Cut depth d_{cut} [mm]	Depth ratio R_d	Ring insert pitch p_r [mm]	Ring space ratio R_r	Number of rings	Heat flux $\dot{q}$ [kW/m^2]
PUCTT1	1.89	0.105	0	0	none	1.35
PUCTTR11	1.89	0.105	22.5	1.25	234	1.35
PUCTTR12	1.89	0.105	45	2.5	117	1.35
PUCTTR13	1.89	0.105	90	5	58	1.35
PUCTT2	3.89	0.216	0	0	none	1.35
PUCTT22	3.89	0.216	0	0	none	2
PUCTTR21	3.89	0.216	22.5	1.25	234	1.35
PUCTTR22	3.89	0.216	45	2.5	117	1.35
PUCTTR23	3.89	0.216	90	5	58	1.35

The rings were soldered into the PUCTT inserts to increase the disturbances on the inside of the tube and to decrease the thermal boundary layer thickness. This is because as the fluid flowed from one ring to another the boundary layer redevelops. As indicated in Fig. 3.6(c) the PUCTT inserts (Fig. 3.6(a)) only disturbed the flow on the periphery of the tape (area D) and at the tape surfaces (area E). However, Fig. 3.6(d) indicates that the PUCTTR inserts shown in Fig. 3.6(b) caused increased disturbances, flow recirculation and mixing on the periphery of the tape (area D) and the tape surfaces (area E) as well as between the ring surface and the inner wall of the test section (area F).

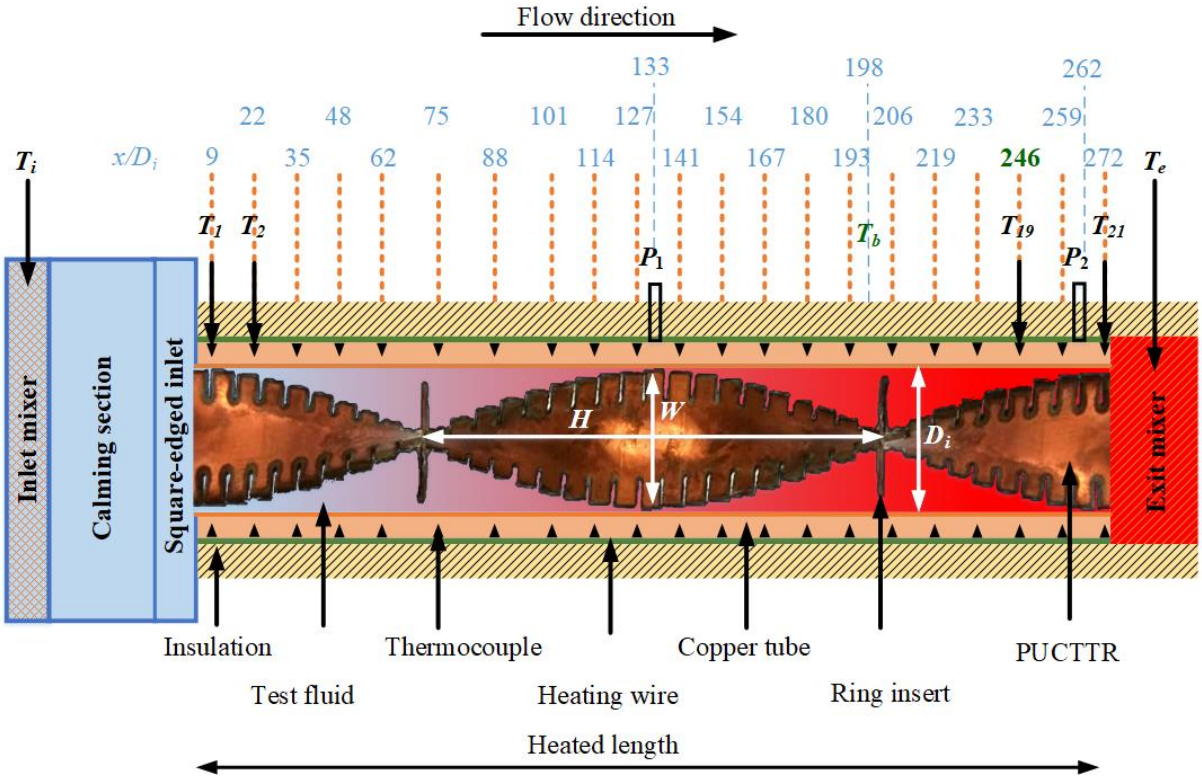

Fig. 3.7. Schematic diagram (not to scale) showing the test section with PUCTT and PUCTTR inserts, the 21 measuring stations (T_1 – T_{21}), station used for bulk temperatures and corresponding bulk Reynolds number, as well as the two pressure taps (P_1 and P_2) and the x/D_i values of each measuring station.

A pressure transducer (11) was connected to two pressure taps, located at $x = 2.52$ m and $x = 4.97$ m from the inlet of the test section as shown in Fig. 3.3. The distance between the two pressure taps, $L_{\Delta P}$, was thus 2.45 m. Holes with a diameter of 1.6 mm were drilled through the pressure taps and test section using a high-speed drill to prevent burr formations on the inside of the test section. The diameter of the holes were less than 10% of the inner diameter, as prescribed by Rayle [230], to prevent localized eddies from affecting the pressure drop measurements. Three differential pressure transducers were used depending on the pressure drops measured. A 0.86 kPa diaphragm was used for the smooth tube experiments, while for the twisted tape inserts, the 0.86 kPa diaphragm was used at lower mass flow rates and a 1.4 kPa as well as a 3.5 kPa diaphragm at higher mass flow rates. The diaphragms were calibrated within an accuracy of 2.15 Pa, 3.5 Pa and 8.75 Pa respectively over a pressure range of 0 Pa to their respective maximum pressures.

A total of 84, T-type thermocouples (0.25 mm diameter) were used to measure the surface temperatures at 21 measuring stations along the test section (Fig. 3.3(a)). At each measuring station, four thermocouples (Fig. 3.3(b)) were soldered at the angles of 0° (top), 90° (left), 180° (bottom) and 270° (right). Care was taken to ensure that the top and bottom thermocouples corresponded to the vertical plane, and the left and right thermocouples corresponded to the horizontal plane. The measuring stations were spaced at 250 mm intervals with the first measuring station located 170 mm from the inlet of the test section ($x/D_i = 9$) and the last measuring station located 5.17 m from the inlet ($x/D_i = 272$). The thermocouples were calibrated within an accuracy of 0.1 °C against a calibrated Pt100 probe over a range of temperature of 17 – 60 °C using a thermostat-controlled bath.

Two insulated constantan heating wires, each with a diameter of 0.81 mm, were tightly coiled around the test section and connected in parallel to the power supply (12) to obtain constant heat flux boundary condition. Care was taken that the gaps between the heating wires and the thermocouple stations were very small (approximately 1 mm) to ensure that the applied heat flux on the outer tube remained constant in an axial length, but that the wires did not touch the thermocouples. The heating wires were connected in parallel to reduce the total electrical resistance, and prevent the heating wires from melting, as the required current for the heat fluxes would have been too high for one wire. The power supply, as identified in Fig. 3.1, was rated as 1.5 kW, with a current and voltage ranges of 0 - 15 A and 0 - 360 V respectively. The error of the current and the voltage from this power supply was 0.2% of maximum value.

The exit mixer (13) as shown in Fig. 3.8 was connected to the exit of the test section. It was fabricated from acetal and had an inner diameter of 19 mm, an outer diameter of 50 mm and a length of 200 mm. Two copper mixer (twisted) plates were placed inside the exit mixer to ensure that the water exiting the test section was mixed to uniform temperature. A Pt100 probe was installed at the exit mixer to measure the bulk exit water temperature. The Pt100 probes installed at the inlet and exit mixers were calibrated to within 0.06 °C in a thermostat-controlled bath against a digital thermometer with an accuracy of 0.03 °C. After leaving the test section and the exit mixer, the water was returned to the reservoir (1) and then pumped to

the chiller unit (2) for continuous cooling to the temperature of 20 °C, before it was recirculated to the test section.

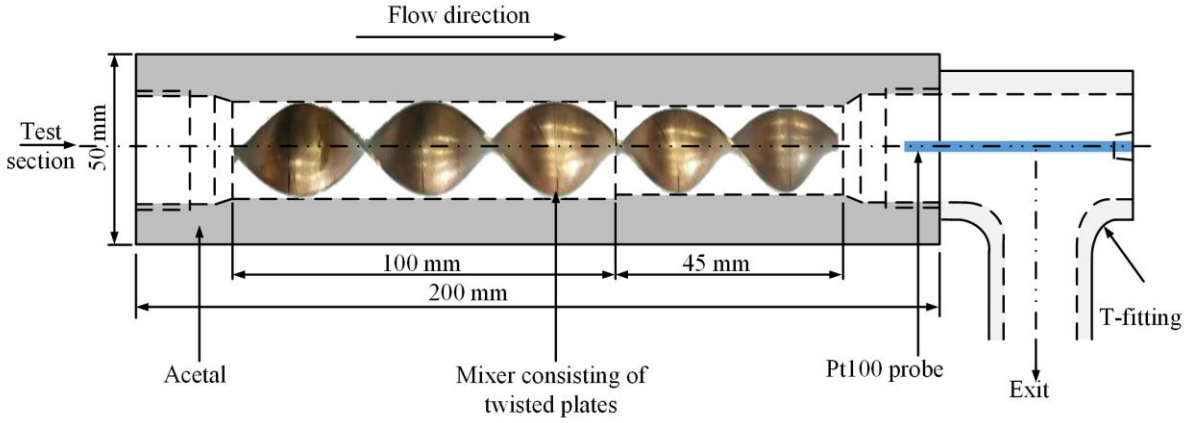

Fig. 3.8. Schematic diagram of the exit mixer with the copper mixer plates and a Pt100 to measure the exit water temperature.

The test section was connected in a longitudinal direction to the stainless-steel calming section and the exit mixer. The thermal conductivity values of the stainless steel, copper tube and acetal were 17, 401 and 0.25 W/mK respectively. Since the thermal conductivity of the stainless steel and acetal were both at least one order of magnitude lower than that of the copper tube, axial heat conduction to the calming section and mixer were limited.

The inlet mixer, calming section, square-edged inlet, test section and exit mixer were adequately insulated to reduce heat losses to the surroundings. The insulating material used was a flexible, closed-cell, elastomeric nitrile rubber material with a low thermal conductivity of 0.037 W/mK. The overall thickness of the insulation used was 144 mm. With this insulation thickness, the heat losses were estimated with one-dimensional conduction resistance calculations to be less than 1% of the power input.

A computerized data acquisition system (14) was used to record all the mass flow rates, temperatures and pressure drop measurements. The data streamed from this acquisition system was then used for the data reduction.

3.3 Instrumentation

The bias of the instruments was obtained from manufacturers' specification sheets. The precision was determined for each of the measuring instruments (Pt100 probes, thermocouples and pressure transducers) using the product of standard deviation of the 400 measuring points logged and corresponding student's t-variable to fall within a confidence level of 95%.

3.3.1 Pt100 probes

Two Pt100 probes with an accuracy of 0.06 °C were used for the measurement of the inlet and exit bulk water temperatures. The Pt100 probes were calibrated in a thermostat-controlled bath over a temperature range 17 – 60 °C at intervals of 2.5 °C, using a DigiCal

DCS2 digital thermometer with an accuracy of 0.03 °C. A calibration curve was obtained as it was possible to generate a linear curve fit between the Pt100 probes and the digital thermometer. The calibration and uncertainty methods described in the work of Everts [231] were used in this study. The uncertainties of the inlet and exit Pt100 probes were determined as 0.0308 °C and 0.0306 °C respectively. The accuracy of the Pt100 probes (0.06 °C) was thereafter used since it was higher than that of the digital thermometer.

3.3.2 Thermocouples

T-type thermocouples with wire diameter of 0.25 mm and accuracy of 0.1 °C were used to measure the surface temperatures of the test section. All the thermocouples used for the temperature measurements were calibrated against the two calibrated Pt100 probes with an accuracy of 0.06 °C in a thermostat-controlled bath over a temperature range of 17 – 60 °C at intervals of 2.5 °C. In general, the same approach used for Pt100 probes was also used for the thermocouples. During the calibration of the thermocouples, one of the Pt100 probes was inserted in the inlet mixer of the calming section, while the other Pt100 probe was inserted in the exit mixer. As a linear relationship existed between the Pt100 probes and each thermocouple, a linear curve fit was generated between the Pt100 probes and each thermocouple to obtain a calibration curve.

However, in the case of the thermocouple the bias of the Pt100 probes was used, while the precision was determined for each of the 84 T-type thermocouples. The bias of the thermocouple was 0.1 °C. The uncertainty of the thermocouples was determined using the method prescribed by Everts [231]. Using the bias of the Pt100 probes (0.06 °C) used to calibrate the thermocouples, the calibration accuracies of the four thermocouples at the $x/D_i = 246$ were determined as 0.0608 °C (top), 0.118 °C (bottom), 0.136 °C (right) and 0.115 °C (left). Then the higher value between the calibration accuracy and the manufacturer accuracy was used. This means that for the top thermocouple accuracy of 0.1 °C was used, while for the other three thermocouples.

3.3.3 Coriolis flow meters

Two Coriolis flow meters with different flow capabilities were used to measure the mass flow rate. The bias of these flow meters was 0.05% of full-scale. The first Coriolis flow meter with a maximum flow capacity of 108 ℓ/h was used for lower mass flow rate measurement. The second flow meter with a maximum capacity of 2 180 ℓ/h was used for higher mass flow rate measurement. The corresponding manufacturer accuracies of the flow meters are 0.054 ℓ/h (1.51×10^{-5} kg/s) and 1.09 ℓ/h (3.03×10^{-5} kg/s) respectively. The precision was determined by multiplying the student's t-values with the standard deviation of the 400 mass flow rate values logged at 95% confidence level.

3.3.4 Pressure transducers

Pressure measurements on the test section were obtained using Validyne differential pressure transducers (DP15) with interchangeable diaphragms. They were installed in the fully developed region over the length of 2.45 m. The diaphragms had a bias of 0.25% of the full-scale. Three diaphragms were used in this study. The three diaphragms used were 0.86 kPa

(for the smooth tube and tube with twisted tape inserts at low mass flow rates), while 1.4 kPa and 3.5 kPa were used for the tube with twisted tape inserts, at higher mass flow rates. The diaphragms 0.86 kPa and 1.4 kPa were calibrated using a Betz manometer with an accuracy of 2.5 kPa, while the 3.5 kPa was calibrated using a water column. When determining the accuracy of the differential pressure transducers, the bias used was 0.25% of full scale, this translated to 2.15 Pa, 3.5 Pa and 8.75 Pa respectively. For the 0.86 kPa diaphragm, the accuracy of the Betz manometer was used as bias because it was higher than that of the diaphragm, while for the 1.4 kPa and 3.5 kPa diaphragms, the 0.25% of the full-scale values were used. The precision was determined using the method prescribed by Everts [231]. When calibrating the pressure transducer, a total of 19 data points, each having a 400 measuring points were logged from 0 kPa to the maximum of the diaphragms. A regression analysis carried out established a linear mathematical relationship between manometer and pressure transducers, this relationship was used to obtain the calibration equation.

3.3.5 Power supply

A power supply with a capacity of 1.5 kW was used to heat the test section. The power supply had a maximum current and voltage drop ratings of 15 A and 360 V respectively. The current and voltage drop accuracies were 0.2% of the nominal value. The maximum current supplied and voltage drop were 4.15 A and 293 V respectively, translating to a maximum heat flux of 4 kW/m^2.

3.3.6 Data acquisition system and control

The frequency drive connected to the electronically-controlled positive displacement pump was used to control the mass flow rate of the pump and the data were streamed through a computerized data acquisition system. The computerized data acquisition system was used to log the mass flow rates data from the flow meters, temperatures data from the Pt100 probes and thermocouples and pressure drops data from the pressure transducers.

The data acquisition was achieved with the use of National Instrument LabVIEW software installed on a personal computer. The data acquired were temperatures, mass flow rates and pressure drops. The data acquisition system consisted of an SCXI 1001 twelve-slot chassis on which SCXI (Signal Conditioning eXtensions for Instrumentation) products were installed; these included terminal blocks and analog-digital converters and multiplexers. The eighty-four thermocouples were connected to three thirty-two channel SCXI 1303 terminal blocks. Additional two thermocouples were connected to measure the ambient temperature and the temperature on the insulating material. Two Pt100 probes were connected to SCXI 1306 terminal block. Since the flow meter, pump and the DP15 were current output, they were all connected to a SCXI 1308 terminal block. The cards on which the terminal blocks for the thermocouples and Pt100 probes were connected are SCXI 1102c and SCXI 1505 respectively. The card for the pump, flow meters and DP15 was a SCXI 1102c. These cards were first installed in the chassis and the respective terminal blocks were then connected to the rear of each card. Microsoft Excel spreadsheet was used for processing the data.

3.4 Data reduction

The method used for the data reduction was in general the same as in previous studies conducted by our research group at the University of Pretoria [22, 24, 26, 29-33, 49, 222, 231-233]. A linear increase in the mean water temperature within the test section was obtained, because a constant heat flux boundary condition was applied to the test section. The mean water temperatures, $T_m(x)$, at each measuring station, x, on the test section were determined using the measured inlet water temperatures, T_i, measured exit water temperatures, T_e, over the measured heated length, L_h, of the test section. Eq. 3.1 therefore allowed for the determination of the water temperature at any position, x, from the inlet where, $x = 0$, to the exit where, $x = L_e$.

$$T_m(x) = T_i + \left[\frac{T_e - T_i}{L_h}\right] x \tag{3.1}$$

The properties of water were determined at the measuring stations on the test section as a function of the mean water temperature using the thermophysical correlations of water developed by Popiel and Wojtkowiak [234]. The properties were densities, $\rho(x)$, dynamic viscosities, $\mu(x)$, specific heat capacities, $Cp(x)$, thermal conductivities, $k(x)$, and Prandtl numbers, $Pr(x)$. The local values were used for heat transfer results, while the bulk values (which would be the average between the two pressure taps) were used for the pressure drop results. The bulk water temperatures, T_b, were not calculated at the centre of the tube, but at $x = 3.77$ m (Fig. 3.3(a)) which is at the centre of the two pressure taps, P_1 and P_2, where the flow was fully developed. Furthermore, the thermophysical properties of all the bulk values were determined at the bulk water temperature.

The mean surface temperatures, $T_s(x)$, were determined as average of the four thermocouples (T_{top}, T_{bottom}, T_{left} and T_{right}) at each measuring station on the test section (Fig. 3.3(b)):

$$T_s(x) = \frac{T_{top} + T_{bottom} + T_{left} + T_{right}}{4} \tag{3.2}$$

The local Reynolds numbers, $Re(x)$, at each measuring station were determined using the measured mass flow rates, $\dot{m}$, of the water that flowed through the test section, the measured inner diameter of the test section, D_i, the local dynamic viscosities, $\mu(x)$, at each measuring station, and the cross-sectional area, $A_c = \pi D_i^2/4$ of the test section:

$$Re(x) = \frac{\dot{m} D_i}{A_c \mu(x)} \tag{3.3}$$

Similarly, the bulk Reynolds numbers, Re_b, between the two pressure taps were determined using the bulk fluid properties.

Everts and Meyer [29] defined the width of the transitional flow regime, ΔRe, as the difference between the Reynolds numbers at which transition ended, Re_{qt} and started, Re_{cr}:

$$\Delta Re = Re_{qt} - Re_{cr} \quad (3.4)$$

The heat transfer rates $\dot{Q}$, to the water were determined using the measured mass flow rates, $\dot{m}$, the differences in measured temperatures between the exit, T_e, and inlet, T_i, of the test section and the bulk specific heat capacities, Cp_b, as:

$$\dot{Q} = \dot{m} Cp_b [T_e - T_i] \quad (3.5)$$

It should be noted that the bulk specific heat capacity in Eq. (3.5) was calculated at the centre of the tube.

The electrical power supplied, $\dot{Q}_e$, to the heating wires was determined using the sum of the product of the currents, I_1 and I_2, through each heating wire and the voltage drops, ΔV_1 and ΔV_2, across each heating wire:

$$\dot{Q}_e = I_1 \Delta V_1 + I_2 \Delta V_2 \quad (3.6)$$

The electrical power supplied, $\dot{Q}_e$, was continuously monitored and compared with the heat transfer rate to the water, $\dot{Q}$, by determining the energy balance error, eb, as:

$$eb = \left| 1 - \frac{\dot{Q}}{\dot{Q}_e} \right| \times 100 \quad (3.7)$$

The heat fluxes, $\dot{q}$, were determined as:

$$\dot{q} = \frac{\dot{Q}}{A_s} \quad (3.8)$$

where the inner surface area, A_s, was determined using the measured inner diameter, D_i, and measured heated length, L_h, of the test section as $A_s = \pi D_i L_h$. The heat fluxes, $\dot{q}$, were determined using the heat transfer rates, $\dot{Q}$, to the water as this was more accurate. The reason is that the electrical power supplied, $\dot{Q}_e$, to the test section was slightly higher than the heat transfer rate to the water, $\dot{Q}$, due to small heat losses that occurred from the heated test section to the surroundings.

The heat transfer coefficients, $h(x)$, at each measuring station were determined using the heat fluxes, $\dot{q}$, the mean surface temperatures, $T_s(x)$, and the mean water temperatures, $T_m(x)$, of the water as:

$$h(x) = \frac{\dot{q}}{[T_s(x) - T_m(x)]} \quad (3.9)$$

The Nusselt numbers, $Nu(x)$, at each measuring station were determined as:

$$Nu(x) = \frac{h(x) D_i}{k(x)} \quad (3.10)$$

while the Colburn *j*-factors, $j(x)$, at each measuring station were determined as:

$$j(x) = \frac{Nu(x)}{[Pr(x)]^{1/3} Re(x)} \tag{3.11}$$

The Grashof numbers, $Gr(x)$, were determined as:

$$Gr(x) = \frac{g\beta(x)[T_s(x) - T_m(x)]D_i^3}{[v(x)]^2} \tag{3.12}$$

while the modified Grashof numbers, $Gr^*(x)$, which is a function of heat flux instead of temperature difference, at each measuring station were determined as:

$$Gr^*(x) = Gr(x)Nu(x) = \frac{g\dot{q}\beta(x)D_i^4}{k(x)[v(x)]^2} \tag{3.13}$$

where, the gravitational acceleration, g, was 9.81 m/s^2, and the kinematic viscosities, $v(x)$, were determined as the ratio of densities, $\rho(x)$, to dynamic viscosities, $\mu(x)$.

The friction factors, f, across the measured pressure drop length, $L_{\Delta P,}$ between the two pressure taps, were determined as:

$$f = \frac{\Delta P \rho_b D_i^5 \pi^2}{8\dot{m}^2 L_{\Delta p}} \tag{3.14}$$

Similar to the local parameters, the bulk modified Grashof numbers between the two pressure taps, were calculated using the bulk fluid properties in Eq. (3.13).

3.5 Experimental procedure and test matrix

In general, most experiments commenced at the maximum mass flow rate of 0.15 kg/s. The electrical power supply was switched on and the required currents and voltages were adjusted to obtain one of the required heat fluxes.

The experimental matrix of the experiments conducted for both the smooth tube and the tube with CTT inserts is summarized in Table 3.5. The smooth tube was tested at heat fluxes of 2, 3 and 4 kW/m^2. Three different CTT inserts with twist ratios of 3, 4 and 5 were then tested at heat fluxes of 2, 3 and 4 kW/m^2. The matrix shows that, for the smooth tube experiments, measurements were taken at 219 different mass flow rates, while experiments were conducted at 646 different mass flow rates for the twisted tape inserts. The total number of experimental conditions investigated (different mass flow rates) on was 865.

The CCCTT inserts experiments were conducted at 60 different mass flow rates to cover the transitional flow regime as well as sufficient parts of the laminar and turbulent flow regimes. CCCTT insert with three different connection angles (θ = 0°, 30° and 60°) were tested at four different heat fluxes of 1.35, 2, 3 and 4 kW/m^2. This resulted in a total of 720 mass flow rates for the different combinations of connection angles and heat fluxes.

Table 3.5. Experimental matrix of the smooth tube and the tube with CTT inserts

Tube condition	Heat flux, $\dot{q}$ [kW/m^2]	Twist ratio, y	Number of different mass flow rates, Re
Smooth	2	--	75
	3	--	76
	4	--	68
Subtotal		--	**219**
CTT inserts	2	3	79
		4	71
		5	71
	3	3	78
		4	69
		5	70
	4	3	76
		4	64
		5	68
Subtotal			**646**
Total			**865**

The PUCTT and PUCTTR inserts were each tested at two different depth ratios of 0.105 and 0.216 and at heat fluxes of 1.35 kW/m^2 (for all the cases of the PUCTT and PUCTTR inserts) and 2 kW/m^2 (only one case of PUCTT22 insert to compare with a CTT insert). A total of 540 experiments were conducted at 60 different mass flow rates for nine different combinations of depth ratios, ring space ratios and heat fluxes.

Each time the experimental set-up was started, an approximate period of three hours was allowed for the system to reach the initial steady-state condition. This condition was assumed to have been met when the standard deviation of the mass flow rates, temperatures and pressure drops remained constant for a period of 10 – 15 min. Once this condition was satisfied, a total of 400 data points of mass flow rates, temperatures (inlet and exit water temperatures and surface temperatures on the test section), and pressure drops were logged at a frequency of 20 Hz using a data acquisition system connected to a personal computer. The currents and voltage drops were also recorded from the power supply. The average of the 400 data points was then regarded as one measurement.

The mass flow rate was changed by approximately 1.7% to the next Reynolds number increment. As the changes in the mass flow rates were small, reaching steady-state conditions were faster for the subsequent changes in the mass flow rates. In the turbulent flow regime, steady-state was reached within 10 – 15 min, while 20 – 30 min were required in the transitional flow regime and 10 – 20 min in the laminar flow regime. The energy balance errors (Eq. 3.7) were continuously monitored and varied from one flow regime to another. The energy balance error ranges were 3 – 5%, 2 – 3% and 2 – 4% in the laminar, transitional and turbulent flow regimes respectively. The maximum error balance errors were found in the laminar flow regime where maximum surface temperatures were obtained due to the small mass flow rates.

3.6 Uncertainties

The uncertainties were determined as suggested by Dunn [235] using a 95% confidence level. The manufacturer specified accuracies (Table 3.6) were used to determine the bias errors, while the precision errors were calculated from standard deviation of 400 data points taken at each mass flow rate. The equations and the method described in the work of Everts [231] were followed when determining the uncertainties.

Table 3.6. Ranges and accuracies of the experimental instrumentation.

Instrument		Range	Accuracy
Flow meters	CMF 010	0 – 108 ℓ/h	0.054 ℓ/h (0.05% of full scale)
	CMF 025	0 – 2 180 ℓ/h	1.09 ℓ/h (0.05% of full scale)
Thermocouples		<150 °C	0.1 °C
Pt100 probes		0 – 250 °C	0.06 °C
Power supplies	Current	0 – 15 A	0.2% of maximum value
	Voltage	0 – 360 V	0.2% of maximum value
Pressure transducers	0.86 kPa diaphragm	0 – 0.86 kPa	2.15 Pa (0.25% of full scale)
	1.4 kPa diaphragm	0 – 1.4 kPa	3.5 Pa (0.25% of full scale)
	3.5 kPa diaphragm	0 – 3.5 kPa	8.75 Pa (0.25% of full scale)

To investigate the effect of different twisted tape inserts on the uncertainties, Fig. 3.9 compares the local Reynolds number uncertainties (Fig. 3.9(a)), local Colburn *j*-factor uncertainties (Fig. 3.9(b)) and friction factor uncertainties (Fig. 3.9(c)) of a PUCTT insert, CCCTT insert, CTT insert at a twist ratio of 5, as well as a smooth tube without any inserts, at a heat flux of 2 kW/m^2. The comparison of the PUCTT, CCCTT as well as the CTT inserts and a smooth tube is done to explain the differences in the uncertainties and transition. The uncertainties were plotted as a function of local Reynolds number, $Re(x)$, in Fig. 3.9(a) and Fig. 3.9(b), but as a function of bulk Reynolds number in Fig. 3.9(c). The reason being that the heat transfer values were local values, while the friction factor values were the averages between the two pressure taps in Fig. 3.3(a). Fig. 3.9 also identifies the laminar flow data (using the nomenclature of "*L*") which was distinguishable from the transition and turbulent data as described in Meyer and Abolarin [49]; as well as the width of the transitional flow regime, ΔRe.

Fig. 3.9(a) shows that the Reynolds number uncertainties decreased as the mass flow rates (which are directly proportional to the Reynolds number) increased. The discontinuity between points "*A*" and "*B*" occurred when the Coriolis mass flow meters had to be swapped, because the meter measuring the smallest mass flow rates was running out of its specified maximum range. For Reynolds numbers greater than point "*B*", the flow meter with a larger full scale was used. However, all the uncertainties were less than 1.7%. Because the mass flow rate meter was located upstream of the test section, the increased Reynolds number uncertainties in the transitional flow regime, due to the mass flow rate fluctuations in the smooth tube, were not visible. However, these fluctuations have been confirmed by Everts and Meyer [29] who had a mass flow rate meter downstream of the test section.

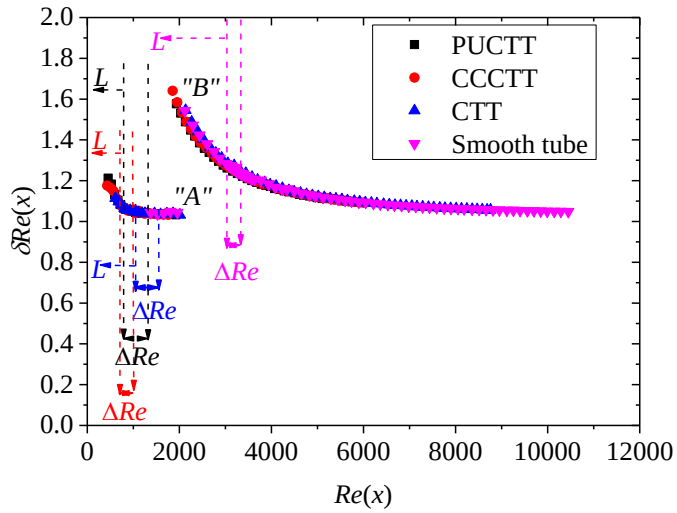

(a)

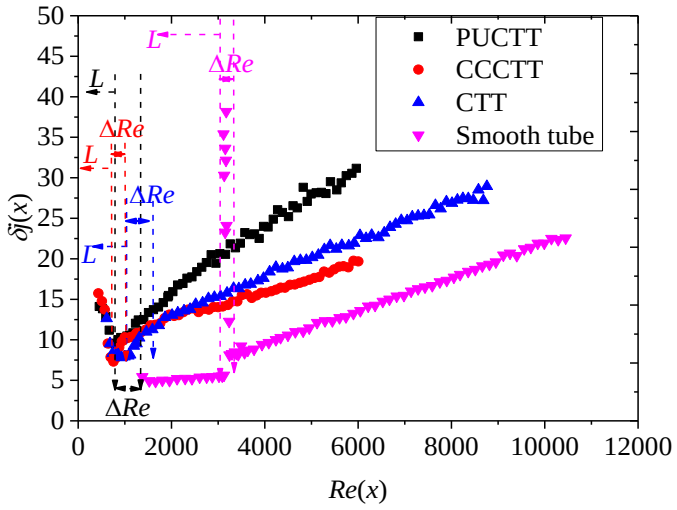

(b)

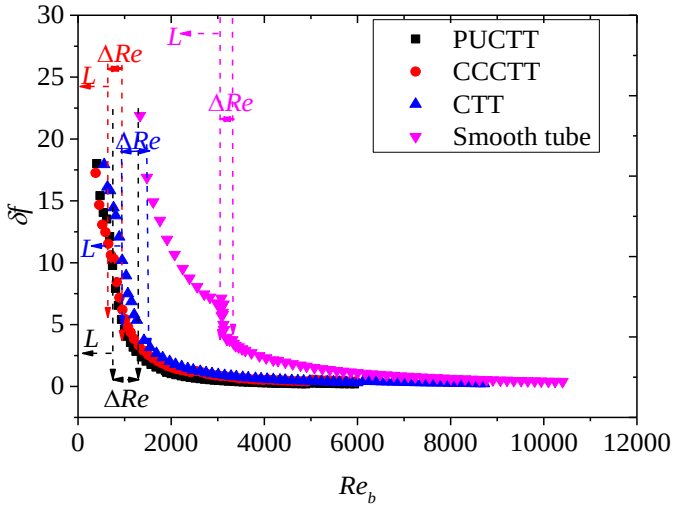

(c)

Fig. 3.9. Comparison of (a) Reynolds number uncertainties, (b) Colburn *j*-factor uncertainties as a function of Reynolds number at the measuring station of x/D_i = 246, and (c) friction factor uncertainties as a function of bulk Reynolds number (at x/D_i = 198) at the heat flux of 2 kW/m^2, for the PUCTT insert, CCCTT insert, CTT insert at the twist ratio of 5 and smooth tube. "*L*" identifies the laminar flow regime and Δ*Re*, the width of the transitional flow regime.

In the laminar flow regime, the Colburn *j*-factor uncertainties (Fig. 3.9(b)) of the smooth tube were less than 6%; however, it increased to 38% in the transitional flow regime. The significant increase was due to the temperature fluctuations [29] that increased the standard deviation of the 400 temperature measuring points, in comparison with the laminar and turbulent flow regimes. For the PUCTT, CCCTT and CTT inserts the uncertainties in the laminar and transitional flow regimes varied between 16% and 8%. The uncertainties of the three tape inserts in the transitional flow regimes were much lower than those of a smooth tube, because the inserts suppressed the transitional flow fluctuations that occurred in the smooth tube without any inserts. In the turbulent flow regime, the general trend of all four tubes was that the uncertainties increased with Reynolds number. This is anticipated as the temperature differences between the wall and fluid decreased as the mass flow rates (Reynolds numbers) increased. However, all the uncertainties were less than 30% for the PUCTT inserts, and specifically in the transitional flow regime, which was the focus of this study, it was less than 12%.

Fig. 3.9(c) indicates that in all the flow regimes, the friction factor uncertainties decreased with increasing Reynolds number. At any Reynolds number, the smooth tube had the highest uncertainty because its pressure drops were much lower than for the tubes with twisted tape inserts. In the laminar flow regime, the maximum friction factor uncertainty was 22% in the smooth tube, while it was approximately 18% for the PUCTT, CCCTT and CTT inserts. In the transitional flow regime, the maximum uncertainties varied between 12% and 3% for all four tubes. Similar to the Colburn *j*-factor uncertainties in Fig. 3.9(b). Fig. 3.9(c) indicates that the twisted tape inserts suppressed the pressure drop fluctuations in the transitional flow regime, because there was no significant increase in the friction factor uncertainties. In the turbulent flow regime, the uncertainties of all four tubes were less than 5%.

3.7 Summary and conclusions

The experimental set-up describing the components of the experimental loop, calming section and test section, instrumentation, data reduction method, experimental procedure, and uncertainty analysis have been presented in this chapter. The test section used consisted of a smooth circular copper tube with an inner diameter, an outer diameter and a length of 19 mm, 22 mm and 5.27 m, respectively. Water was used as test fluid within the range of Reynolds number of 300 to 11 404, covering a wide range of data in the laminar, transition and turbulent flow regimes.

The instrumentation consisted of Pt100 probes, thermocouples, pressure transducers, flow meters, power supply and data acquisition system and control. The Pt100 probes, thermocouples and pressure transducers were calibrated to ensure accurate measurements. The Pt100 probes were installed in the inlet and exit mixers to measure the bulk inlet and exit water temperatures respectively. The thermocouples were used to measure temperatures on the surface of the test section. The pressure transducers were used to measure pressure drop of the test section over the length of 2.45 m.

The test section used was electronically heated using two constantan wires with a diameter of 0.81 mm each that were tightly coiled around the test section to obtain constant heat flux boundary condition. The test section was insulated with armaflex insulating material and the maximum heat loss from the test section to the surrounding less than 1% of power input.

In the test section experiments were conducted for both smooth circular tube and tube with CTT, CCCTT, PUCTT and PUCTTR inserts. The twist ratios of the CTT inserts considered were 3, 4, and 5. Each tape insert was tested at the heat flux of 2, 3 and 4 kWm^2. The CCCTT inserts were of the connection angles of $\theta = 0°$, 30° and 60°, at the twist ratio of 5. Each connection angle was tested at the heat of 1.35, 2, 3 and 4 kWm^2. The PUCTT inserts were of the depth ratio of 0.105 and 0.216, each tested with ring space ratios of 1.25, 2.5 and 5 at the heat flux of 1.35 kW/m^2. All of the above conditions were investigated using the square-edged inlet section.

When the experiments started, sufficient time was allowed for the system to reach a steady-state condition. This condition was assumed to have been met when the standard deviation of the mass flow rates, temperatures and pressure drops remained the same for a period of 10 – 15 min. Once the steady state conditions were satisfied, a set of 400 data points of the temperatures (inlet water temperatures, surface temperatures on the test section and exit water temperatures), mass flow rates and pressure drops were logged.

After a set of data had been logged, data reduction was done and uncertainty analysis was conducted to determine the uncertainties of the Reynolds numbers, Colburn *j*-factors and friction factors. The maximum and minimum Reynolds number uncertainties were 1.7% and 1% respectively in the laminar and turbulent flow regimes. The Colburn *j*-factor uncertainties in the laminar and transitional flow regimes in the smooth tube were about 6% and 38% respectively. The PUCTT, CCCTT and CTT uncertainties in the laminar flow regime varied from 16% to 7.8%. In the transitional flow regime, the Colburn *j*-factor uncertainties were less than 12%, while in the turbulent the maximum was 30%. The maximum friction factor uncertainty of about 22% was determined in the smooth tube while, the uncertainties of the tape inserts were in the order of 18% in the laminar flow regime. In the transitional flow regime, the maximum uncertainties varied between 12% and 3% for all four tubes. In the turbulent flow regime, the uncertainties for all four tubes were less than 5%.

4. Validation

4.1 Introduction

This chapter focuses on validation of the heat transfer and pressure drop data obtained from the experimental set-up and data reduction method with literature. Prior to the comparison, the results were first analyzed in order to determine whether the flow was thermally fully developed or not. Thereafter, heat transfer and pressure drop results obtained from the experiments were compared with well-known and relevant correlations in literature. The local heat transfer coefficients in the smooth tube and tube with CTT inserts were validated in Section 4.2. The Colburn *j*-factors were validated in Section 4.3, while the friction factors were validated in Section 4.4.

4.2 Local heat transfer coefficients

Prior to commencement of the experiments with the twisted tape inserts, validation experiments were conducted on a smooth tube without any twisted tape inserts so that the experimental methodology, accuracy of measurements, repeatability, and data reduction method could be verified. As this study concentrated on the transitional flow regime, the experiments were conducted in the upper laminar flow regime, through the transitional flow regime, and into the turbulent flow regime. Before the results could be compared to literature studies, it was also important to determine if the flow was fully developed; not only for the smooth tube experiments, but also for the experiments with the tubes with twisted tape inserts. For the smooth tube, the flow should theoretically be thermally fully developed in the laminar flow regime (at a Reynolds number of 1 000 and Prandtl number of 7) at a distance of $x = 0.12RePrD_i = 16$ m, for forced convection [31] and for turbulent flow regime at $x = 10D_i = 0.19$ m. Thus, theoretically if only forced convection existed, thermally fully developed flow should not occur as the test section is 5.27 m in length.

In Fig. 4.1 the local heat transfer coefficient results are given for the smooth tube (Fig. 4.1(a)) and for a tube with a CTT insert (Fig. 4.1(b)) as a function of a dimensionless tube length-to-diameter ratio (x/D_i) at a heat flux of 2 kW/m^2. In Fig. 4.1(a) results are given for the smooth tube at two laminar bulk Reynolds numbers of 1 331 and 2 558 (close to the start of transition as indirectly indicated later in Fig. 4.3) and at a turbulent bulk Reynolds number of 6 170.

Several observations were made when the results were compared to literature. At a bulk Reynolds number of 1 331 in the laminar flow regime, the local heat transfer coefficients of this study compared well with the correlation of Everts [219]. The average deviation was 17%. It was also compared with the correlation of Morcos and Bergles [236], with an average deviation 6%. The results also showed that the heat transfer coefficients remained constant in an axial direction, except at the first measuring station. It can therefore be assumed that the flow was thermally fully developed, except for the first measuring station.

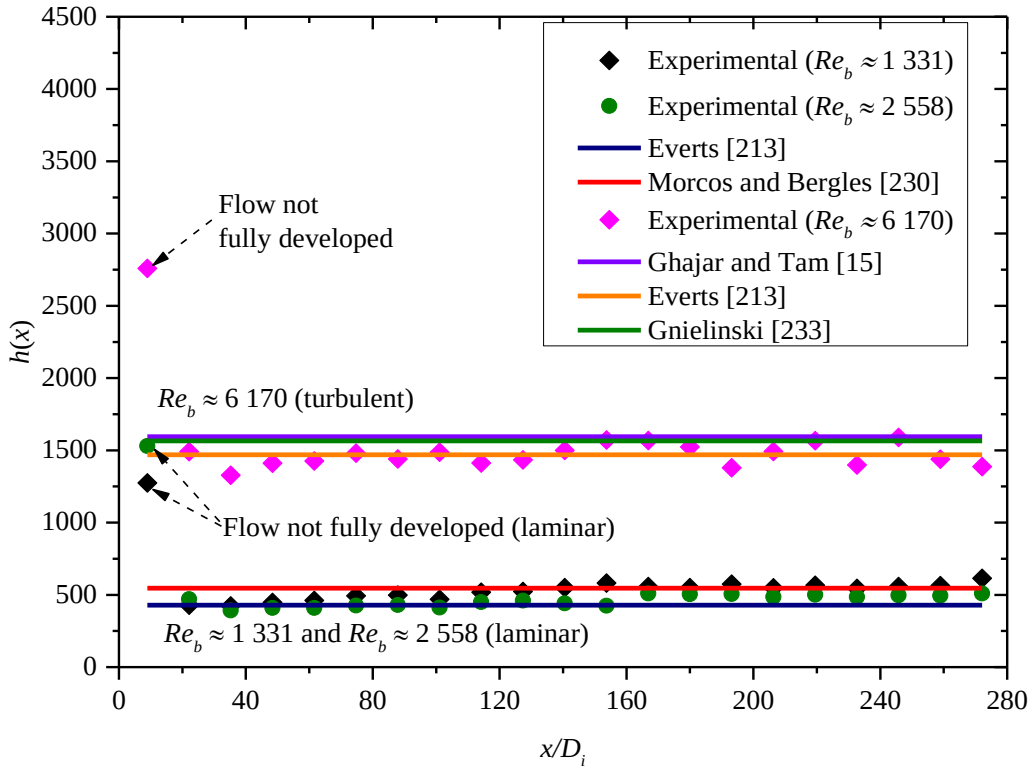

(a)

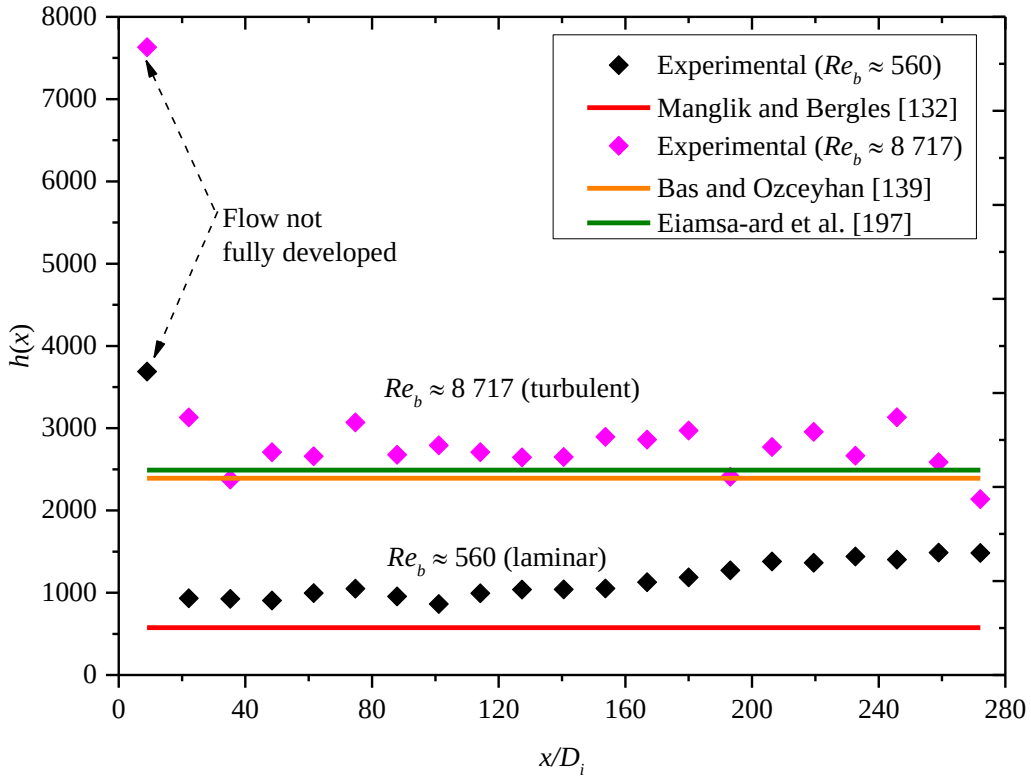

(b)

Fig. 4.1. Comparison of local heat transfer coefficients with literature for the (a) smooth tube at three bulk Reynolds numbers of 1 331, 2 558 (laminar) and 6 170 (turbulent), and the (b) the tube with CTT inserts at two bulk Reynolds numbers of 560 (laminar) and 8 717 (turbulent). The twist ratio, y = 5, and the heat flux was 2 kW/m^2.

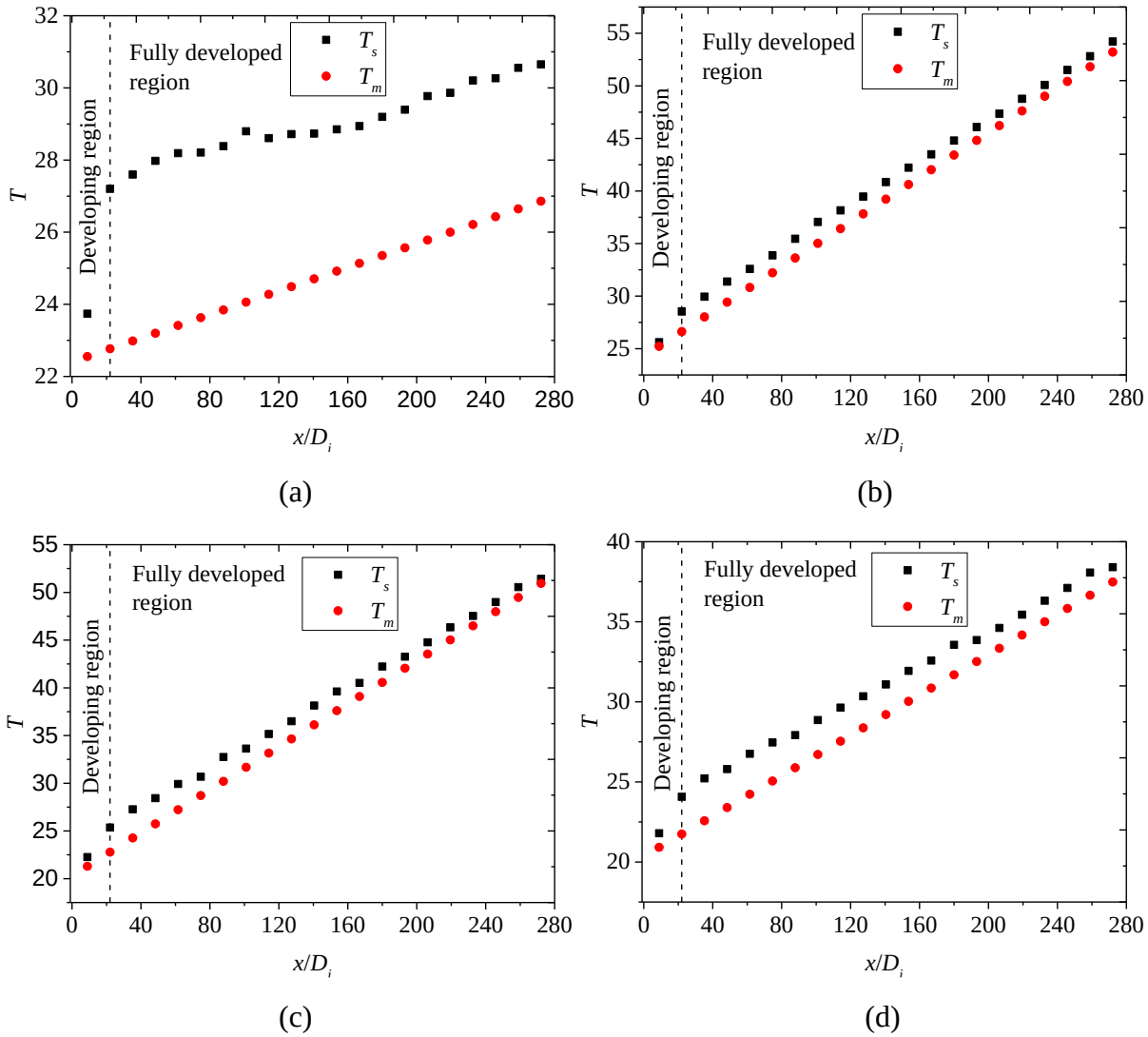

Fig. 4.2. Variation of tube surface and fluid mean temperatures as a function of x/D_i for the (a) smooth tube (Re_b = 2 558, heat flux of 2 kW/m^2), (b) CTT insert (Re_b = 560, heat flux of kW/m^2, y = 5), (c) CCCTT insert (Re_b = 520, heat flux of 2 kW/m^2, y = 5) and (d) PUCTT insert (Re_b = 525, heat flux of 1.35 kW/m^2, y = 5).

The additional laminar experiments at a bulk Reynolds number of 2 558 were included to show that all the local heat transfer coefficients in the laminar flow regime indicated that the flow was fully developed, except at the first measuring station. The reason why the flow was so quickly fully developed was because the flow with heating was not in the forced convection flow regime, but in the mixed laminar flow regime [15]. In this regime, free convection effects occur, which ensured that fully developed flow develops sooner. This was confirmed with surface temperature (T_s) and fluid mean temperature (T_m) measurements as illustrated in Fig. 4.2 as a function of x/D_i for (a) smooth tube, (b) CTT insert, (c) CCCTT insert and (d) PUCTT insert. Fig. 4.2 illustrates that the surface temperature measurements in the fully developed flow region increased linearly from the second measuring station in the direction of flow (as x/D_i increased). It also followed that the temperatures at the top of the tube were not equal to the temperatures at the bottom of the tube. The average ratio of these temperatures for a Reynolds number of 2 558 was 0.9. The observations that the flow was fully developed along the test section length was observed for all the experimental conditions.

In turbulent flow regime, at a Reynolds number of 6 170, again except for the first measuring station, $x/D_i = 9$, all the other local heat transfer coefficients were independent of axial tube location. This was to be expected as the general guideline is that fully developed turbulent flow occurs after 10 diameters from the tube inlet [237, 238]. All the local heat transfer coefficients were within 6% of the average heat transfer coefficient. Furthermore, the results compared well with the correlations of Ghajar and Tam [15], Everts [219] and Gnielinski [239]. The average deviations with these studies were 9%, 1% and 7% respectively.

Similar trends were found in experiments with twisted tape inserts, as shown in Fig. 4.1(b). The results illustrated are for a tube with a CTT insert, with a twist ratio of 5. In the laminar flow regime at the bulk Reynolds number of 560, except at the first measuring station, the values of the heat transfer coefficients were constant and not a function of the axial length. Towards the end of the test section, the local heat transfer coefficients increased gradually. This increase is associated with the loss effect at the exit of the test section. A similar trend of exit losses when using a tube with a twisted tape insert was also reported in the work carried out by Chang et al. [35, 208] and Chang and Zhen [240]. The average value of the heat transfer coefficient was 1 145 W/m^{2}K, and the heat transfer coefficients of all the measuring stations, excluding the first one, were within an absolute deviation of 14% of this value. Furthermore, the results of this study were higher than the correlation of Manglik and Bergles [135]. It was therefore assumed from the results in the laminar flow regime that the heat transfer coefficients at all the measuring stations were fully developed, except at the first measuring station.

In the turbulent flow regime, at a bulk Reynolds number of 8 717 (Fig. 4.1(b)), the heat transfer coefficients were also generally constant and independent on the axial tube length. The only exception, again, was the first measuring station. The average heat transfer coefficient was 2 741 W/m^{2}K, and the heat transfer coefficients of all stations were within 10% of this value. Therefore, it was assumed that the heat transfer coefficients of all the stations, except the first one, were fully developed. Furthermore, the results were within 10% of the equation of Eiamsa-ard et al. [203] and within 13% of the equation of Bas and Ozceyhan [145].

In general, the local heat transfer coefficients in Fig. 4.1 (as well as at the other experimental conditions listed in Section 3.2.3) showed that the flow was thermally fully developed. The exceptions, for both laminar and turbulent flow, were at the first measuring station where the flow was developing.

4.3 Colburn *j*-factors

In Fig. 4.3 the Colburn *j*-factors as a function of Reynolds numbers at $x/D_i = 246$ and a heat flux of 2 kW/m^2 are presented over the Reynolds number range of 1 377 - 10 449. In general, the results compared well with literature. The results of the Colburn *j*-factors in the laminar flow regime were compared to the correlation of Morcos and Bergles [236] with maximum deviation of 7%. The transition occurred at Reynolds numbers between 3 053 - 3 331. In the turbulent flow regime, the Colburn *j*-factor results were compared to the correlation of

Gnielinski [239], with minimum and maximum deviations of 6% and 12% respectively. A maximum deviation of 5% was obtained with the correlation of Ghajar and Tam [15].

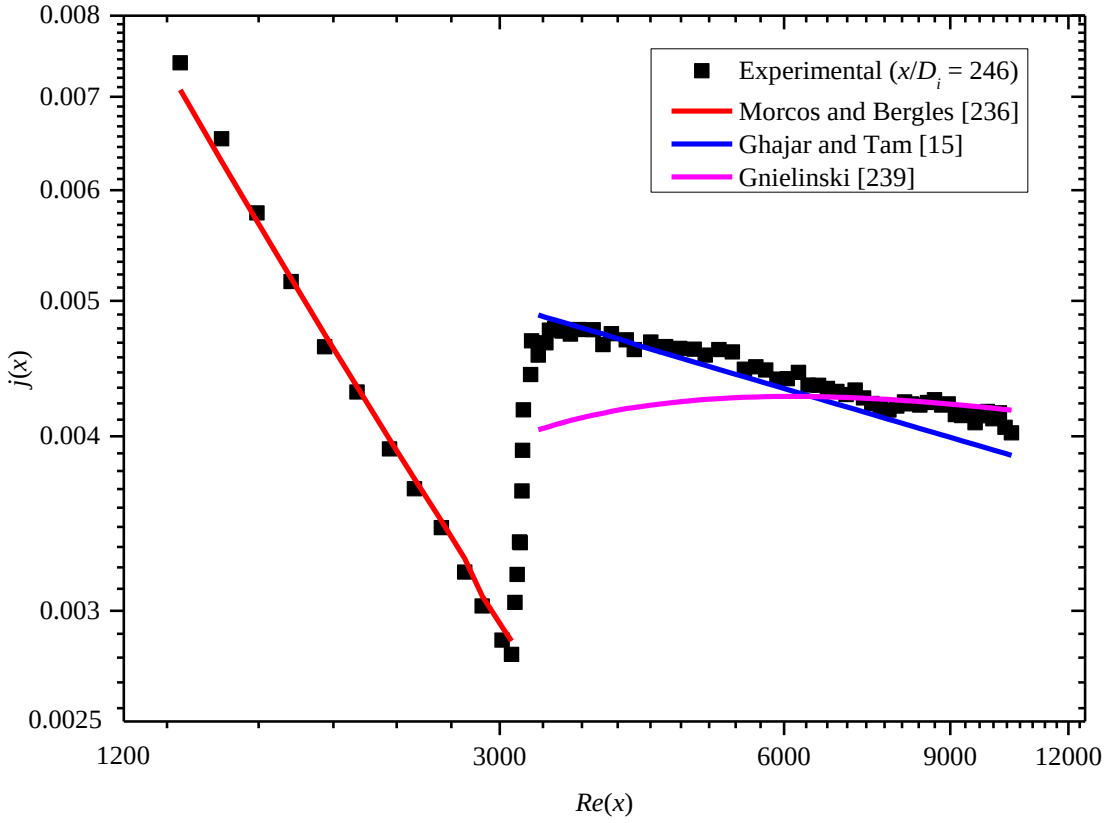

Fig. 4.3. Comparison of the Colburn *j*-factors as a function of Reynolds numbers at x/D_i =246 and a heat flux of 2 kW/m^2, with literature.

4.4 Friction factors

In Fig. 4.4 the diabatic friction factors against the bulk Reynolds numbers of the smooth tube at a heat flux of 2 kW/m^2 are shown over the fully developed pressure drop length of 2.45 m. The friction factor results in the laminar flow regime were compared to Tam and Ghajar [20] and Test [241] with a maximum deviation of 5%. The diabatic friction factors in the turbulent flow regime were compared to those of Blasius [242] and Allen and Eckert [243], and most of the data were predicted with a deviation of 5%.

Although only results of 2 kW/m^2 were shown in this section, similar results were found for heat fluxes of 1.35, 3 and 4 kW/m^2. It has been found that when the smooth tube and twisted tape measurements of this section were repeated 14 months later, after the completion of the twisted tape inserts in chapters 5-7, the results in Fig. 4.3 and Fig. 4.4 compared with errors of less than 1%. It was therefore concluded that the results were repeatable and that negligible drift occurred in all instrumentation and/or measurements that were conducted in this study over the period of experimentation.

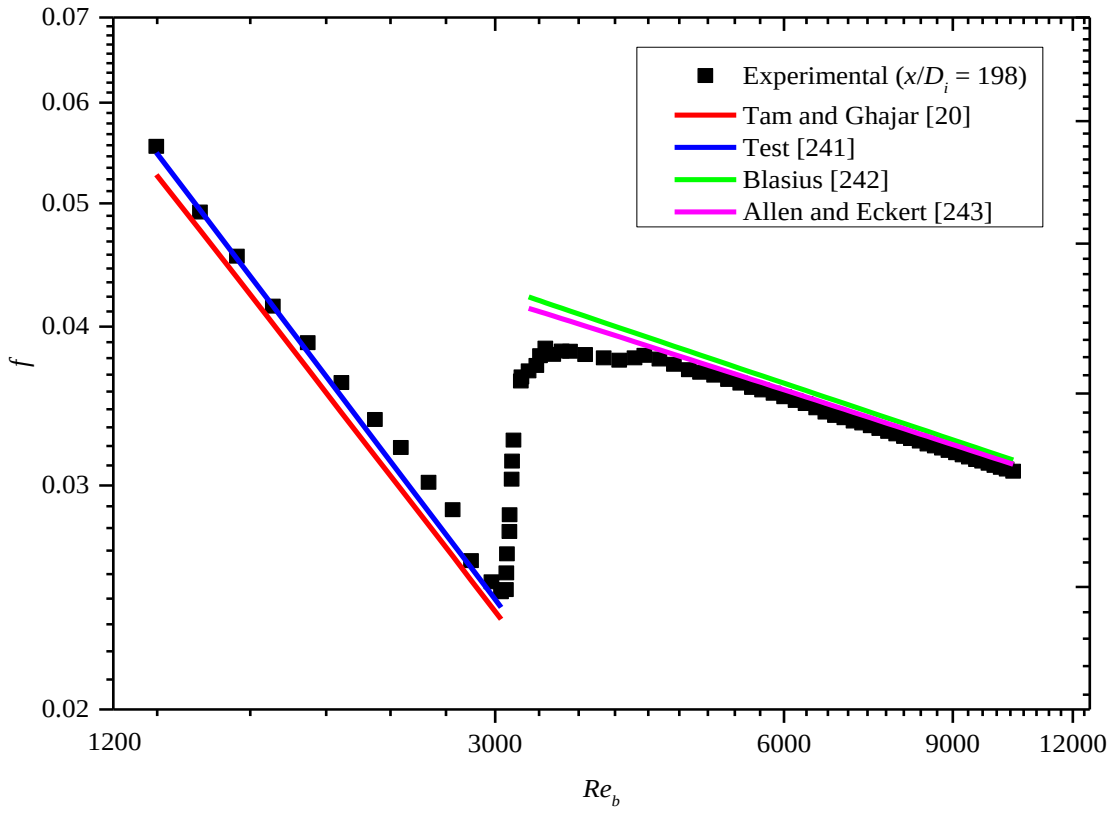

Fig. 4.4. Comparison of the smooth tube diabatic friction factors against bulk Reynolds numbers at a heat flux of 2 kW/m^2, with literature.

4.5 Summary and conclusions

The validation of the heat transfer and pressure drop experiments with literature was presented in this chapter. The validation was done for the smooth tube and the tube with CTT inserts. This was to ensure that experimental set-up and data collected correlated with literature and of high accuracy. Furthermore, the validation ensured that the results presented in subsequent chapters can be relied on with very high level of confidence.

Thermally fully developed flow was first investigated using local heat transfer coefficients of smooth tube and tube with CTT inserts. The local heat transfer coefficients were plotted as a function of the measuring stations. The results revealed that except for the first measuring station, the heat transfer coefficients were in general independent of the measuring stations. This then showed that the heat transfer results were thermally fully developed from the second measuring station to the end of the test section. The results were compared with literature in the laminar and turbulent flow regimes.

After establishing that the heat transfer results were thermally fully developed, the Colburn *j*-factors in smooth tube were plotted as a function of Reynolds number at the measuring station with $x/D_i = 246$. The results were compared with literature with maximum deviations of 7% (in the laminar) and 12% (in the turbulent flow regime).

The friction factors in smooth tube were plotted as a function of bulk Reynolds number at the measuring station with x/D_i = 198, which is the centre of the two pressure taps. The friction factors were compared with literature with a maximum deviation of 5% in the laminar and turbulent flow regimes.

In general, the excellent agreement of the heat transfer coefficients, Colburn *j*-factors and the friction factors results with literature demonstrates that the experimental set-up, procedures and data reduction method used in chapters 3 and 5-7 can be relied on with a high level of confidence.

5. Heat transfer and pressure drop in the transitional flow regime with conventional twisted tape inserts

5.1 Introduction

This chapter contains experimental results of the heat transfer and pressure drop characteristics in a smooth tube heat exchanger with conventional twisted tape (CTT) inserts of three twist ratios of 3, 4 and 5. Each twist ratio was tested at three heat fluxes of 2, 3 and 4 kW/m^2. The heat transfer results were presented in terms of Colburn *j*-factors, while the pressure drop results in terms of friction factors. The techniques used to determine the transitional flow regime, the influence of twist ratios and heat flux on the start and end of the transitional flow regime were discussed as well as the correlations developed. The results contained in this chapter were published in Meyer and Abolarin [49].

The general conclusion that was reached in Chapter 4 was that the results for both the smooth tube and the tube with the CTT inserts represented thermally fully developed flow. The exceptions were the results for the first measuring station, which were in the developing flow regime. Therefore, the results can be presented as the average of measuring stations 2 to 21, or alternatively at one specific station. The latter was used, and therefore all the results related to temperature measurements, Colburn *j*-factors and Reynolds number calculations in this chapter were specifically the local values from the measurements at station 19, where, $x/D_i = 246$. It has also been found that, if the bulk temperature calculation, as shown in Eq. (3.1), is adjusted to exclude/include the distance from the first measuring station, the difference between the fully developed local and bulk Reynolds numbers were negligible.

The average or bulk results (Colburn *j*-factors, Nusselt numbers, Reynolds numbers) were also compared to the local values at measuring station, $x/D_i = 246$, and it was found that the results deviated by less than 3%. The friction factors were, of course, not a local value, as it was the pressure drop over the last part of the test section (Fig. 3.3), at $x/D_i = 198$. These results were presented as a function of bulk Reynolds number. There was a negligible difference between the bulk Reynolds number based on the temperature at the centre of the two pressure taps at $x = 3.77$ m and the bulk Reynolds number based on the mean temperature at the centre of the tube at $x = 2.64$ m.

5.2 Transition

The boundaries of the start and end of transition were identified using two methods: a standard deviation method and a linear line method.

5.2.1 Standard deviation method

With the standard deviation method, the standard deviation, σ, of the 400 surface temperature measurements as a function of time were evaluated and compared as illustrated in Fig. 5.1.

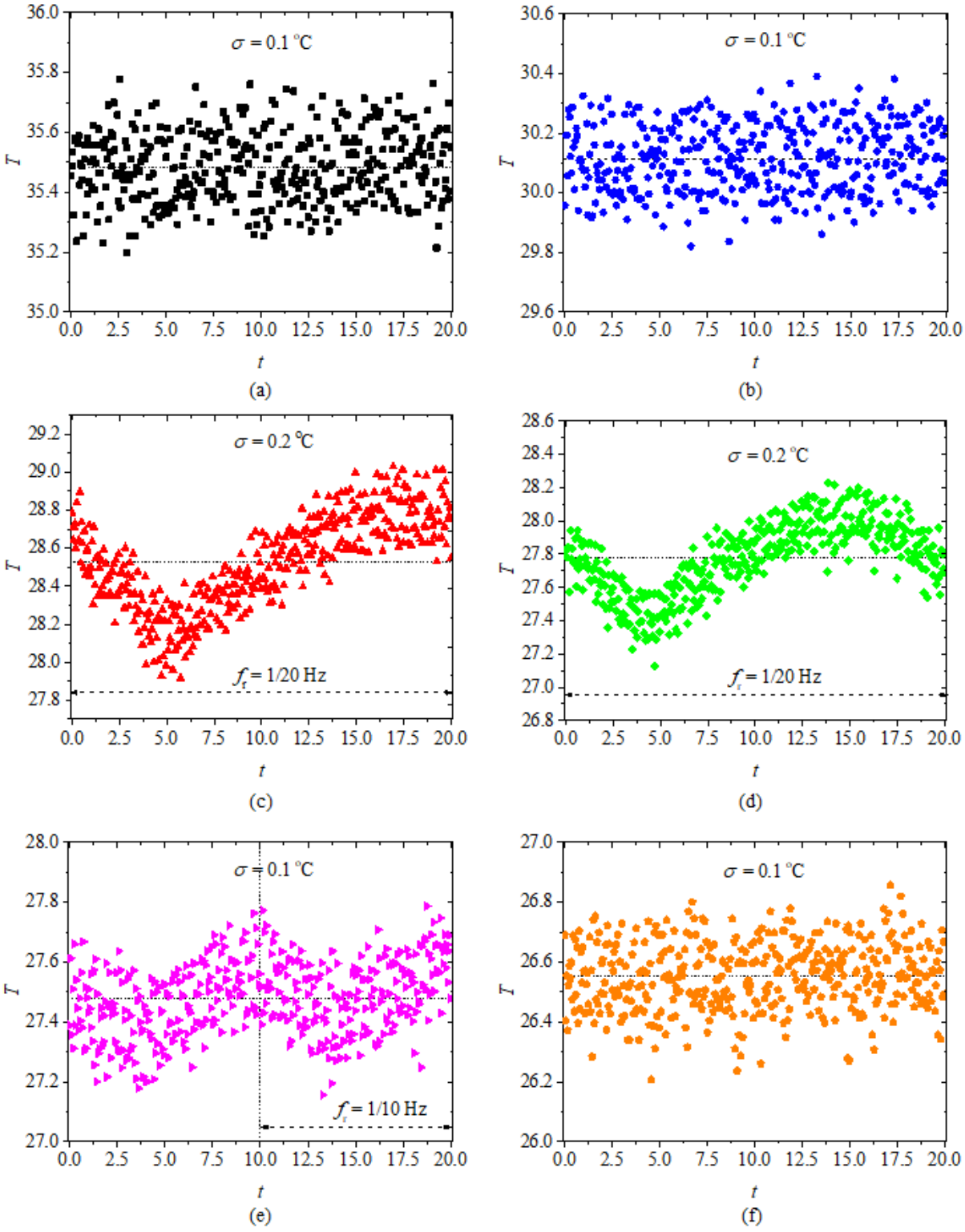

Fig. 5.1. Deviation of the local surface temperatures in the smooth tube against time at x/D_i = 246, a heat flux of 2 kWm^2 and Reynolds numbers of: (a) 1 377; (b) 2 755; (c) 3 173; (d) 3 179; (e) 3 297 and (f) 4 497. The labels (a) to (f) correspond to the labels in Fig. 5.2.

These evaluations were conducted for 20 of the 21 measuring stations (the first measuring station was excluded). As the Reynolds number during experiments was decreased from the maximum to the minimum Reynolds number, it was found that three flow regimes could be identified. In the turbulent flow regime, the standard deviations of the measurements were all 0.1 °C (which corresponds to the uncertainty of temperature measurements of this study). It then increased to 0.2 °C or higher in the transitional flow regime, and reduced to 0.1 °C in the laminar flow regime. In Fig. 5.1 the results are presented for the smooth tube with Reynolds numbers 1 377 (Fig. 5.1(a) laminar flow), 2 755 (Fig. 5.1(b) close to the end of the laminar flow regime), 3 173 (Fig. 5.1(c) beginning of the transitional flow regime), 3 179 (Fig. 5.1(d) close to the end of the transitional flow regime), 3 279 (Fig. 5.1(e) in probably the low-Reynolds-number end of the transition) and 4 497 (Fig. 5.1(f) turbulent flow). The low-Reynolds-number end results could be distinguished from the transitional and turbulent results by the change in frequency. In the transitional flow regime, the average frequency, f_r, of the fluctuations was approximately 1/20 Hz (Fig. 5.1(c) and (d)) with a standard deviation temperature of 0.2 °C, while in the low-Reynolds-number end the frequency, this changed to 1/10 Hz (Fig. 5.1(e)) with a standard deviation temperature of 0.1 °C.

5.2.2 Linear line method

From the smooth tube results, it was found that the transitional flow regime can be well described with three linear curve fits on a log-log scale, as illustrated in Fig. 5.2.

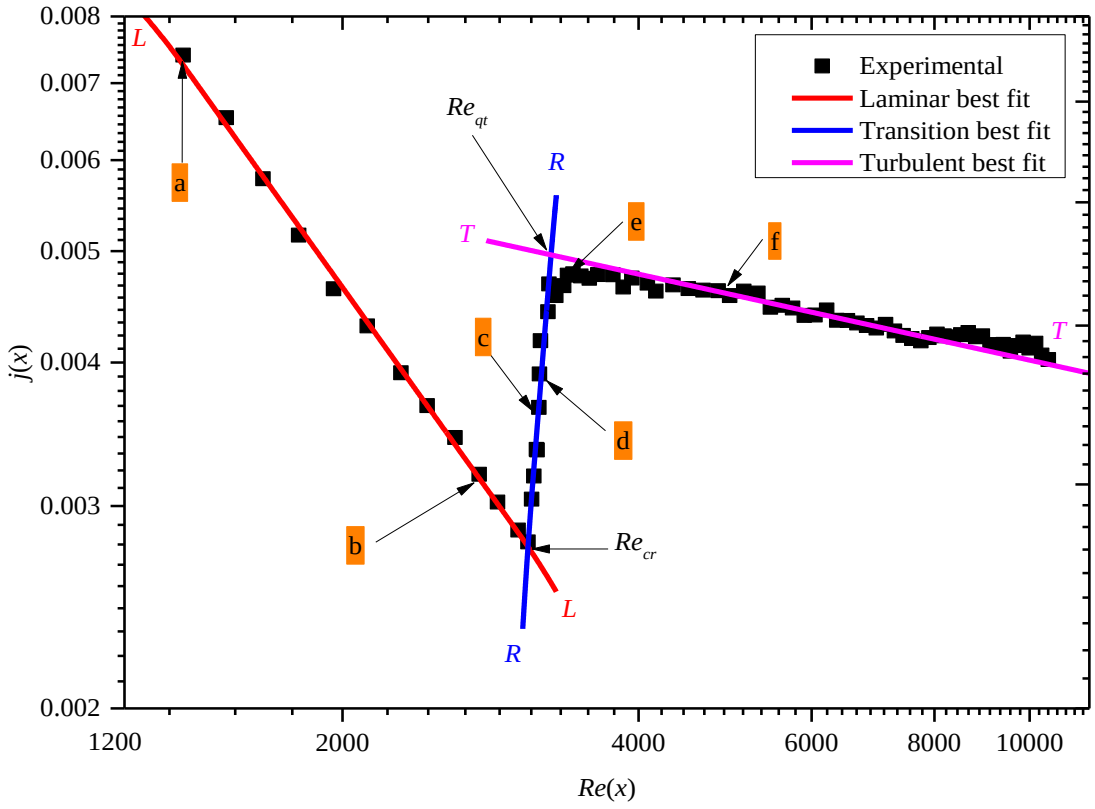

Fig. 5.2. Colburn *j*-factors as a function of Reynolds number in the smooth tube at x/D_i = 246 and a heat flux of 2 kWm^2.

The results that could be confidently identified as turbulent are shown with the lines connecting the "*T-T*" markers in Fig. 5.2. These results were for Reynolds numbers larger than 4 000. The results close to the transitional flow regime were not taken into consideration. A linear-line curve fit was then constructed through the laminar points, indicated by the "*L-L*" markers. These values were identified as all the laminar results with Reynolds numbers smaller than 3 000. The remaining line was constructed with a curve fit from Reynolds numbers 3 114 to 3 250, that connected the two "*R-R*" markers. Care was taken not to select data close to the points where transition started and ended.

5.2.2.1 Smooth tube

Fig. 5.2 illustrates the linear line method for the identification of the three flow regimes in smooth tube. The Reynolds numbers at the two intersections of the "*R-R*" transition line, with the "*L-L*" laminar line and the "*T-T*" turbulent line, were identified for the purposes of this study as the start, Re_{cr}, and end, Re_{qt}, of transition and the width of transition as, ΔRe. The start of transition in Fig. 5.2 was at, $Re_{cr} = 3\,053$ and the end of transition was at, $Re_{qt} = 3\,331$. The width of transition was defined as the difference between the Reynolds numbers at the end and at the start of transition, thus, $\Delta Re = Re_{qt} - Re_{cr} = 278$.

5.2.2.2 CTT inserts

The same approach was also used for the tube with twisted tape inserts, as shown in Fig. 5.3 for the standard deviation method and Fig. 5.4 for the linear line method. The results are for a tube with a CTT insert with a twist ratio of 5 and a heat flux of 2 kW/m^2. In the turbulent flow regime, the "*T-T*" line was constructed for Reynolds numbers larger than 2 000. In the laminar flow regime, the "*L-L*" line was constructed for Reynolds numbers lower than 1 000. The transitional flow regime line, "*R-R*", was constructed for Reynolds numbers between 1 098 and 1 289. The start of the transitional flow regime in Fig. 5.4 was at, $Re_{cr} = 1\,023$, and the end of transition was at, $Re_{qt} = 1\,604$. A summary of the Reynolds numbers indicating the start, end and width of the transitional flow regime for all the cases of the smooth tube, as well as the tube with CTT inserts is given in Table 5.1.

Table 5.1. Ranges of transitional flow regime Reynolds numbers of the Colburn *j*-factors with the smooth tube and twisted tape inserts at different heat flux boundary conditions.

$\dot{q}$ [kW/m^2]	Smooth			Twist ratios								
				$y = 3$			$y = 4$			$y = 5$		
	Re_{cr}	Re_{qt}	ΔRe	Re_{cr}	Re_{qt}	ΔRe	Re_{cr}	Re_{qt}	ΔRe	Re_{cr}	Re_{qt}	ΔRe
Colburn *j*-factor, *j*												
2	3 053	3 331	278	593	1 125	532	669	1 027	358	1 023	1 604	581
3	3 164	3 452	288	819	1 274	455	951	1 418	467	1 108	1 683	575
4	3 266	3 565	299	1 093	1 404	311	1 172	1 524	352	1 278	1 775	497
Friction factor, *f*												
2	3 041	3 292	251	540	1 091	551	609	977	368	980	1 561	581
3	3 152	3 411	259	739	1 167	428	873	1 308	435	1 067	1 630	563
4	3 177	3 507	330	983	1 361	378	1 049	1 485	436	1 182	1 670	488

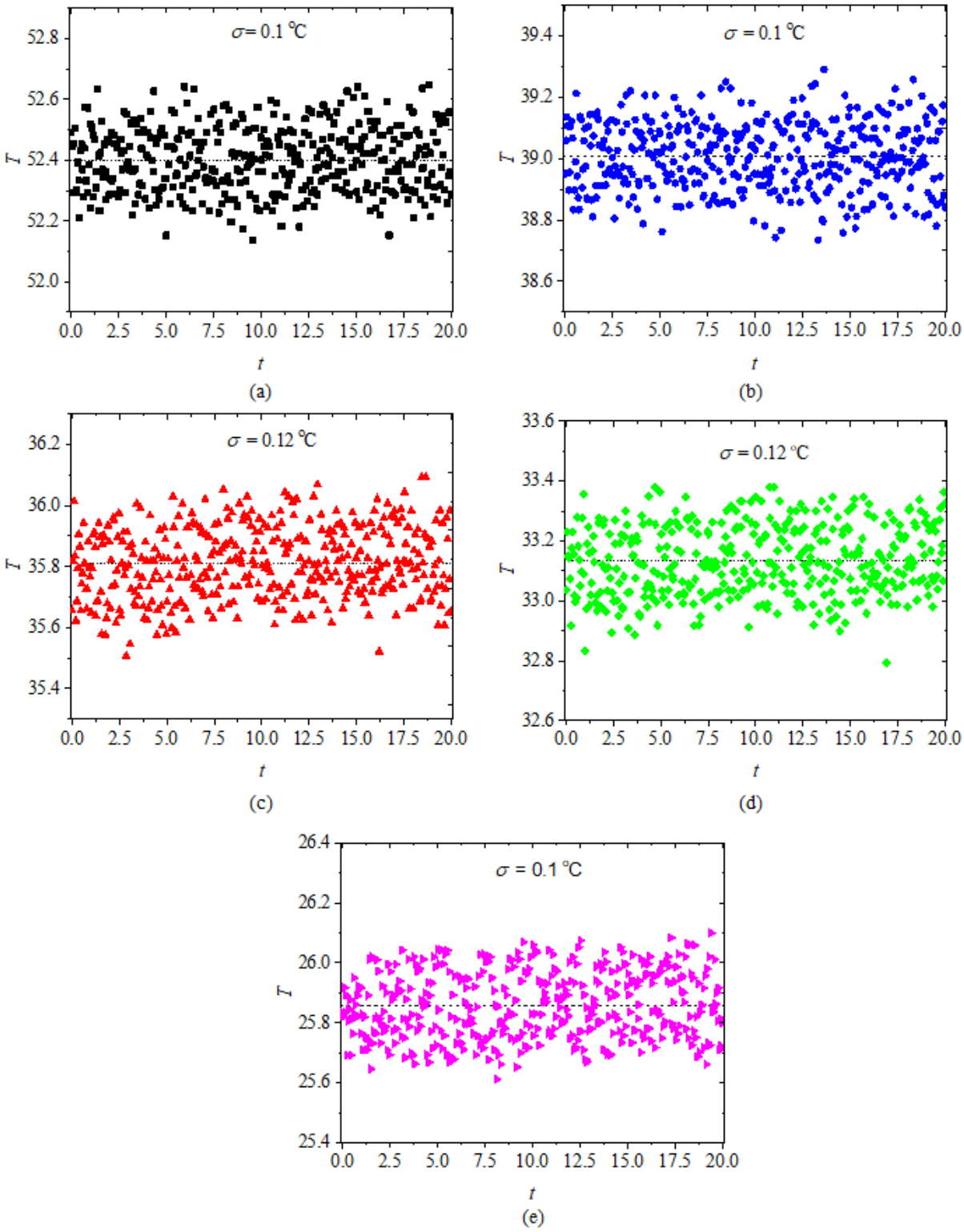

Fig. 5.3. Deviation of the local surface temperatures in the smooth circular tube with twisted tape insert with a twist ratio of $y = 5$ against time at $x/D_i = 246$, a heat flux of 2 kW/m^2, and Reynolds numbers of: (a) 610; (b) 995; (c) 1 193; (d) 1 461 and (e) 4 492. The labels (a) to (e) correspond to the labels in Fig. 5.4.

Although the two methods used to identify the transitional flow regimes, relied in some cases on subjective decisions (which data to include and/or exclude in a flow regime), it was found that reasonable results could be obtained if the two methods were used complementary to each other, and in some cases by iterating between the two methods. However, it was found

that the linear line method was quicker to implement than the standard deviation method, especially if enough data points were available in all three the flow regimes (laminar, transitional and turbulent). For some experiments at low mass flow rates (and thus low Reynolds numbers), the outlet temperatures became too high, which resulted in a very limited number of experimental data points in the laminar flow regime. In these cases, the transitional to turbulent flow points could be described well, but not the laminar to transitional flow points. In some of these cases, only one or two laminar data points could be identified, with Reynolds numbers of approximately 500.

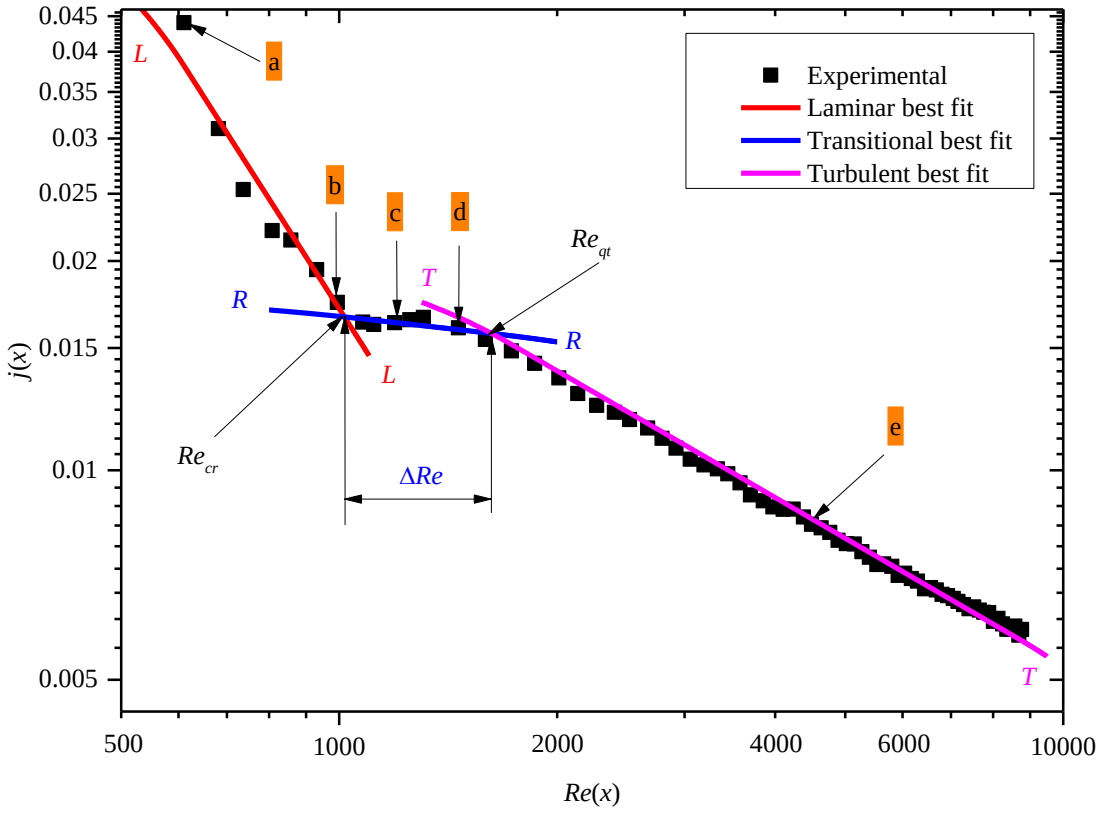

Fig. 5.4. Colburn *j*-factors as a function of local Reynolds numbers at measuring station $x/D_i = 246$ and a heat flux of 2 kW/m^2, for a tube with a CTT insert with a twist ratio of $y = 5$.

5.3 Twist ratio

Fig. 5.5 compares the Colburn *j*-factor results for the same heat flux of 2 kW/m^2, but with twist ratios of 3, 4 and 5 at measuring station $x/D_i = 246$. The results are also compared to the smooth tube at the same x/D_i, value. The results showed that the Colburn *j*-factors increased as the twist ratios decreased from, $y = 5$ to $y = 3$. This can be expected as the twist ratio of, $y = 3$ induced more radial rotation to the flow (when compared to the other twist ratios) and increased the longitudinal flow path through the tube. For this reason, there were less experimental data points in the laminar flow region, and transition occurred earlier.

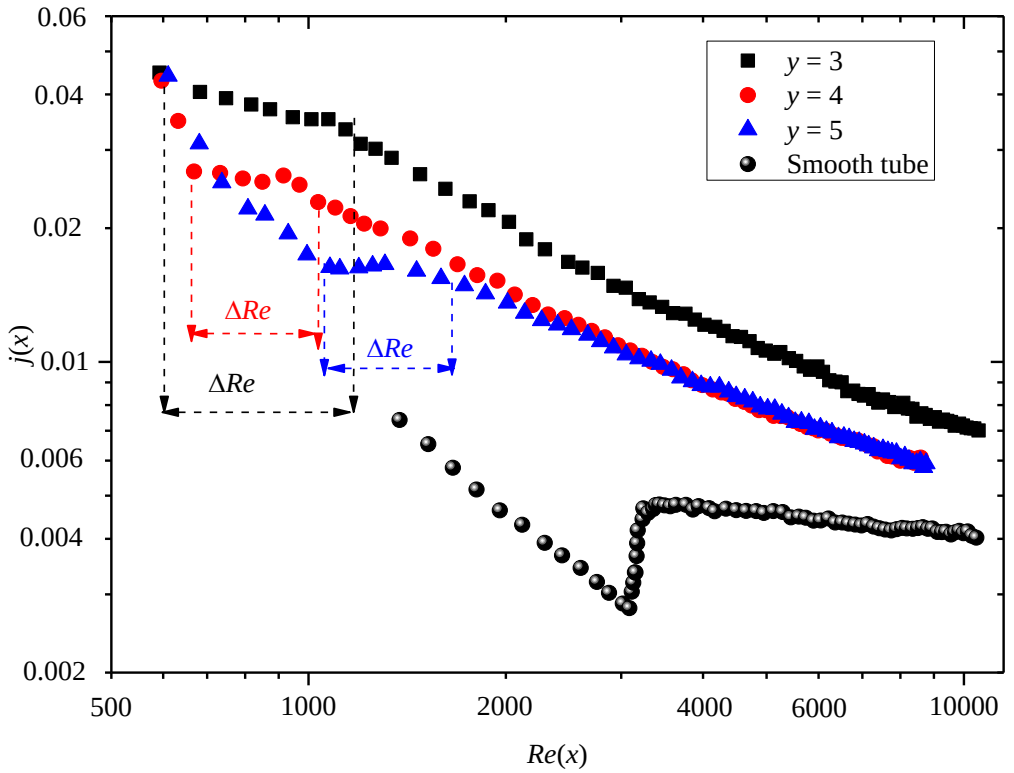

(a)

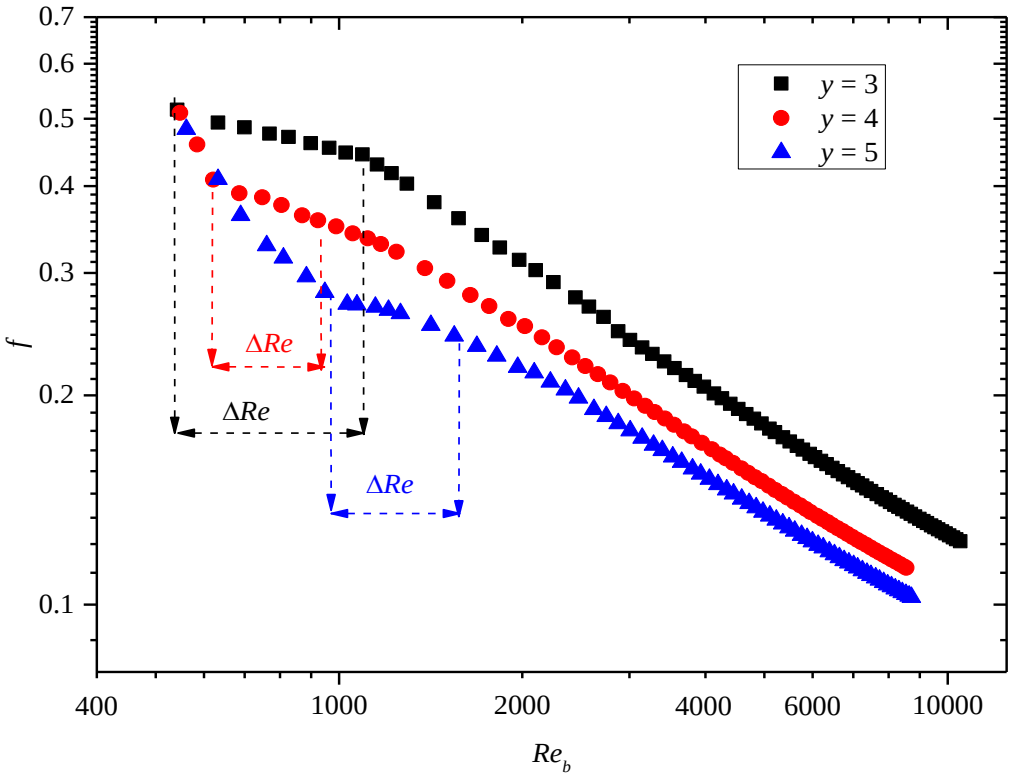

(b)

Fig. 5.5. (a) Colburn *j*-factors as a function of Reynolds numbers at, $x/D_i = 246$, (b) friction factors at $x/D_i = 198$, a heat flux of 2 kW/m^2 and for twist ratios of 3, 4 and 5 for the smooth tube. ΔRe is the transitional flow regime, so that $\Delta Re = Re_{qt} - Re_{cr}$.

In general, transition started earlier as the twist ratio decreased. Transition in Fig. 5.5(a) for a twist ratio of $y = 3$ started at a Reynolds number of 593. For a twist ratio of, $y = 4$, it was at a Reynolds number of 669, and for a twist ratio of $y = 5$, it was at a Reynolds number of 1 023. For the smooth tube case, transition started at a Reynolds number of 3 053 for a heat flux of 2 kW/m^2. For a heat flux of 3 kW/m^2, it was at a Reynolds number of 3 164, and for a heat flux of 4 kW/m^2, it was at a Reynolds number of 3 266. It ended for the smooth tube at the Reynolds numbers 3 331, 3 452 and 3 565 for heat fluxes of 2, 3 and 4 kW/m^2 respectively.

The early transition is attributed to the increased flow disturbances as the twist ratio reduced. As illustrated in Fig. 5.5 for the same heat flux, the twisted tape insert with the lowest twist ($y = 3$), ratio caused most disturbances, and produced the earliest transition ($Re = 593$). This caused a thinner thermal boundary layer and thus the highest heat transfer coefficients. If twisted tapes only are compared the twisted tape with the highest twist ratio ($y = 5$), delayed transition ($Re = 1\,023$) the most as it caused the smallest disturbances in the thermal boundary. The tube that will cause no disturbances in the development of the thermal boundary layer is the smooth tube. For this reason, it delayed transition ($Re = 3\,053$) the most and it had the lowest heat transfer coefficients.

The results of the friction factors for the tube with CTT inserts with twist ratios of 3, 4 and 5 are presented in Fig. 5.5(b) for a heat flux of 2 kW/m^2. The results showed that the transitional flow regimes were well defined as the heat transfer data. It correctly shows that the friction factor increased as the twist ratio decreased. The reason is that, as the twist ratio decreased, the average lateral flow path length increased. The twisted tape surface area for friction also increased. Furthermore, the widths of the transitional flow regime, ΔRe, decreased as the twist ratios increased.

Comparing the start of transition results Re_{cr}, end of transition results, Re_{qt}, and Coburn j-factor values with the friction factor data in Table 5.1 reveals small differences of a maximum of 14%. The reason is that, for the Colburn j-factor data, the local Reynolds number was based on the local temperatures at measuring station, $x/D_i = 246$, while the friction factor was based on the bulk temperature positioned in the centre of the two pressure taps at $x/D_i = 198$.

In general, it was also found that the difference between the Reynolds numbers at the end of transition and at the start of transition (ΔRe) increased as the twist ratio increased. At a heat flux of 3 kW/m^2, the ΔRe values were 455, 467 and 575 respectively for the Colburn j-factors and the ΔRe values were 428, 435 and 563 for the friction factors. This trend was found in all the data except for one point at a heat flux of 4 kW/m^2 and a twist ratio of 3. At this point, the transition point was probably not that accurate, as experimental data points in the laminar flow regime were challenging to collect. At these low Reynolds numbers, the associated low mass flow rates caused the water outlet temperatures to rise beyond the maximum material specifications of the experimental set-up.

5.4 Heat flux

The effects of different heat fluxes on a tube with a CTT insert with a twist ratio of 5, as a function of the Reynolds number are illustrated in Fig. 5.6. (a). Similar to the results obtained by Tam and Ghajar [20] and Everts [219], it follows from Fig. 5.6. (a) that higher heat fluxes delayed the transition from laminar to transitional flow. Although these works were conducted at a constant heat flux the delayed transitions were also found by Meyer and Olivier [1, 24, 26]. In the laminar flow regime, the heat transfer coefficients increased with heat flux as the thermal gradient between the fluid and wall increased. This increased the strengths of the free convection effects which decreased the thermal boundary layer thickness. The heat transfer coefficients increased as the thermal boundary layer decreased. Higher heat fluxes increased both the upper and lower limits of the transitional flow regime. The effect of heating is that transition is delayed or to stabilize the flow [20] and thus transition occurred at a higher critical Reynolds number. Furthermore, the width of the transitional flow regime, ΔRe, decreased as the heat fluxes increased (Table 5.1). In the turbulent flow regime, the results were independent of heat flux. This can be expected as similar results were found for all the heat fluxes in smooth tubes and tube with twisted tape inserts.

The effect of heat flux on friction factor for a tube with a CTT insert and a twist ratio of $y = 5$ is given in Fig. 5.6. (b). It shows that, in the laminar and transitional flow regimes, an increase in heat flux decreased the friction factor. The higher heat fluxes increased the wall surface temperature, which decreased the water viscosity and thus shear stress on the wall. Most probably, the free convection effects (that would increase the friction factors) were negligible as, in general, no temperature differences were found between the top of the wall and the bottom of the wall at the same measuring station. In the turbulent flow regime, the heat flux had no effect on the friction factor. This can be expected as the heat transfer data (Fig. 5.6. (a)) performed similarly, and the same trend was found when using the linear line method.

The physical mechanisms that caused the changes in the friction factors as function of Reynolds number, critical Reynolds number, twist ratio and heat fluxes are the same as for the heat transfer data. For the same heat flux, the flow disturbances caused by the twisted tapes increased (as the twist ratios decreased) the flow velocity gradients and thus shear stresses on the wall. This increased the pressure drops and thus friction factors.

A higher heat flux increased the temperature differences in the fluid. The fluid near the wall had a higher temperature and lower density than those close tube centre. This temperature difference produced mixed convection (Nusselt numbers higher than 4.36 in the smooth tube showed that the flow regime was not forced convection but mixed convection). The changes in flow regime caused the velocity profile of the fluid to change. In these cases, it changed the shear stress and fluid density of the flow. The shear stress increased when the heat fluxes increased, but the fluid density decreased. However, the increases in the shear stresses were more than the decreases in density and therefore the friction factors increased [20].

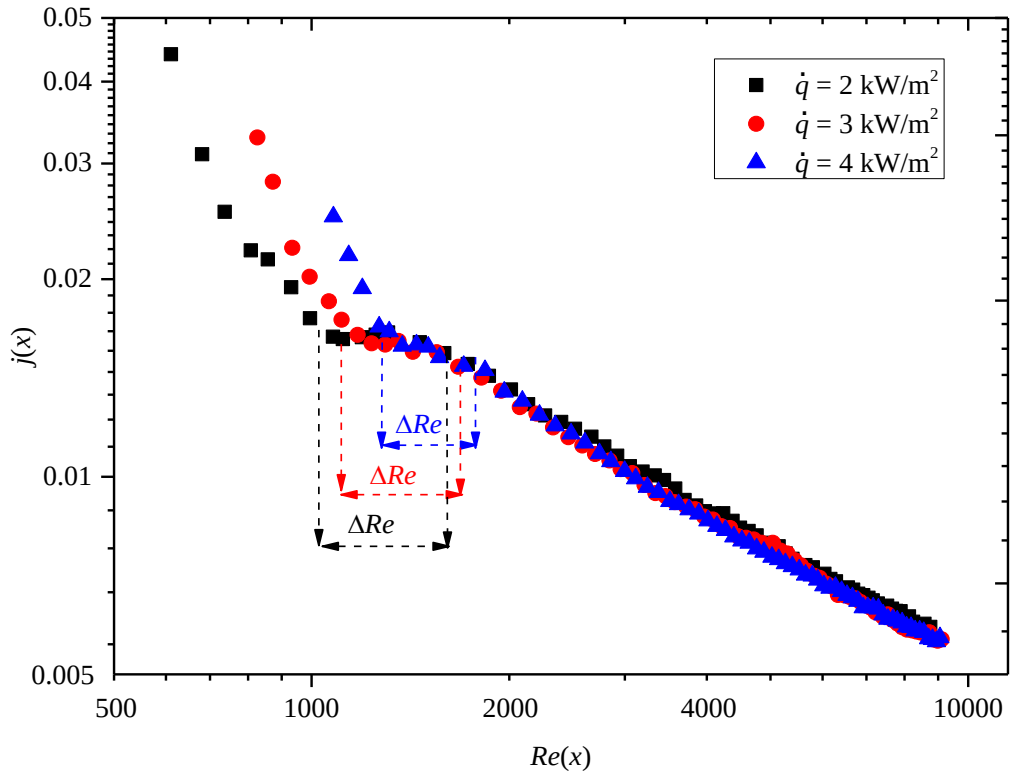

(a)

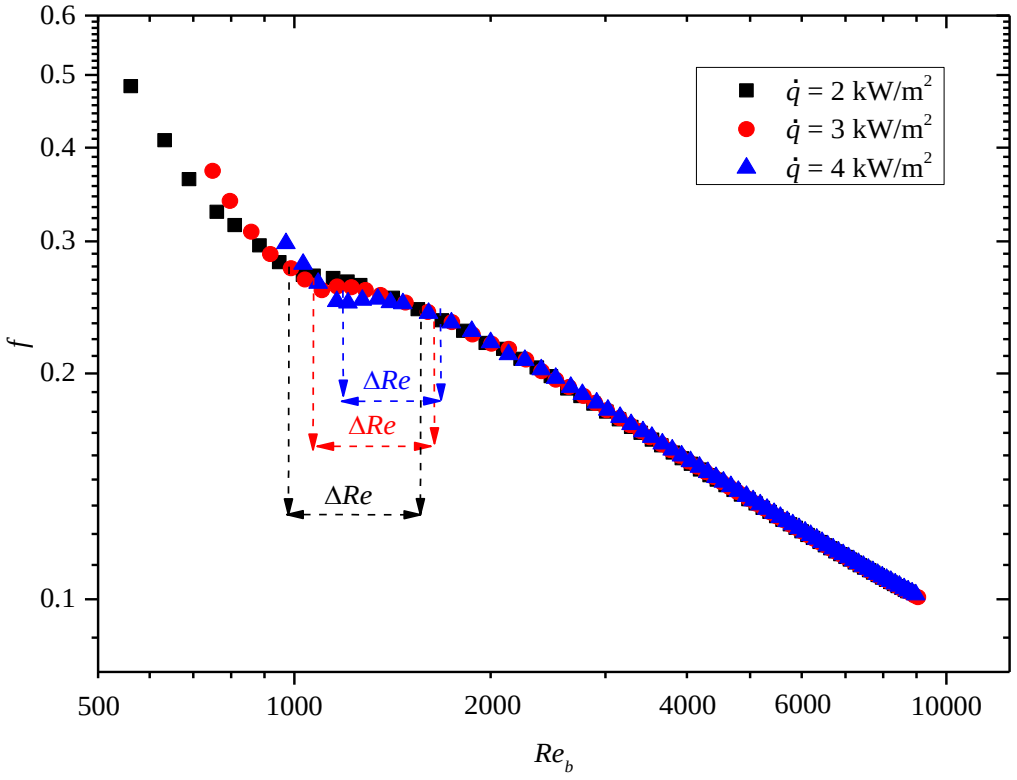

(b)

Fig. 5.6. Colburn *j*-factors as a function of local Reynolds numbers at x/D_i = 246, and (b) friction factors at x/D_i = 198, in a tube with a twist ratio of y = 5, and varying heat fluxes of 2, 3 and 4 kW/m^2. ΔRe is the transitional flow regime, so that $\Delta Re = Re_{qt} - Re_{cr}$.

5.5 Correlations

5.5.1 Colburn *j*-factor

For simplicity, the following correlations were developed using curve fits of the Colburn *j*-factors that represent the non-dimensional heat transfer coefficients for the smooth tube results:

$$j(x) = d[Re(x)]^c \left(\frac{\mu_b}{\mu_s}\right)^{0.14} \quad 5.1$$

With, *d*, being the *y*-axis intercept and, *c*, being the slope. It was found that inserting the term, $(\mu_b/\mu_s)^{0.14}$ gave better results, although the viscosity ratios only varied in the range of $1.01 \leq \mu_b/\mu_s \leq 1.09$. The Colburn *j*-factors, Reynolds numbers and viscosities were all obtained using the local values per measuring station. To reflect the influence of the twisted tape inserts, as a function of twist ratio, *y*, Eq. (5.2) was adapted for CTT inserts:

$$j(x) = ay^b[Re(x)]^c \left(\frac{\mu_b}{\mu_s}\right)^{0.14} \quad 5.2$$

With, $d = ay^b$. It was also found that a value of $b = 0.3$ gave acceptable results for all the experiments that were conducted. The values of the variables, *a*, *c*, and *d* were determined for each case and are summarized in Table 5.2. The average and maximum deviations of each curve fit with the experimental data, using the values of, Re_{cr}, Re_{qt} and ΔRe are also included. Thus, for laminar results, all the data with Reynolds numbers smaller than, $Re_{cr,}$ was used. To further distinguish the variables in the table, the *a, c* and *d* values were used together with the subscripts of *L*, *R* and *T* to identify the laminar, transitional, and turbulent flow regimes respectively.

For the smooth tube (Fig. 5.2), the resulting equation for laminar flow is:

$$j_L(x) = 43[Re(x)]^{-1.2} \left(\frac{\mu_b}{\mu_s}\right)^{0.14} \quad 5.3$$

The transitional flow regime is described by:

$$j_R(x) = 1.13 \times 10^{-41}[Re(x)]^{11} \left(\frac{\mu_b}{\mu_s}\right)^{0.14} \quad 5.4$$

The turbulent flow regime is described by:

$$j_T(x) = 0.0248[Re(x)]^{-0.2} \left(\frac{\mu_b}{\mu_s}\right)^{0.14} \quad 5.5$$

Table 5.2. The heat transfer values of the variables in Eqs. 5.1 and 5.2 for the Colburn *j*-factor equations, for different heat fluxes at the measuring station, $x/D_i = 246$.

	Smooth			Twist ratios								
				$y = 3$			$y = 4$			$y = 5$		
$\dot{q}$	2	3	4	2	3	4	2	3	4	2	3	4
Re_{cr}	3053	3164	3266	593	819	1093	669	951	1172	1023	1108	1278
Re_{qt}	3331	3452	3565	1125	1274	144	1027	1418	1524	1604	1683	1775
ΔRe	278	288	299	532	455	311	358	467	352	581	575	497
Laminar values												
a_L	--	--	--	--	--	--	7.06×10^{9}	31910	2.23×10^{8}	2100	36180	291180
$_{CL}$	-1.2	-1.2	-1.2	--	--	--	-4.1	-2.12	-3.33	-1.77	-2.15	-2.4
d_L	43	51	57	--	--	--	1.06×10^{10}	48367	3.52×10^{8}	3403	58635	471903
Transitional values												
a_L	--	--	--	0.31	0.31	0.31	0.113	0.162	0.284	0.023	0.094	0.262
$_{CL}$	11	5	7.7	-0.37	-0.382	-0.393	-0.282	-0.342	-0.425	-0.117	-0.315	-0.456
d_L	1.13×10^{-41}	9.63×10^{-21}	2.36×10^{-30}	0.431	0.431	0.431	0.171	0.246	0.43	0.037	0.152	0.425
Turbulent values												
a_L	--	--	--	3.76	3.76	3.76	1.66	1.66	1.66	0.628	0.628	0.628
$_{CL}$	-0.2	-0.2	-0.2	-0.734	-0.734	-0.734	-0.665	-0.665	-0.665	-0.571	-0.571	-0.571
d_L	0.0248	0.0248	0.0248	5.23	5.23	5.23	2.52	2.52	2.52	1.02	1.02	1.02
Deviations from experimental data												
Ave	1	3	2	5	2	4	9	9	10	2	2	2
Max	9	6	6	7	3	16	14	14	15	5	5	5

By substituting the Colburn *j*-factors as $Nu/RePr^{1/3}$ into Eq. 5.5 the Nusselt number equation was derived for the smooth tube in the turbulent flow regime (similar equations can be derived for the laminar and transitional flow regimes) as:

$$Nu_T(x) = 0.0248[Re(x)]^{0.8}[Pr(x)]^{1/3}\left(\frac{\mu_b}{\mu_s}\right)^{0.14} \quad 5.6$$

which compares reasonably well with the equation of Ghajar and Tam [15]:

$$Nu_T = 0.023Re^{0.8}Pr^{0.385}\left(\frac{x}{D}\right)^{-0.0054}\left(\frac{\mu_b}{\mu_s}\right)^{0.14} \quad 5.7$$

The results for the tubes with a CTT insert with a twist ratio of $y = 5$ and a heat flux of 2 kW/m^2 (results shown in Fig. 5.4 and variables from Table 5.2) are as follows for laminar flow:

$$j_L(x) = 2100y^{0.3}[Re(x)]^{-1.77}\left(\frac{\mu_b}{\mu_s}\right)^{0.14} \quad 5.8$$

and for transitional flow:

$$j_R(x) = 0.023y^{0.3}[Re(x)]^{-0.117}\left(\frac{\mu_b}{\mu_s}\right)^{0.14} \quad 5.9$$

and for turbulent flow:

$$j_T(x) = 0.628y^{0.3}[Re(x)]^{-0.571}\left(\frac{\mu_b}{\mu_s}\right)^{0.14} \quad 5.10$$

Although only the Colburn *j*-factor equations for a heat flux of 2 kW/m^2 and a twist ratio of 5 were given above, the equations for the heat fluxes of 3 and 4 kW/m^2 and twist ratios of 3 and 4 can be determined directly from Table 5.2.

The equations developed for the Colburn *j*-factors were compared to the experimental data and it was found that the equations estimated the experimental data on average to within 6%, with a maximum error of 16%.

5.5.2 Friction factors

Using the transition results, (Re_{cr}), and (Re_{qt}), of the Colburn *j*-factor data, friction factor correlations similar to the Colburn *j*-factor equations were developed. For the smooth tube, the friction factor correlation was of the form:

$$f = d[Re_b]^c\left(\frac{\mu_b}{\mu_s}\right)^{0.14} \quad 5.11$$

For the tube with the twisted tape insert, the following equation was used:

$$f = ay^b[Re_b]^c\left(\frac{\mu_b}{\mu_s}\right)^{0.14} \quad 5.12$$

Thus, for the case of a heat flux of 2 kW/m^2 and in the laminar flow regime for a smooth tube, the friction factor can be described as:

$$f_L = 74[Re_b]^{-1}\left(\frac{\mu_b}{\mu_s}\right)^{0.14} \quad 5.13$$

In the transitional flow regime, the equation is:

$$f_R = 3.37 \times 10^{-37}[Re_b]^{10}\left(\frac{\mu_b}{\mu_s}\right)^{0.14} \quad 5.14$$

In the turbulent flow regime, the equation is:

$$f_T = 0.26[Re_b]^{-0.23}\left(\frac{\mu_b}{\mu_s}\right)^{0.14} \quad 5.15$$

For a tube with a twisted tape insert, a heat flux of 2 kW/m^2 and a twist ratio of y = 5 in the laminar flow regime, it is:

$$f_L = 183y^{0.3}[Re_b]^{-1.02}\left(\frac{\mu_b}{\mu_s}\right)^{0.14} \quad 5.16$$

In the transitional flow regime, the equation is:

$$f_R = 1.04y^{0.3}[Re_b]^{-0.262}\left(\frac{\mu_b}{\mu_s}\right)^{0.14} \quad 5.17$$

In the turbulent flow regime, it is:

$$f_T = 7y^{0.3}[Re_b]^{-0.52}\left(\frac{\mu_b}{\mu_s}\right)^{0.14} \quad 5.18$$

The ranges of Reynolds numbers in the transitional flow regime with diabatic friction factors are given in Table 5.3 and the appropriate constants for Eqs. (5.11) and (5.12) are summarized in Table 5.3 for different twist ratios and heat fluxes. In Table 5.3 the predicted results from the correlations are compared to the measurements of this study and a maximum error of 4% was obtained. Comparing the start of transition results (Re_{cr}), end of transition results (Re_{qt}) as well as Coburn j-factor values with the friction factor data in Table 5.1 reveals small differences of a maximum of 14%. The reason is that, for the Colburn j-factor data, the local Reynolds number was based on the local temperatures at measuring station x/D_i = 246, while the friction factor was based on the bulk temperature positioned in the centre of the two pressure taps, between stations 15 and 16 at x/D_i = 198.

Table 5.3. The values of the variables in the friction factor Eqs. 5.11 and 5.12 for different heat fluxes between the pressure taps, at the measuring station, x/D_i = 198.

	Smooth			Twist ratios								
				y = 3			y = 4			y = 5		
$\dot{q}$	2	3	4	2	3	4	2	3	4	2	3	4
Re_{cr}	3041	3152	3177	540	739	983	609	814	1049	980	1067	1182
Re_{qt}	3292	3411	3507	1091	1167	1361	977	1308	1485	1561	1630	1670
ΔRe	251	259	330	551	428	378	368	494	436	581	563	488
Laminar values												
a_L	--	--	--	--	--	--	22300	167	3500	183	192	205
$_{CL}$	-1	-1	-1	--	--	--	-1.76	-0.98	-1.4	-1.02	-1.02	-1.02
d_L	74	76	79	--	--	--	33800	253	5305	297	311	332
Transitional values												
a_L	--	--	--	1.4	1.4	1.4	2.2	0.85	0.773	1.04	0.85	0.746
$_{CL}$	10	6	5	-0.211	-0.22	-0.235	-0.328	-0.2	-0.19	-0.262	-0.265	-0.22
d_L	3.37×10^{-37}	2.45×10^{-23}	6.79×10^{-20}	1.93	1.93	1.93	3.33	1.3	1.17	1.69	1.38	1.21
Turbulent values												
a_L	--	--	--	16	16	16	10.5	10.5	10.5	7	7	7
$_{CL}$	-0.23	-0.23	-0.23	-0.564	-0.564	-0.564	-0.548	-0.548	-0.548	-0.52	-0.52	-0.52
d_L	0.26	0.26	0.26	22.4	22.4	22.4	16	16	16	11.3	11.3	11.3
Deviations from experimental data												
Ave	1	1	1	1	1	1	1	1	1	1	1	1
Max	4	4	2	4	3	3	3	3	3	2	2	2

5.6 Summary and conclusions

An experimental investigation of the transitional flow regime with three CTT inserts with twist ratios of 3, 4 and 5 were conducted. The range of Reynolds numbers in the experiments in general spanned all three flow regimes of laminar, transitional and turbulent. A calming section and square-edged inlet were used. Experiments were conducted at three different heat fluxes (2, 3 and 4 kW/m^2) and the heat transfer coefficients and friction factors were determined. The results were also compared to a smooth tube without any twisted tape inserts. A total of 865 experiments were conducted.

Two independent, yet complementary methods, were used to determine the boundaries where transition started and ended. The first method was the standard deviation method in which the temperature deviations at each measuring station were determined. The second method was to construct three linear curve fits on a log-log scale of Colburn *j*-factors as a function of the Reynolds numbers. The curve fits made it possible for correlations to be developed for the non-dimensionalized heat transfer coefficients (Colburn *j*-factors) and friction factors, which took into consideration the twist ratio, heat flux and Reynolds number.

When the CTT inserts were compared at the same heat flux, it was found that the Colburn *j*-factors increased as the twist ratio decreased, and transition started earlier. When the twist ratio was kept constant, and the heat flux were varied, higher heat flux delayed the transition from laminar to transitional flow. Furthermore, the width of the transitional flow regime decreased as the heat flux increased.

For friction factors of the CTT inserts, it was found that friction factors increased as the twist ratio decreased. The width of the transitional flow regime also decreased as the twist ratios increased. When both the twist ratio and the Reynolds number were kept constant, an increase in heat flux was found to decrease the friction factor.

Heat transfer and pressure drop correlations were developed for the CTT inserts as a function Reynolds number, twist ratio and heat flux.

6. Heat transfer and pressure drop in the transitional flow regime with clockwise and counter clockwise twisted tape inserts

6.1 Introduction

This chapter presents the experimental results of heat transfer and pressure drop characteristics in a smooth tube heat exchanger with alternating clockwise and counter clockwise twisted tape (CCCTT) inserts of connection angles of 0°, 30° and 60° at the twist ratio of 5. Each connection angle was tested at four heat fluxes of 1.35, 2, 3 and 4 kW/m^2. The heat transfer results were presented in terms of Colburn *j*-factors, while the pressure drop results in terms of friction factors. The performance of the CCCTT insert was compared with the PUCTT and CTT inserts. The influence of connection angle and heat flux on the transitional flow regime were discussed as well as the correlations developed. The results contained in this chapter have been published in Abolarin et al. [50].

For forced convection laminar flow (at a Reynolds number of 1 000 in a smooth tube) the flow was expected to be fully developed at $x/D_i = 0.12RePr = 840$ [31] and for turbulent flow at $x/D_i \approx 10$. Although the test section considered was not a smooth tube this should at least give an order of magnitude estimate. However, similar to the results obtained by Meyer and Abolarin [49], the local Nusselt numbers indicated that in all three flow regimes (laminar, transitional and turbulent) the flow was developing at the first measuring station, $x/D_i = 9$, and fully developed for $x/D_i \geq 22$ when CCCTT inserts were used. The significant decrease in the laminar thermal entrance length was due to the fluid rotation caused by the tape inserts as well as free convection effects that led to mixed convection [31]. The heat transfer results could thus be presented in two ways: either as the average between $x/D_i = 22$ and $x/D_i = 272$, or at a specific measuring station as was used in the work of Ghajar and Tam [15, 16, 21]. Similar to Ghajar and Tam [15, 16, 21] and Meyer and Abolarin [49], the results were presented at a specific measuring station, $x/D_i = 246$. Furthermore, due to the direct relationship between heat transfer and pressure drop that exists in all flow regimes, the heat transfer results were investigated in terms of the Colburn *j*-factors [31].

The transitional flow regime, which was the main focus of this study, was identified using the linear line method prescribed by Meyer and Abolarin [49]. As illustrated in Fig. 6.1 for a CCCTT inserts with a twist ratio of $y = 5$, connection angle of $\theta = 60°$, and heat flux of 1.35 kW/m^2, this method involved linear fits (on a log-log scale) of the data in the laminar, transitional and turbulent flow regimes when the Colburn *j*-factors or friction factors were plotted as a function of Reynolds number. The laminar flow regime was identified by the "*L-L*" line which excluded the data points close to the critical Reynolds number. The transitional

flow regime was marked by the "*R-R*" line and the data points near the start and the end of the transitional flow regime were excluded in the fitting of this line. The turbulent flow regime was identified by the "*T-T*" line. The intersection of the laminar "*L-L*" and transitional "*R-R*" curve fits indicated that transition started at a Reynolds number of 529. Also, the intersection of the transitional "*R-R*" and turbulent "*T-T*" curve fits, indicated that the transitional flow regime ended at a Reynolds number of 847.

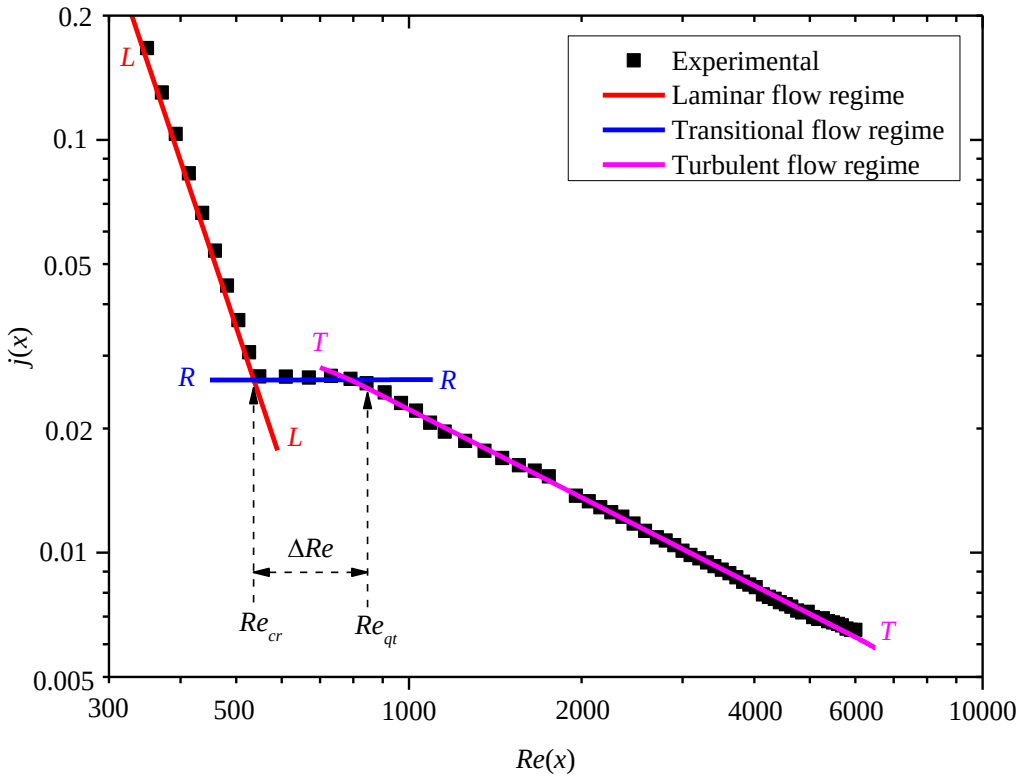

Fig. 6.1. Illustration of the linear line method [49] used to identify the three flow regimes for the heat transfer results as a function of Reynolds number at x/D_i = 246, a heat flux of 1.35 kW/m^2 and connection angle of 60°. The "*L-L*", "*R-R*" and "*T-T*" lines represent the laminar, transitional and turbulent flow regimes respectively.

6.2 Comparison of the CCCTT insert with the PUCTT and CTT inserts

Fig. 6.2 compares the Colburn *j*-factors (Fig. 6.2(a)) and friction factors (Fig. 6.2(b)) as a function of Reynolds number of the CCCTT insert (changing the flow direction every 450 mm) at a connection angle of 60°, with a PUCTT22 insert (peripheral u-cuts) [51] with a depth ratio of 0.216 and CTT insert that rotated the flow in only one direction. All the twisted tape inserts had a twist ratio of y = 5 and the experiments were conducted at a heat flux of 2 kW/m^2. It should be noted that for the Colburn *j*-factors, the lowest uncertainties occurred in the laminar flow regime where temperature differences were high, while the lowest friction factor uncertainties were found in the turbulent flow regime where pressure drops were higher. Therefore, in the laminar flow regime the Colburn *j*-factor data is more accurate while the friction factor data is more accurate in the turbulent flow regime. In cases where small differences occurred between the CCCTT, PUCTT22 and CTT inserts in the laminar flow regime (as in some cases in this chapter); the Colburn *j*-factor data are more representative of

the real differences. For cases with small differences in the turbulent flow regime, the friction factors are more representative of the real differences. This has been shown by the heat transfer and pressure drop analogy work of Everts and Meyer [30].

Similar to the results reported in literature [45, 133, 135, 149, 244-246], the Colburn *j*-factors (Fig. 6.2(a)) indicate that there were very small differences in the results of the three twisted tapes in the laminar flow regime. Therefore, changing the flow rotation direction or modifying the twisted tape inserts were not effective heat transfer techniques in the laminar flow regime. In the turbulent flow regime, the heat transfer enhancement varied between approximately 4% and 15%.

Significant heat transfer enhancement was obtained in the transitional flow regime. At a Reynolds number of 1 000, the Colburn *j*-factors of the CCCTT insert were approximately 30% and 46% higher than those of the PUCTT22 insert and CTT insert respectively. Furthermore, the transitional flow regime occurred significantly earlier (at lower Reynolds numbers) when a CCCTT insert was used. The transitional flow regime started, Re_{cr}, and ended, Re_{qt}, at Reynolds numbers of 1 023 and 1 604 for the CTT insert, at 796 and 1 344 for the PUCTT22 insert and at 685 and 978 for the CCCTT insert. Similar results were obtained in the friction factor data in Fig. 6.2(b). This can be expected as Everts and Meyer [30], determined that the Colburn analogy is also valid in the transitional flow regime and that the start and end of transitional flow regime will always occur at the same mass flow rate for heat transfer and pressure drop data. For the results in this study (with heat transfer results as a function of local Reynolds numbers and friction factors as a function of bulk Reynolds number), the Reynolds numbers for the start and end of transition were not exactly the same. This is due to the different temperatures at which the fluid properties, mainly the viscosities, were calculated.

No significant difference was found in the laminar friction factor data in Fig. 6.2(b). In the transitional flow regime, it was found that at a Reynolds number of 1 000, the friction factors of the CCCTT insert were approximately 24% higher than that of the CTT insert and 18% lower than that of the PUCTT insert. Similar to the Colburn *j*-factors, the transitional flow regime started and ended first for the CCCTT insert. For the CTT insert the start and end of transition were at Reynolds numbers of 923 and 1 504, while 747 and 1298 for the PUCTT22 insert and for the CCCTT insert they were at 637 and 932 respectively.

In the turbulent flow regime, the friction factors of the CCCTT insert were slightly higher than for the CTT insert and significantly lower than the PUCTT22 insert. For instance, at Reynolds numbers of 1 540 and 5 897, the friction factors of the CCCTT insert were 12% and 7% respectively higher than those of the CTT insert, while they were 22% and 58% respectively lower than those of the PUCTT22 insert. Because the CCCTT insert caused the flow path to change rotation direction (from clockwise to counter clockwise) 12 times, the flow was continually disturbed and the flow path length was increased. This led to the slight increase in friction factors compared with the CTT insert. The discontinuity at "*C*" as illustrated in the Fig. 6.2(b) occurred because different pressure transducer diaphragms were used due to the range limitations.

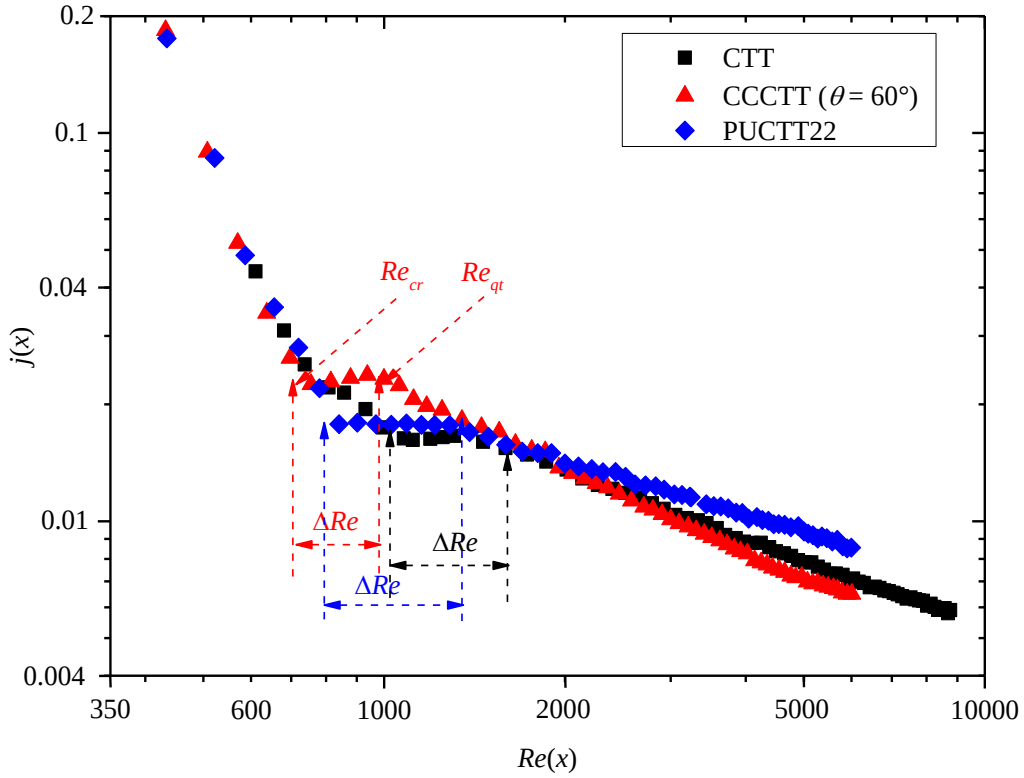

(a)

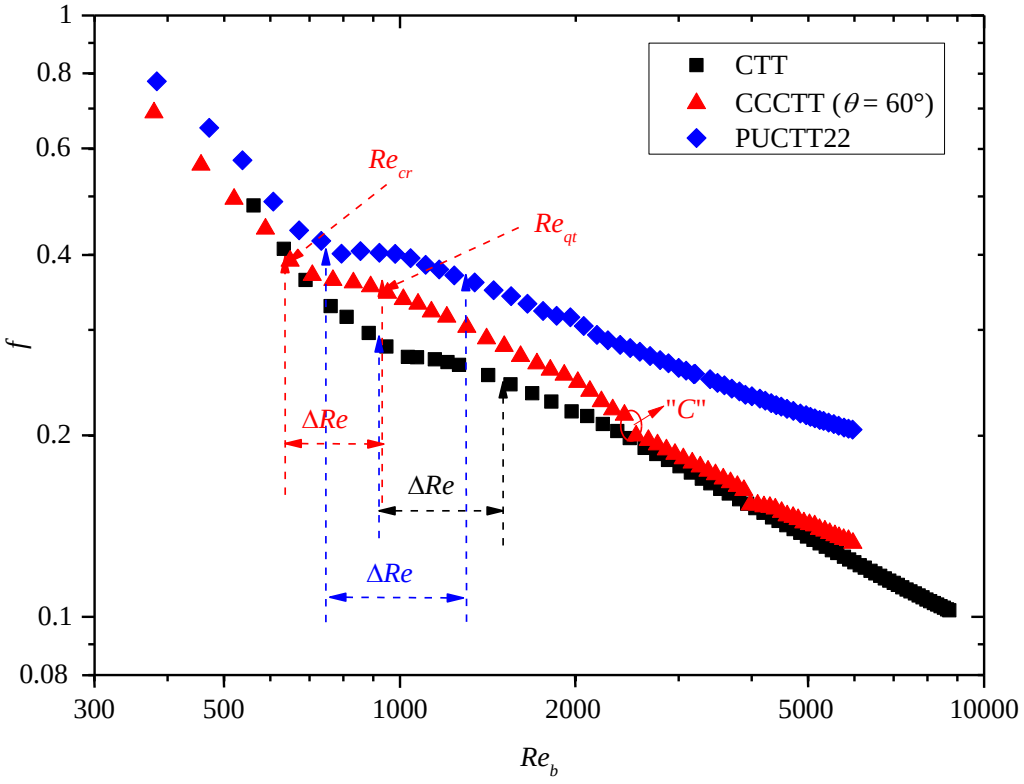

(b)

Fig. 6.2. Comparison of (a) the Colburn *j*-factors as a function of local Reynolds number at $x/D_i = 246$, and (b) the friction factors as a function of bulk Reynolds number at $x/D_i = 198$, for the CTT insert [49], CCCTT insert with a connection angle of 60° and PUCTT22 insert with depth ratio of 0.216 [51]. The experiments were conducted at a heat flux of 2 kW/m^2 and all tapes had a twist ratio of 5.

It can therefore be concluded that no enhancement occurred in the laminar and turbulent flow regimes with a CCCTT insert compared with PUCTT and CTT inserts. However, significant heat transfer enhancements were observed in the transitional flow regime and transition occurred earlier when CCCTT inserts were used.

6.3 Connection angle

Fig. 6.3 compares the Colburn *j*-factors (Fig. 6.3(a)) and friction factors (Fig. 6.3(b)) as a function of Reynolds number for different connection angles (θ = 0°, 30° and 60°) at a heat flux of 3 kW/m^2. Fig. 6.3(a) indicates that using different connection angles had no heat transfer enhancement effect in the laminar flow regime. In the turbulent flow regime at a Reynolds number of 2 000, an increase of 13% and 23% compared to a connection angle of 0°, occurred for connection angles of 30° and 60° respectively. Similar enhancement trends occurred in the turbulent flow regime for the friction factors in Fig. 6.3(b). Therefore, the increased disturbance caused by the connection angle enhanced mixing inside the test section which led to increased heat transfer coefficients. However, this enhancement decreased with increasing Reynolds numbers, because the effect of the disturbance caused by the connection became less significant compared with the turbulent inertia of the fluid.

For the Colburn *j*-factors (Fig. 6.3(a)) the transition started and ended at Reynolds numbers of 997 and 1 308, 973 and 1 271, and 920 and 1 200 for the respective connection angles of 0°, 30° and 60°. The transitional flow regime was thus occurred earlier as the connection angle increased. At a Reynolds number of 1 000, the Colburn *j*-factors were 0.0175, 0.0190 and 0.0219 respectively, for connection angles of 0°, 30° and 60°. Thus, the Colburn *j*-factors also increased with connection angles and were 25% higher for a connection angle of 60° than for a connection angle of 0°. The Reynolds numbers at which the transitional flow regime started, Re_{cr}, ended, Re_{qt}, as well as the width of the transitional flow regime, ΔRe [29], are summarized in Table 6.1. It should be noted that the Colburn *j*-factor results and friction factor results were very similar and the same conclusions can be made from both.

Table 6.1 indicates that for all heat fluxes, the critical Reynolds number decreased with increasing connection angle. This was due to the increased disturbance and swirl caused by the connection angle, combined with the sudden change in flow direction, that disturbed the boundary layer. Table 6.1 also indicates that similar to the start of the transitional flow regime, the end of the transitional flow regime, Re_{qt}, occurred earlier with increasing connection angle. Furthermore, as the connection angle was increased from 0° to 60° the width of the transitional flow regime, ΔRe, decreased from a Reynolds number range of 311 to 280.

It can therefore be concluded that an increase in connection angle caused a greater disturbance inside the test section that not only enhanced the heat transfer in the transitional flow regime, but also caused transition to occur earlier and the width of the transitional flow regime to decrease. However, there were no significant enhancements in the laminar and turbulent flow regimes.

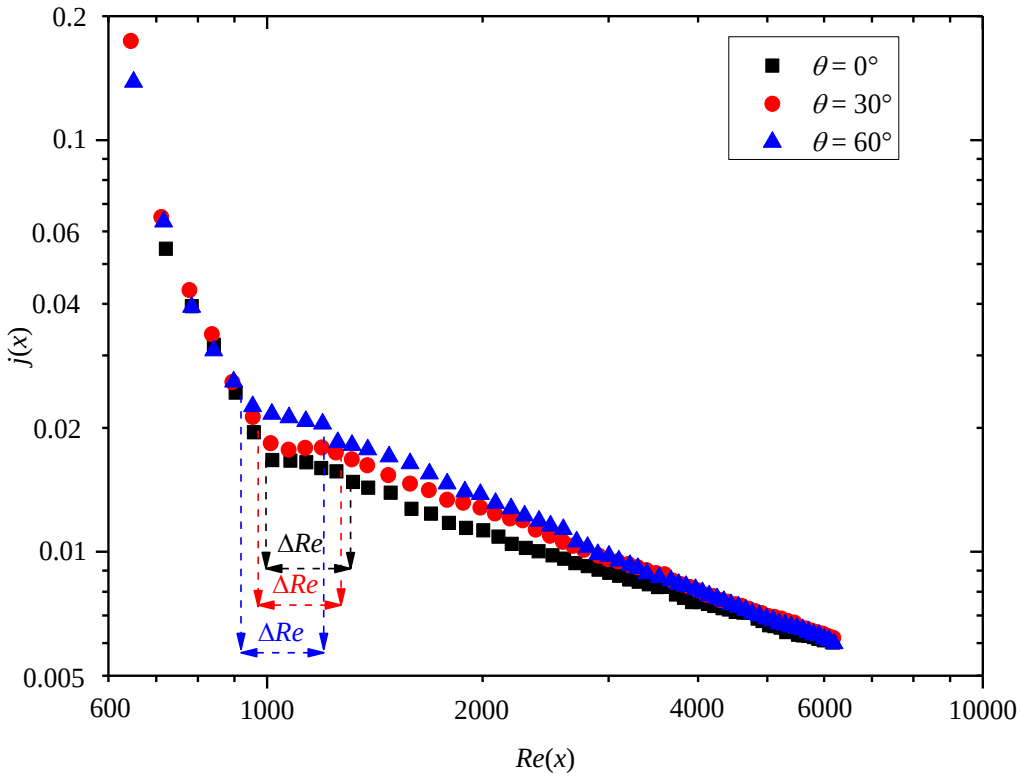

(a)

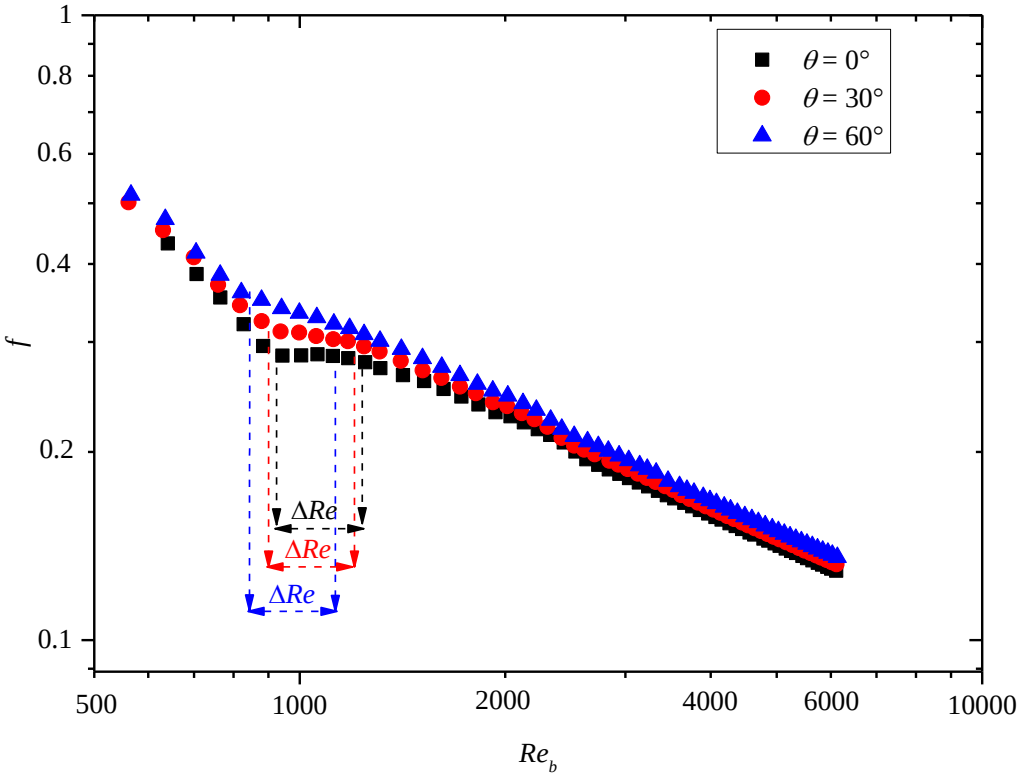

(b)

Fig. 6.3. Comparison of (a) Colburn *j*-factors as a function of local Reynolds number at $x/D_i = 246$ and (b) friction factors as a function of bulk Reynolds number at $x/D_i = 198$, for CCCTT inserts at the heat flux of 3 kW/m^2 and at different connection angles.

Table 6.1. Summary of the start, end and width of transitional flow regime for the Colburn *j*-factors and friction factors with CCCTT inserts.

Connection angle, θ	Symbols	Heat flux, $\dot{q}$ [kW/m^2]							
		1.35	2	3	4	1.35	2	3	4
		Colburn *j*-factors, *j*				Friction factors, *f*			
0°	Re_{cr}	584	722	997	1 212	553	675	980	1 108
	Re_{qt}	948	1 055	1 308	1 502	917	1 010	1 237	1 404
	ΔRe	363	333	311	290	364	335	314	296
30°	Re_{cr}	563	705	973	1 184	532	657	898	1 082
	Re_{qt}	894	1 008	1 271	1 465	864	962	1 200	1 368
	ΔRe	331	303	298	281	332	305	302	286
60°	Re_{cr}	529	685	920	1 173	498	637	844	1 070
	Re_{qt}	847	978	1 200	1 413	818	932	1 127	1 314
	ΔRe	318	289	280	240	320	295	283	244

6.4 Heat flux

Fig. 6.4 compares the Colburn *j*-factors (Fig. 6.4(a)) and friction factors (Fig. 6.4(b)) as a function of Reynolds number at different heat fluxes for a CCCTT insert with a connection angle of θ = 30°. This figure indicates that the increasing free convection effects due to the increased heat flux caused the Colburn *j*-factors and friction factors in the laminar flow regime to increase [29, 30, 135, 187]. At a laminar Reynolds number of 500, the Colburn *j*-factor enhancement was 103% when the heat flux was increased from 1.35 kW/m^2 to 2 kW/m^2. As expected, the heat flux did not affect the results in the turbulent flow regime, because free convection effects were negligible compared with the inertia forces [29].

The Colburn *j*-factors in Fig. 6.4(a) also indicate that the start, end and width of the transitional flow regime were significantly affected by free convection effects. At a heat flux of 1.35 kW/m^2, the transitional flow regime started and ended at Reynolds numbers of 563 and 894, respectively. As the heat flux was increased to 4 kW/m^2, both the start and end of transition were delayed to Reynolds numbers of 1 184 and 1 465, respectively. Furthermore, the width of the transitional flow regime, ΔRe, decreased from a Reynolds number range of 331 at a heat flux of 1.35 kW/m^2, to 281 at a heat flux of 4 kW/m^2. The same trends were found in the friction factor results (Fig. 6.4(b) and Table 6.1), the results of the other connection angles, as well as previous studies [15, 29-32, 49, 232]. Everts and Meyer [29] explained that although free convection effects caused the transitional flow regime to occur at lower mass flow rates, the Reynolds numbers at which transition started and ended increased. The gradient of the fluid temperature along the test section increased with increasing heat flux, which led to decreasing viscosities and increased Reynolds numbers. Furthermore, Everts and Meyer [29, 30, 232] also found that as free convection effects were increased, a shorter tube length was required for the flow to transition from laminar to turbulent along the tube length, which explains why the width of the transitional flow regime decreased with increasing heat flux.

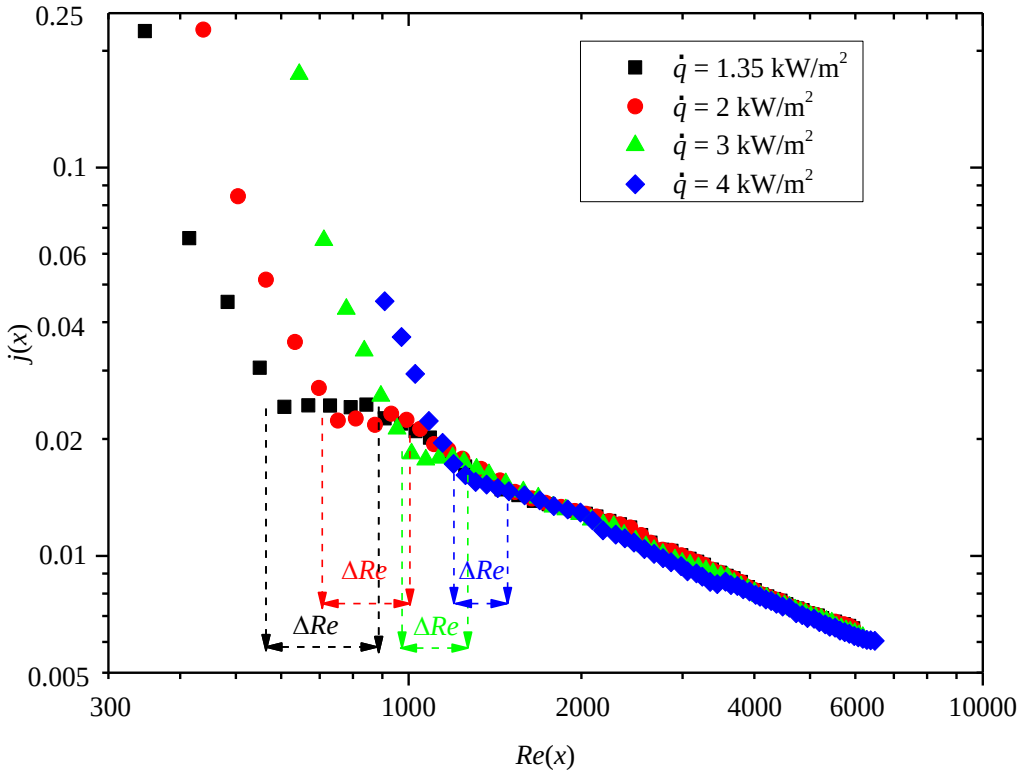

(a)

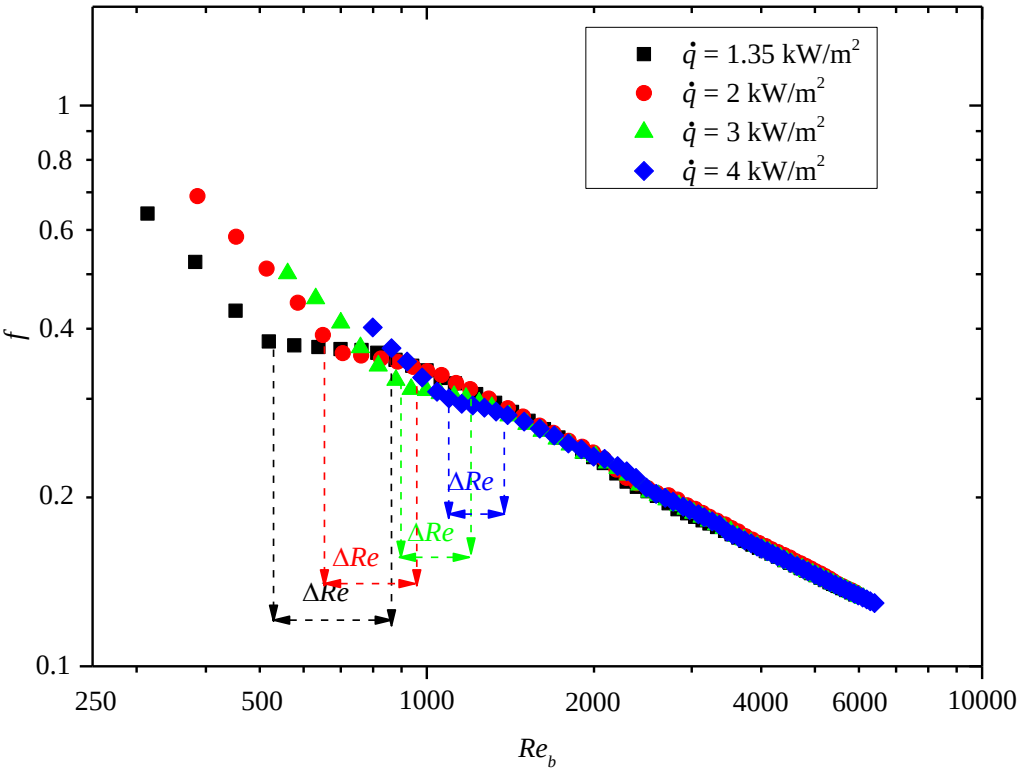

(b)

Fig. 6.4. Comparison of (a) Colburn *j*-factors as a function of local Reynolds number at $x/D_i = 246$ and (b) friction factors as a function of bulk Reynolds number at $x/D_i = 198$, for CCCTT inserts with a connection angle of 30° and for heat fluxes of 1.35, 2, 3 and 4 kW/m².

In general, it can therefore be concluded that an increase in heat flux significantly enhanced the heat transfer in the laminar flow regime, delayed transition and decreased the width of the transitional flow regime. However, an increase in the heat flux had no significant effect in the turbulent flow regime.

6.5 Correlations

Three sets of correlations were developed to predict the experimental data of this study: (1) Correlations to predict the start and the end of the transitional flow regime as a function of connection angle (Fig. 6.5). (2) Correlations to predict the Colburn *j*-factors in the laminar, transitional and turbulent flow regimes (Fig. 6.6). (3) Correlations to predict the friction factors in the same three flow regimes. The ranges and performance of the different correlations are summarized in Table 6.2. In Fig. 6.5 the filled markers represent the Colburn *j*-factor data, while the empty markers represent the corresponding friction factor data. As illustrated in Fig. 6.6 the filled black markers represent the data at a heat flux of 1.35 kW/m^2, while the empty red, blue and magenta markers represent the results at heat fluxes of 2 kW/m^2, 3 kW/m^2 and 4 kW/m^2 respectively. Furthermore, the squares, circles and triangles represent the connection angles of 0°, 30° and 60°.

6.5.1 Start and end of the transitional flow regime

Fig. 6.3 and Fig. 6.4 indicated that the start and the end of the transitional flow regime were influenced by connection angle, θ, and free convection effects (heat flux). To account for different connection angles, a cosθ-term was introduced, while the modified Grashof number, Gr^*, was used to account for free convection effects. The critical Reynolds numbers, Re_{cr}, in Table 6.1 were divided by $[Gr^*(x)]^{0.416}$ and plotted as a function of cosθ in Fig. 6.5(a). The exponent 0.416 was found through power curve. A power curve fit was done through the data points to obtain the following correlation to predict the start of the transitional flow regime:

$$Re_{cr}(x) = 1.46[Gr^*(x)]^{0.416}[cos\theta]^{0.158} \quad (6.1)$$

A similar approach was followed to determine the end of transitional flow regime from the results in Fig. 6.5(b):

$$Re_{qt}(x) = 19.4[Gr^*(x)]^{0.275}[cos\theta]^{0.143} \quad (6.2)$$

The corresponding bulk Reynolds numbers for the start, Re_{crb}, and end, Re_{qtb}, of the transitional flow regime in terms of the friction factors were obtained by replacing the $Gr^*(x)$ in Eqs. (6.1) and (6.2) with the bulk modified Grashof number, Gr^*_b. The ranges and performance of Eqs. (6.1) and (6.2) are summarized in Table 6.2. This table indicates that the start and end of transitional flow regime of both the Colburn *j*-factor and friction factor results could be determined within 6%.

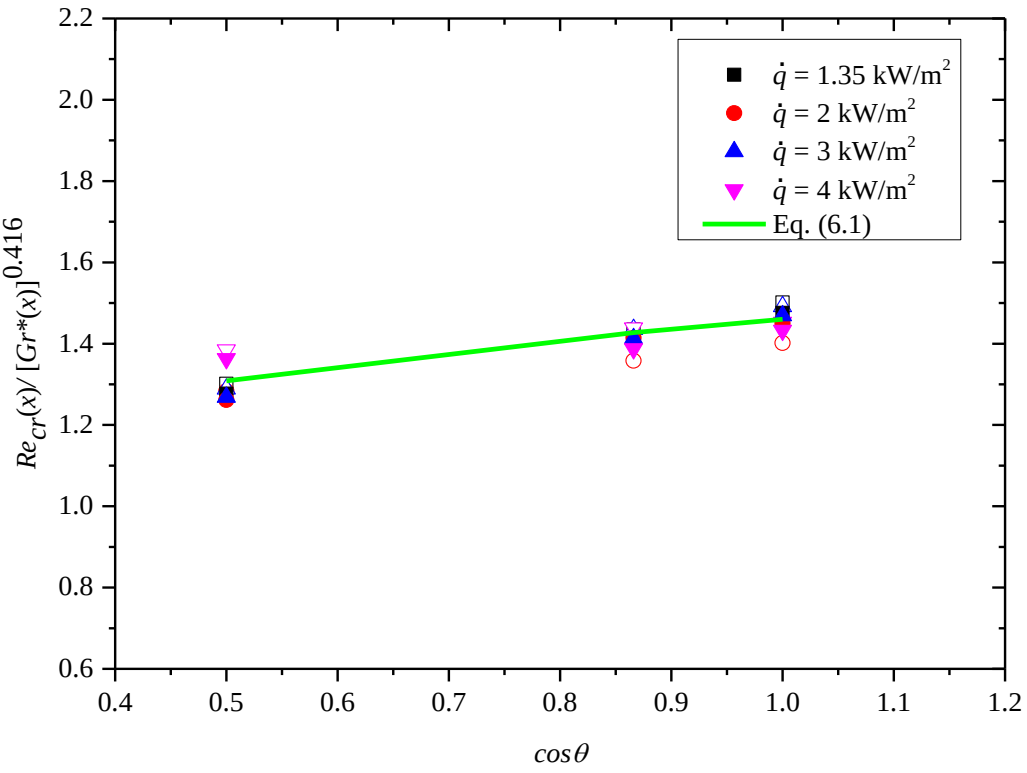

(a)

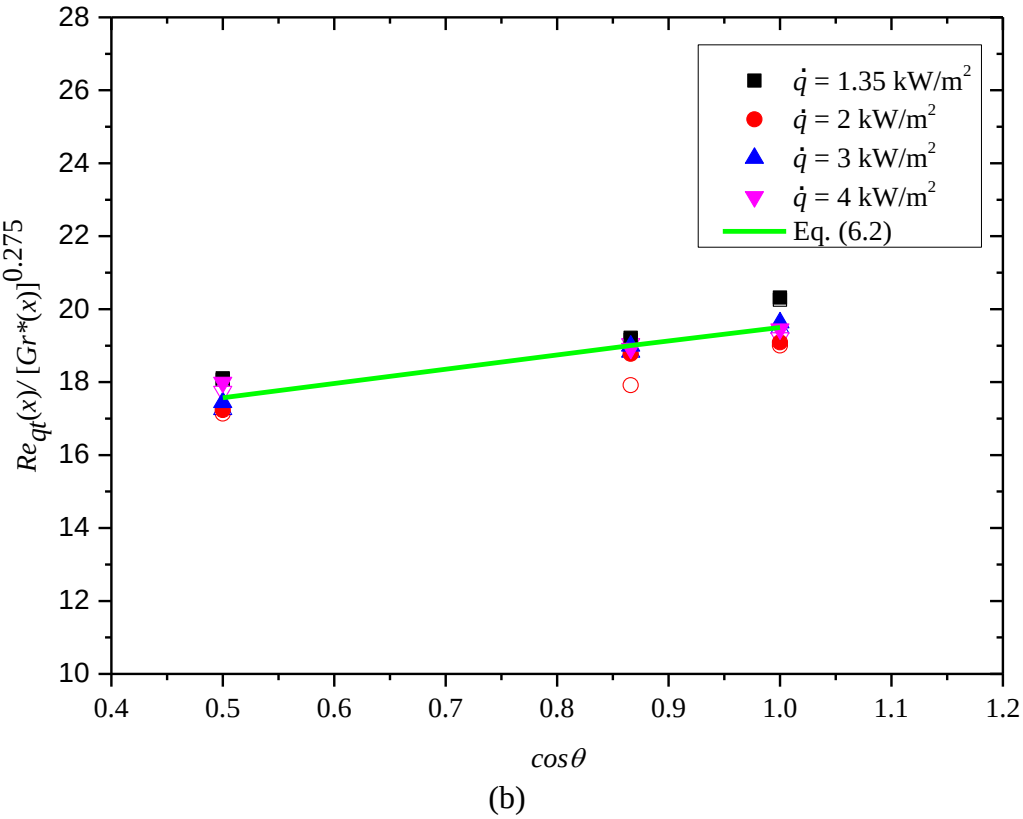

(b)

Fig. 6.5. Heat transfer and pressure drop results in terms of (a) $Re_{cr}(x)/[Gr^*(x)]^{0.416}$ to obtain the start of the transitional flow regime (Eq. 6.1) and (b) $Re_{qt}(x)/[Gr^*(x)]^{0.275}$ to obtain the end of the transitional flow regime (Eq. 6.2), as a function of cosθ.

6.5.2 Colburn *j*-factors

The laminar Colburn *j*-factors decreased with increasing Reynolds number (Fig. 6.1) and increased with increasing free convection effects (Fig. 6.4(a)), but were not significantly affected by the connection angle (Fig. 6.3(a)). Therefore, the laminar Colburn *j*-factors were divided by $[Gr^*(x)]^{0.61}$ to account for free convection effects and the results were plotted as a function of Reynolds number in Fig. 6.6(a). Again, the power of 0.61 was determined through power curve. The following laminar Colburn *j*-factors correlation was obtained through a power curve fit:

$$j_L(x) = 6.52[Re(x)]^{-2.25}[Gr^*(x)]^{0.61} \quad 6.3$$

Table 6.2 indicates that the average and maximum deviations were 3 and 12% respectively.

In the transitional flow regime, it was found that the Colburn *j*-factors were significantly influenced by the Reynolds number (Fig. 6.1), connection angle (Fig. 6.3(a)), as well as the free convection effects (Fig. 6.4(a)). Therefore, the following correlation was developed to predict the Colburn *j*-factors in the transitional flow regime:

$$j_R(x) = 2.37[Re(x)]^{-0.337}[Gr^*(x)]^{-0.168}[cos\theta]^{-0.356} \quad 6.4$$

Table 4 indicates that Eq. 6.4 was able to predict all the Colburn *j*-factors in the transitional flow regime with an average deviation of 3% and a maximum deviation of 13%.

Fig. 6.3(a) and Fig. 6.4(a) indicated that the turbulent Colburn *j*-factors were a function of Reynolds number and connection angle, but not a function of modified Grashof number because free convection effects were suppressed by the inertia forces of the fluid [29]. The turbulent Colburn *j*-factor correlation was developed from the results in Fig. 6.6(c):

$$j_T(x) = 1.57[Re(x)]^{-0.641}[cos\theta]^{-0.102} \quad 6.5$$

Eq. (6.5) performed very well and was able to predict the experimental data with average deviation of 2% and a maximum deviation of 13%.

6.5.3 Friction factors

Similarly, the following correlations were developed to predict the friction factors in the laminar, transitional and turbulent flow regimes (friction factor figures that correspond to the Fig. 6.6 were not included in this thesis as it looks similar). For laminar flow:

$$f_L = 10.6[Re_b]^{-0.849}[Gr_b^*]^{0.141}[cos\theta]^{-0.176} \quad 6.6$$

and for transitional flow:

$$f_R = 5.77[Re_b]^{-0.252}[Gr_b^*]^{-0.0815}[cos\theta]^{-0.214} \quad 6.7$$

and for turbulent flow:

$$f_T = 11.6[Re_b]^{-0.517}[cos\theta]^{-0.079} \quad 6.8$$

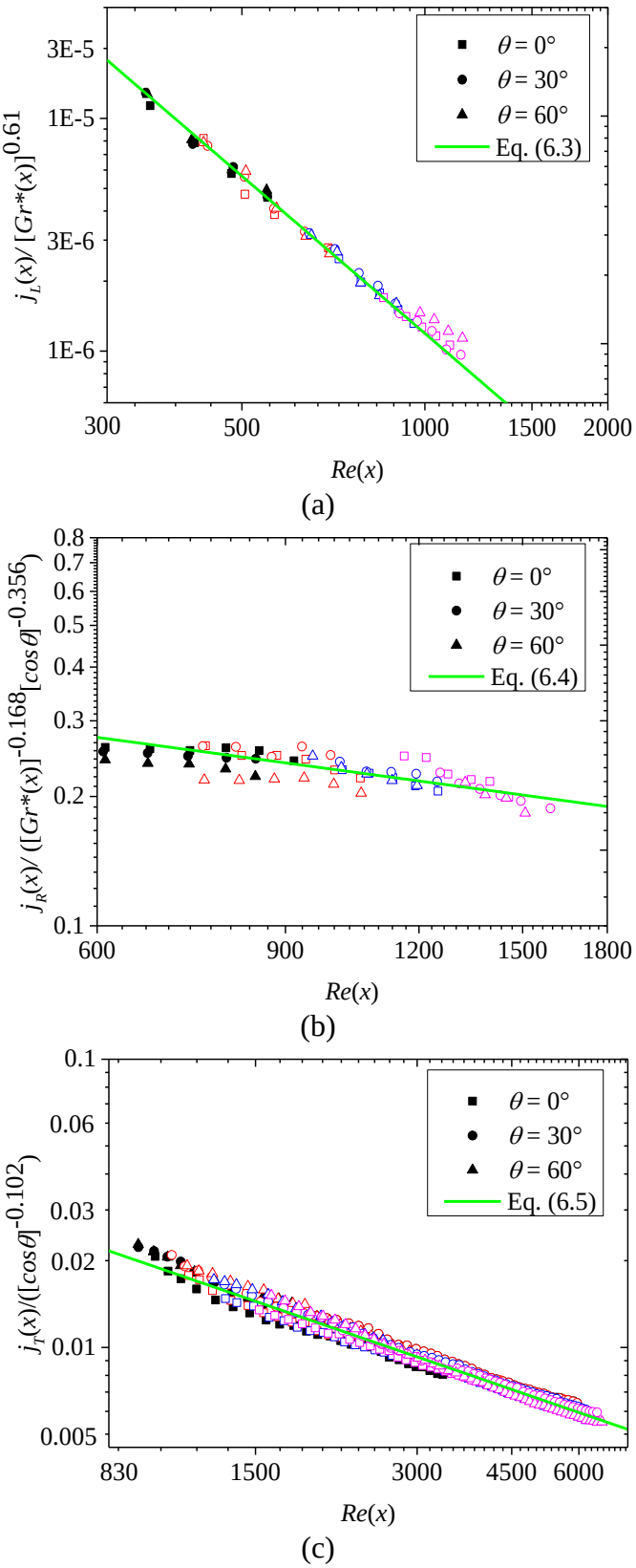

Fig. 6.6. Heat transfer results as a function of Reynolds number to obtain Colburn *j*-factor correlations in the (a) laminar flow regime (Eq. 6.3), (b) transitional flow regime (Eq. 6.4) and (c) turbulent flow regime (Eq. 6.5) for different connection angles and heat fluxes.

Table 6.2. The ranges and performance of the Colburn *j*-factor (section 6.5.2) and friction factor (section 6.5.3) correlations of the CCCTT inserts.

		Eq.	Average deviation [%]	Maximum deviation [%]	Range
Transitional flow regime boundaries	Re_{cr}	(6.1)	1	6	$533 \leq Re(x) \leq 1\,173$ $1.47 \times 10^6 < Gr^*(x) < 1.13 \times 10^7$ $0° \leq \theta \leq 60°$ $y = 5$
	Re_{qt}	(6.2)	0.1	6	$917 \leq Re(x) \leq 1\,413$ $1.03 \times 10^6 < Gr^*(x) < 7.78 \times 10^6$ $0° \leq \theta \leq 60°$ $y = 5$
Colburn *j*-factors	Laminar	(6.3)	3	12	$300 < Re(x) < 1\,200$ $1.83 \times 10^6 < Gr^*(x) < 3.2 \times 10^7$ $0° \leq \theta \leq 60°$ $y = 5$
	Transitional	(6.4)	3	13	$600 < Re(x) < 1\,500$ $1.18 \times 10^6 < Gr^*(x) < 1.2 \times 10^7$ $0° \leq \theta \leq 60°$ $y = 5$
	Turbulent	(6.5)	2	13	$900 < Re(x) < 6\,600$ $8 \times 10^5 < Gr^*(x) < 7.13 \times 10^6$ $0° \leq \theta \leq 60°$ $y = 5$
Friction factors	Laminar	(6.6)	5	17	$300 < Re_b < 1\,200$ $1.52 \times 10^6 < Gr^*_b < 2.3 \times 10^7$ $0° \leq \theta \leq 60°$ $y = 5$
	Transitional	(6.7)	2	10	$570 < Re_b < 1\,400$ $1.06 \times 10^6 < Gr^*_b < 9.26 \times 10^6$ $0° \leq \theta \leq 60°$ $y = 5$
	Turbulent	(6.8)	1	8	$878 < Re_b < 6\,400$ $7.54 \times 10^5 < Gr^*_b < 5.86 \times 10^6$ $0° \leq \theta \leq 60°$ $y = 5$

The ranges and performance of Eqs. (6.6) – (6.8) are summarized in Table 6.2. This table indicates all the correlations performed well and were able to predict the friction factors in the laminar, transitional and turbulent flow regimes with average deviations of 5%, 2% and 1% respectively.

6.6 Summary and conclusions

The heat transfer and pressure drop characteristics of a smooth horizontal tube with CCCTT inserts at different connection angles were experimentally investigated in the laminar, transitional and turbulent flow regimes for different constant heat fluxes. The CCCTT inserts consisted of clockwise and counter clockwise segments with a twist ratio of 5 and length of 450 mm. Therefore, flow rotation was changed every 450 mm and the different segments were connected at connection angles of 0°, 30° and 60°. Experiments were conducted at four different constant heat fluxes and a total of 720 experimental data points was obtained in this study.

The comparison of the Colburn *j*-factor and friction factor results of the CCCTT insert with the CTT and PUCTT inserts showed no enhancement in the laminar flow regime. In the transitional flow regime significant heat transfer enhancements occurred and transition of the CCCTT occurred earlier than with the PUCTT and CTT inserts. In the turbulent flow regime, the heat transfer enhancements of the CCCTT insert were slightly better than that of the CTT insert.

When different connection angles were compared it was found that the increased disturbance created by an increased connection angle enhanced mixing inside the test section, which led to increased heat transfer. Furthermore, it also caused transition to occur at lower Reynolds numbers. However, the connection angle had no significant effect in the laminar and turbulent flow regimes. An increase in heat flux was found to enhance heat transfer in the laminar flow regime and delay transition, however, the turbulent flow regime remained unaffected.

Correlations to predict the start and end of the transitional flow regime, as well as the Colburn *j*-factors and friction factors in the laminar, transitional, and turbulent flow regimes of the CCCTT inserts were developed. These correlations were developed as a function of the Reynolds number, connection angle, and modified Grashof number, to account for different connection angles as well as free convection effects where relevant.

7. Heat transfer and pressure drop in the transitional flow regime with peripheral u-cut twisted tape inserts

7.1 Introduction

This chapter presents the experimental results of the heat transfer and pressure drop characteristics in a smooth tube heat exchanger with peripheral u-cut (PUCTT) inserts with depths of cuts of 0.105 and 0.216 without rings and with rings (PUCTTR) of ring space ratios of 1.25, 2.5 and 5 at the twist ratio of 5 and heat flux of 1.35 kW/m^2. The heat transfer results were presented in terms of Colburn *j*-factors, while the pressure drop results in terms of friction factors. The performance of the PUCTT insert was compared with CCCTT and CTT inserts. Thereafter, the influence of depth ratios and ring space ratios on the transitional flow regime were discussed. Heat transfer and pressure drop correlations were developed as a function of Reynolds number, depth ratio and ring space ratio. The results contained in this chapter were published in Abolarin et al. [51].

Ideally, for the test section (with inner diameter of 19 mm) used in this study, the forced convection laminar thermal entrance was estimated to be $L_{th} = 0.12RePrD_i = 16$ m (at a Reynolds number of 1 000 and Prandtl number of 7 and without any tape inserts) [31]. Although this is longer than the test section, Meyer and Everts [31] found that the thermal entrance decrease significantly for mixed convection conditions, which exist in this study. For turbulent flow, the flow was expected to be fully developed at $x = 10D_i = 0.19$ m. However, similar to the results obtained by Meyer and Abolarin [49], the results of this chapter indicated that in all the three flow regimes (laminar, transitional and turbulent) and for all the cases in Table 3.3 and Table 3.4 only the first measuring station, $x/D_i = 9$, exhibited thermally developing flow characteristics. Subsequently from the second measuring station, $x/D_i \geq 22$, to the last measuring station at the, $x/D_i = 272$, the flow was thermally fully developed as the heat transfer coefficients were independent of the axial length. In the laminar flow regime, it was found that mixed convection conditions existed because a significant difference in the temperature measurements at the top and bottom of tube existed. Furthermore, the recent work of Meyer and Everts [31] and Everts and Meyer [232] also predicted that the flow regime is mixed convection.

The decreased thermal entrance length in the laminar flow regime ($L_{th} \approx 22D_i \approx 0.42$ m) was due to the fluid rotation from the twisted tape inserts as well as free convection effects that led to mixed convection [31]. Therefore, the heat transfer (Colburn *j*-factor) results could be represented in two ways: (1) as the average of the fully developed data ($22 \leq x/D_i \leq 272$) (Fig. 3.7) or (2) at a specific measuring station as was used in the work of Ghajar and Tam [15, 16, 21]. Similar to Meyer and Abolarin [49], the heat transfer results were presented

as local values at $x/D_i = 246$ and compared with the mean values with a maximum deviation of 6%. The pressure drop data were the average between pressure taps at $x/D_i = 133$ and $x/D_i = 262$ and the bulk fluid temperature was obtained at $x/D_i = 198$.

In general, it should be noted when the heat transfer (Colburn *j*-factors) and pressure drop (friction factors) results were evaluated, the trends of the heat transfer and pressure drop characteristics were in many cases not well aligned. There are two reasons for this. Firstly, the results were plotted on log-log graphs and especially the *y*-scales of the Colburn *j*-factors and friction factors differed with an order of magnitude. Secondly, the enhancements of the heat transfer results in the laminar flow regime were more accurate, because the temperature differences were high (low Colburn *j*-factor uncertainties), while the pressure drops were low (high friction factor uncertainties). The opposite was true in the turbulent flow regime. Thus, in the laminar flow regime, the heat transfer results give a better indication of heat transfer enhancement, while in the turbulent flow regimes the pressure drop results are more accurate to investigate the influence of twisted tape inserts. The heat transfer and pressure drop results are directly related in all three flow regimes as has been shown by Everts and Meyer [30]. The transitional flow regime, which was the focus of this experimental study, was identified using the linear line technique proposed by Meyer and Abolarin [49], and also used successfully by Abolarin et al. [50]. With this technique it was possible to determine the start, end and width of the transition for both the Colburn *j*-factors and friction factors.

7.2 Comparison of PUCTT, CCCTT and CTT inserts

Fig. 7.1 compares the Colburn *j*-factors (Fig. 7.1(a)) and friction factors (Fig. 7.1(b)) results as a function of Reynolds number for the PUCTT insert of depth ratio, $R_d = 0.216$ (PUCTT22), with a CCCTT insert [50] and CTT insert [49] (without peripheral cuts). The experiments were conducted at a heat flux of 2 kW/m^2, the CCCTT insert had a connection angle of 60°, while the PUCTT and CTT inserts were twisted only in one direction and all twisted tape inserts had a twist ratio of $y = 5$.

Fig. 7.1(a) indicates that the PUCTT22 insert did not lead to any heat transfer enhancement in the laminar flow regime when compared with the CCCTT and CTT inserts. In the turbulent flow regime, the heat transfer enhancements varied between approximately 4% and 15%, while the friction factors increased by approximately 20% and 40% compared with the CCCTT and CTT inserts respectively Fig. 7.1(b).

Fig. 7.1 indicates that two important changes occurred in the transitional flow regime. Firstly, the transitional flow regime occurred earlier when PUCTT22 insert was compared with CTT insert, while it was delayed when compared with CCCTT insert. The transitional flow regime started, Re_{cr}, and ended, Re_{qt}, at Reynolds numbers of 1 023 and 1 604 respectively when CTT inserts were used, also the Reynolds numbers decreased to 796 and 1 344 respectively, when PUCTT22 inserts were used, while the Reynolds numbers decreased to 685 and 978 when the CCCTT insert was used. Secondly, a heat transfer enhancement of approximately 12% at a Reynolds number of 1 000 occurred in the transitional flow regime when PUCTT22 insert were compared with CTT inserts. Furthermore, in the transitional flow regime, the performance of the CCCTT inserts were approximately 30% higher than PUCTT22 inserts.

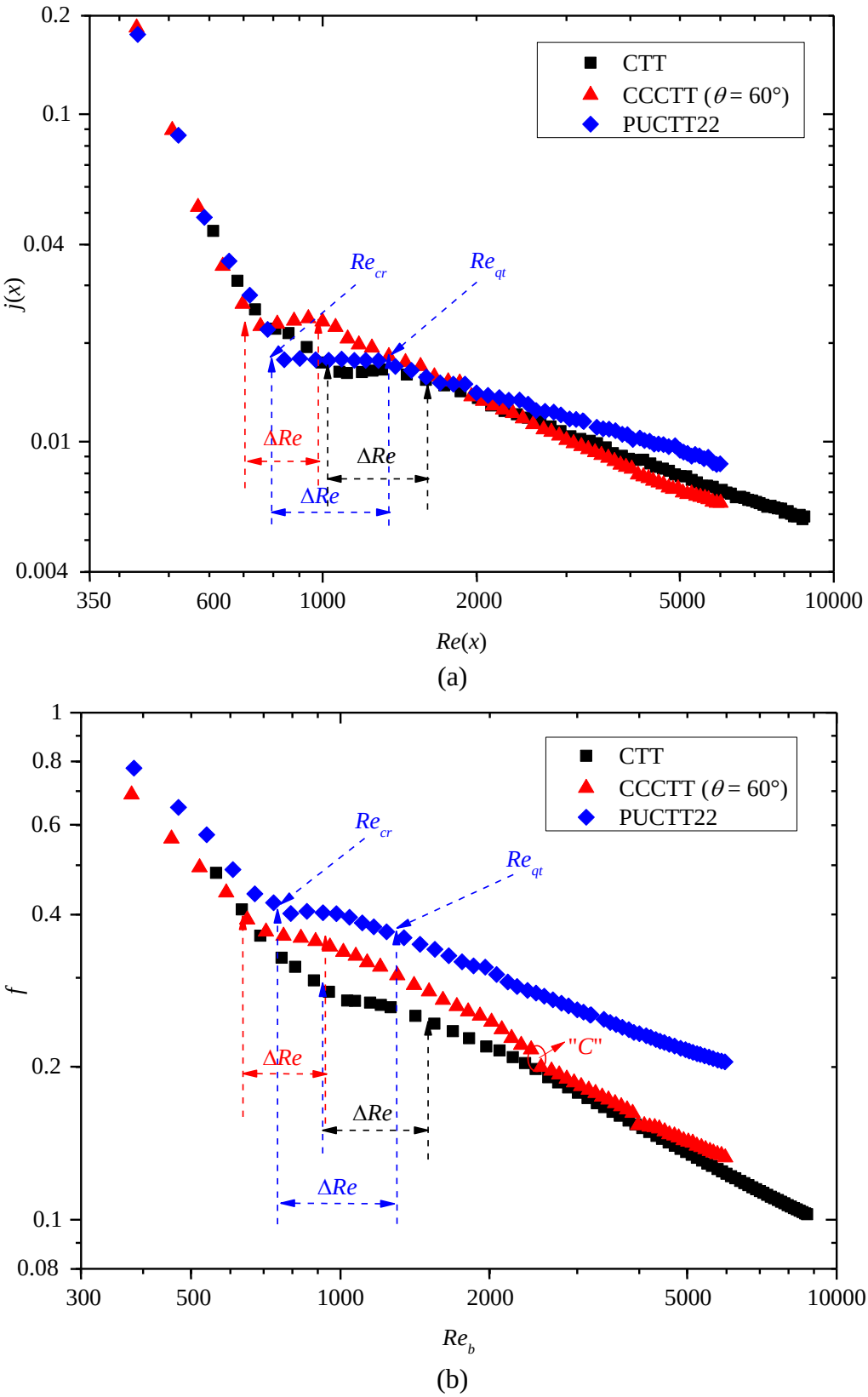

Fig. 7.1. Comparison of (a) Colburn *j*-factors as a function of local Reynolds number at the measuring station, x/D_i = 246, and (b) friction factors as a function of bulk Reynolds number (at x/D_i = 198) for the PUCTT22, CCCTT with connection angle of 60° and CTT inserts. The experiments were conducted at a heat flux of 2 kW/m^2 and all tapes had a twist ratio of 5.

It can therefore be concluded that the u-cuts on the twisted tapes not only enhanced heat transfer in the transitional flow regime, but also caused transition to occur at much lower Reynolds numbers. This was possibly due to the u-cuts that caused recirculation zones and disturbances on the boundary layer near the tube wall. This is not only of academic importance, but is applicable to many industry applications where glycol rather than water needs to be used such as in chillers in cold climates. As the pressure drops are significantly higher when glycol is used than when water is used, the corresponding operating Reynolds numbers can fall in the laminar flow regime where there is poor heat transfer performance (Fig. 7.1(a)).

7.3 Depth ratio

Fig. 7.2 compares the Colburn *j*-factors (Fig. 7.2(a)) and friction factors (Fig. 7.2(b)) as a function of Reynolds number for the PUCTT insert with depth ratios of 0.105 (PUCTT1) and 0.216 (PUCTT2) at the heat flux of 1.35 kW/m^2.

Fig. 7.2(a) indicates that the depth ratio had no significant influence on the laminar Colburn *j*-factors, while the heat transfer results in the transitional flow regime were significantly affected. As the depth ratio was increased from 0.105 (PUCTT1) to 0.216 (PUCTT2), an increase of approximately 27% occurred at a Reynolds number of 1 000, because the Colburn *j*-factors increased from 0.0165 to 0.021. This increase was due to the prevalence of the swirl intensity of the fluid as it flowed in and around the periphery of the PUCTT insert with higher depth ratio [143, 190]. Furthermore, Fig. 7.2(a) also indicates that the start and end of the transitional flow regime occurred at lower Reynolds numbers as the depth ratio was increased from 0.105 to 0.216. Table 7.1 summarizes the Reynolds numbers at which transition started and ended, as well as the width of the transitional flow regime for different depth ratios. From this table it follows that increasing the depth ratio not only caused transition to occur at lower Reynolds numbers, but the width of the transitional flow regime decreased as well. The transitional flow regime occurred earlier with the PUCTT2 insert (depth ratio of 0.216), because this tape with higher depth ratio generated more swirl, which caused a greater disturbance in the boundary layer. In the turbulent flow regime, the Colburn *j*-factors of the PUCTT2 were approximately 10% higher than when PUCTT1 inserts were used. The increased swirl caused by the increased depth ratio enhanced the heat transfer inside the test section and led to increased heat transfer coefficients.

Fig. 7.2(b) compares the friction factors of the PUCTT1 and PUCTT2 inserts. As expected, the same conclusions can be made from the friction factor data as from the Colburn *j*-factor data. The only difference is the quantitative values of the enhancements. As summarized in Table 7.1 the start, end and width of the transitional flow regime obtained from the friction factor results are close (all within 2 - 6%), but not exactly the same from the Colburn *j*-factor results. This is because the Colburn *j*-factor data were based on the local Reynolds numbers (at x/D_i = 246) while the pressure drop results were based on the bulk Reynolds number at x/D_i = 198.

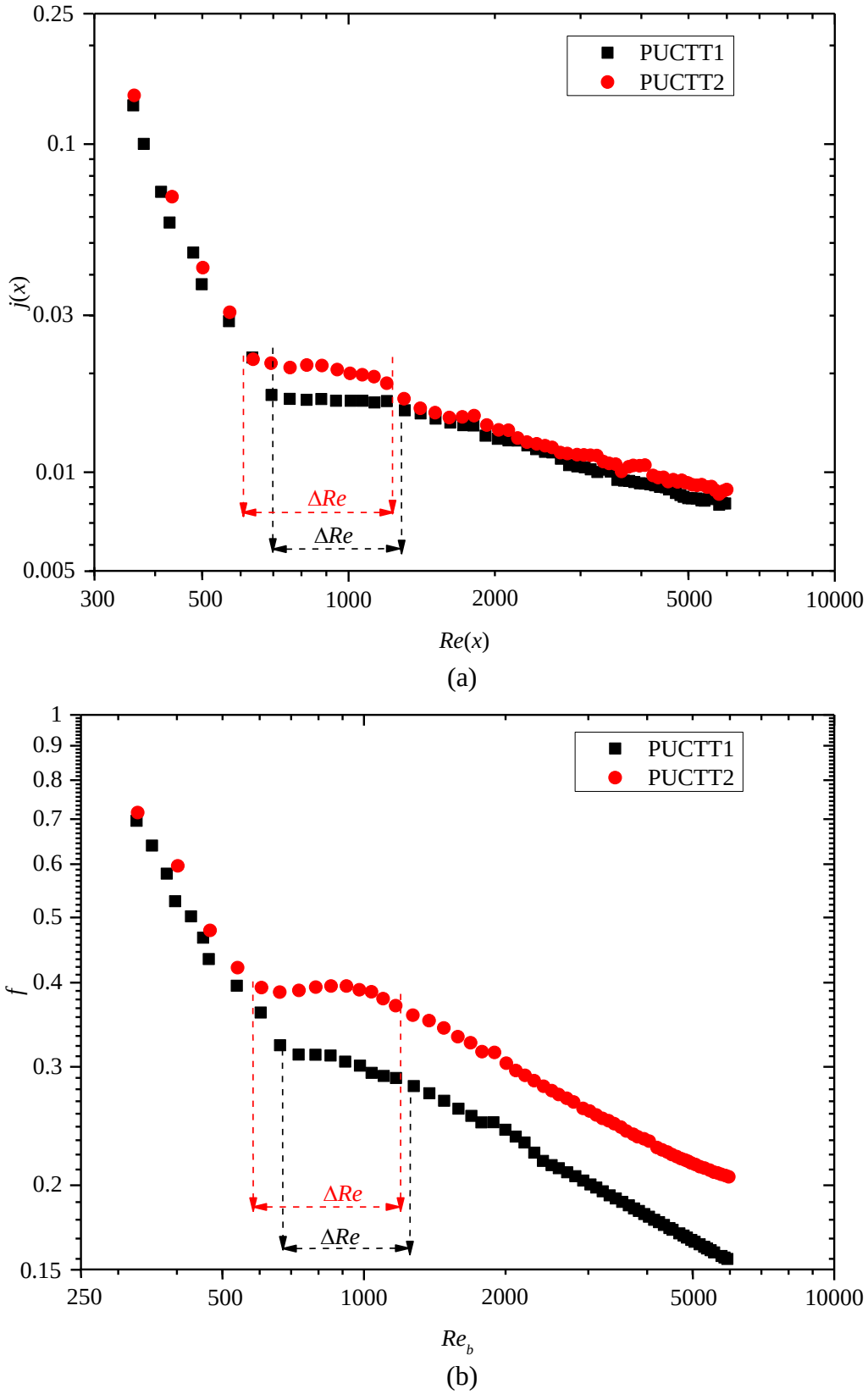

Fig. 7.2. Comparison of the (a) Colburn *j*-factors as a function of local Reynolds number at the measuring station, x/D_i = 246 and (b) friction factors as a function of bulk Reynolds number (at x/D_i = 198) of the PUCTT inserts of depth ratios of 0.105 (PUCTT1), with 0.216 (PUCTT2) and at heat flux of 1.35 kW/m^2.

Table 7.1. Summary of the start, end and width of the transitional flow regime for the Colburn *j*-factors and friction factors with the PUCTT and PUCTTR inserts.

	Depth ratio		Transition boundaries			Heat flux
	R_d	Insert	Re_{cr}	Re_{qt}	ΔRe	$\dot{q}$ [kW/m^2]
Colburn *j*-factor, *j*	0.105	PUCTT1	689	1 281	592	1.35
		PUCTTR11	587	1 079	492	1.35
		PUCTTR12	632	1 125	493	1.35
		PUCTTR13	662	1 157	495	1.35
	0.216	PUCTT2	640	1 225	585	1.35
		PUCTT22	796	1 344	548	2
		PUCTTR21	576	1 043	467	1.35
		PUCTTR22	603	1 084	481	1.35
		PUCTTR23	623	1 132	509	1.35
Friction factor, *f*	0.105	PUCTT1	657	1 265	608	1.35
		PUCTTR11	560	1 031	471	1.35
		PUCTTR12	595	1 096	501	1.35
		PUCTTR13	631	1 134	503	1.35
	0.216	PUCTT2	604	1 195	591	1.35
		PUCTT22	747	1 298	549	2
		PUCTTR21	554	1 037	483	1.35
		PUCTTR22	572	1 066	494	1.35
		PUCTTR23	616	1 116	500	1.35

7.4 Ring space ratio

Fig. 7.3 compares the Colburn *j*-factors (Fig. 7.3(a)) and the friction factors (Fig. 7.3(b)) as a function of Reynolds numbers when ring inserts were soldered on the PUCTT2 inserts at different ring insert pitches to form the PUCTTR21, PUCTTR22 and PUCTTR23 inserts. As summarized in Table 3.4, the PUCTTR21, PUCTTR22 and PUCTTR23 inserts corresponded to the tape insert with ring space ratios of 1.25, 2.5 and 5. Therefore, ring insert pitches were 22.5, 45 and 90 mm respectively.

Fig. 7.3(a) indicates that no significant heat transfer enhancement occurred in the laminar flow regime, while Fig. 7.3(b) indicates that the laminar friction factors increased as the ring space ratio decreased. Although this increase was expected (due to the increased disturbances caused by the ring inserts), it was not convincing, because the pressure drops in the laminar flow regime were very low and most the friction factor differences were within the uncertainties (approximately 20%).

Fig. 7.3 indicates that the ring inserts and ring space ratios had two major influences on the heat transfer and pressure drop characteristics in the transitional flow regime. Firstly, when the ring space ratio was reduced (thus more rings were used), the Colburn *j*-factors increased. For instance, at a Reynolds number of 800, when the ring space ratio was reduced from 5 (PUCTTR23) to 2.5 (PUCTTR22), and from 2.5 (PUCTTR22) to 1.25 (PUCTTR21), the Colburn *j*-factor increased by 17% (from 0.0232 to 0.0271) and 18% (from 0.0271 to 0.0319) respectively. Furthermore, when the Colburn *j*-factors of the PUCTTR21 inserts were compared with the PUCTT2 inserts, the results showed that the ring inserts caused the heat transfer to increase significantly by approximately 53%.

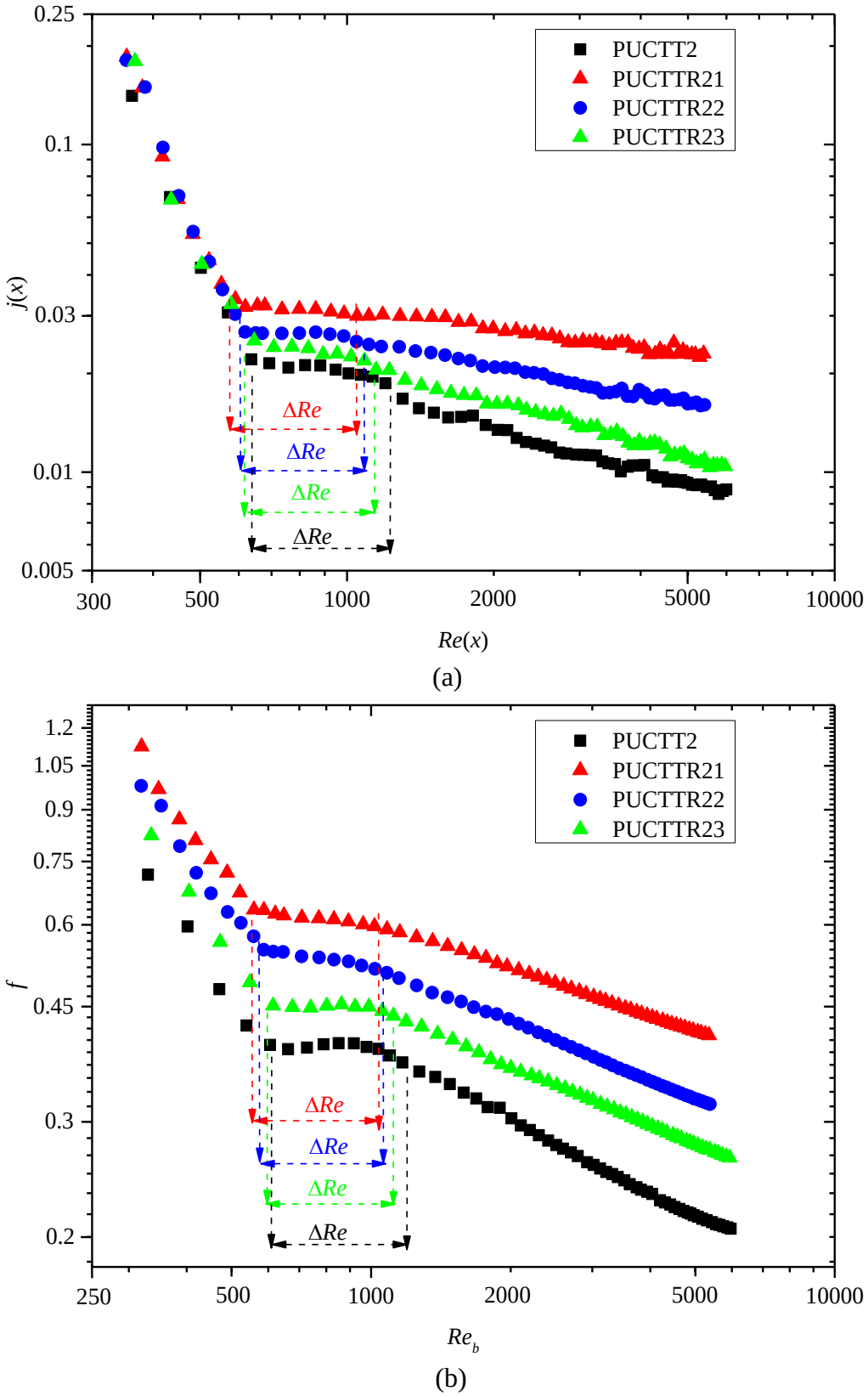

Fig. 7.3. Comparison of the (a) Colburn *j*-factors as a function of local Reynolds numbers at the measuring station, $x/D_i = 246$ and (b) friction factors as a function of bulk Reynolds number (at $x/D_i = 198$) of the PUCTT2, as well as PUCTTR21, PUCTTR22 and PUCTTR23 inserts with respective ring space ratios of 1.25, 2.5 and 5, at heat flux of 1.35 kW/m^2.

Secondly, the Reynolds numbers at which the transitional flow regime started and ended occurred earlier as the ring space ratio was reduced. Fig. 7.3(a) and Table 7.1 indicate that the transitional flow regime of the PUCTTR21 insert (ring space ratio of 1.25) started and ended at Reynolds numbers of 576 and 1 043 respectively. The corresponding Reynolds numbers for the PUCTTR22 and PUCTTR23 inserts were Re_{cr} = 603 and Re_{qt} = 1 084, and Re_{cr} = 623 and Re_{qt} = 1 132, respectively. The insertion of the rings caused the transition to occur earlier, because the rings tripped the laminar boundary layer and caused the laminar-turbulent transition along the tube length to occur faster. The transitional characteristics of the friction factors in Fig. 7.3(b) corresponded quantitatively to the Colburn *j*-factors.

The use of the rings also increased the heat transfer in the turbulent flow regime. For example, Fig. 7.3(a) indicated that at a Reynolds number of 2 000, the ring inserts led to heat transfer enhancements of 20% (PUCTTR23), 53% (PUCTTR22) and 103% (PUCTTR21) respectively compared with the PUCTT2 insert (no rings). Again, this heat transfer enhancement was because the rings increased the mixing of the fluid inside the test section.

7.5 Correlations

Correlations to predict the heat transfer coefficients and friction factors in the laminar, transitional and turbulent flow regimes for the PUCTT and PUCTTR inserts were developed. The correlations were a function of Reynolds number, depth ratio and ring space ratio and the ranges and performance of these correlations are summarized in Table 7.2. The exponents and coefficients of the correlations are within 95% confidence interval.

7.5.1 Colburn *j*-factors

Fig. 7.2(a) indicated that the laminar Colburn *j*-factors were a strong function of Reynolds number were not significantly affected by the depth ratio. Furthermore, when the laminar Colburn *j*-factors of PUCTT inserts (Fig. 7.2(a)) were compared with the PUCTTR inserts (Fig. 7.3(a)) the results indicated that the heat transfer coefficients were not significantly affected by the insertion of rings. Therefore, it was possible to develop a single correlation to predict the laminar Colburn *j*-factors as a function of Reynolds number for both the PUCTT and PUCTTR inserts using a power curve in Fig. 7.4(a):

$$j_L(x) = 1.1 \times 10^7 [Re(x)]^{-3.1} \qquad 7.1$$

As summarized in Table 7.2, the average and maximum deviations of Eq. (7.1) from the experimental data were 5 and 15% respectively.

It follows from the experimental results in Fig. 7.2(a) that the transitional Colburn *j*-factors of the PUCTT inserts were a strong function of Reynolds number and depth ratio. Furthermore, Fig. 7.3(a) indicated that for the PUCTTR inserts, the transitional Colburn *j*-factors were also influenced by the ring space ratio. Therefore, to develop a correlation to predict the Colburn *j*-factors of the PUCTT and PUCTTR inserts in the transitional flow regime, a term R_d, to account for the influence of the depth ratio, as well as a term R_r, to account for the influence of the ring space ratio, were used.

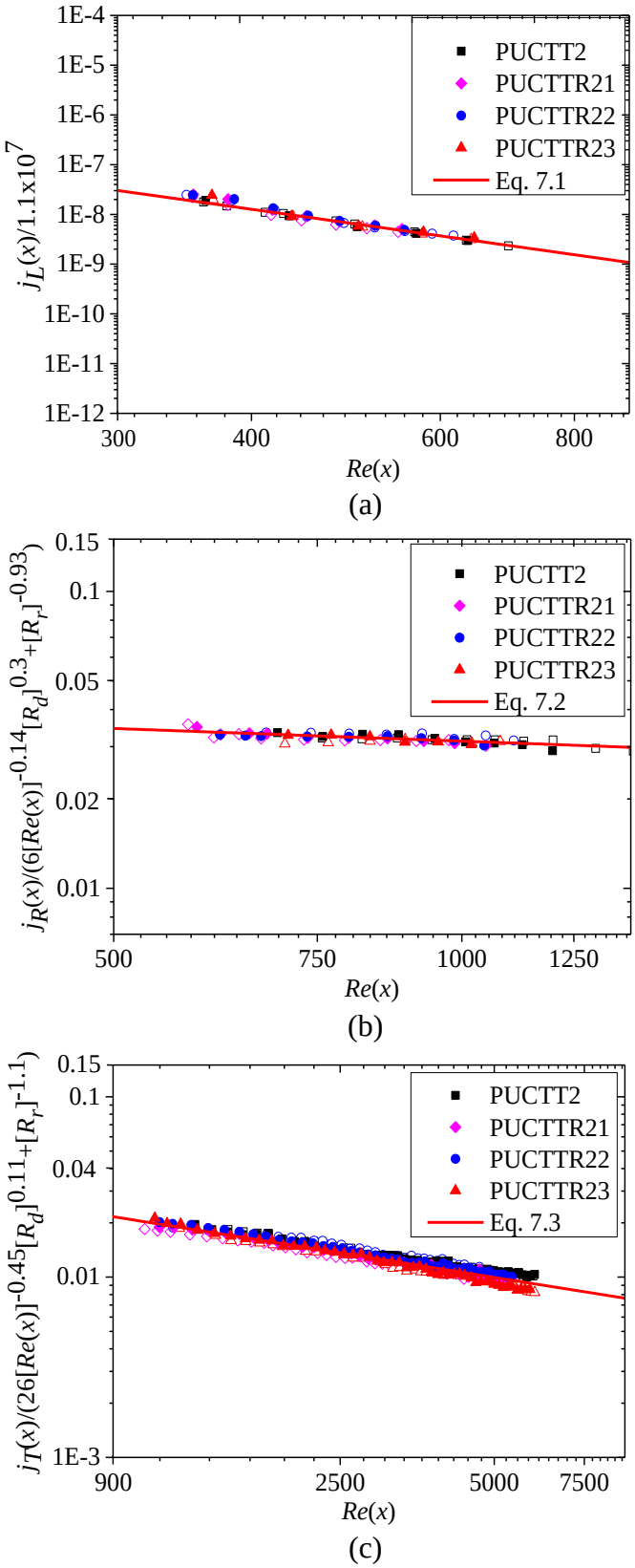

Fig. 7.4. Comparison of the results of the Colburn *j*-factors correlations developed with experimental data in the (a) laminar (Eq. 7.1), (b) transitional (Eq. 7.2), and (c) turbulent (Eq. 7.3) flow regimes for the PUCTT and PUCTTR inserts. The empty markers represent the results of the PUCTT and PUCTTR inserts with the depth ratio of 0.105, while the filled markers represent the results of the PUCTT and PUCTTR inserts with the depth ratio of 0.216. Furthermore, the black squares represent the results of the PUCTT inserts, while the magenta diamonds, blue circles and red triangles represent the results of the PUCTTR inserts with the ring space ratio of 1.25, 2.5 and 5 respectively.

From the results in Fig. 7.4(b), a single correlation was then obtained to predict the experimental transitional Colburn *j*-factors of the PUCTT and PUCTTR inserts as:

$$j_R(x) = 0.014[6[Re(x)]^{-0.14}[R_d]^{0.3}+[R_r]^{-0.93}] \quad 7.2$$

It can be concluded from Fig. 7.4(b) and Table 7.2 that the Eq. 7.2 performed well and able to predict the experimental data with a maximum deviation of 6%.

Table 7.2. The ranges and performances of the Colburn *j*-factors (section 7.5.1) and friction factors (section 7.5.2) correlations of the PUCTT and PUCTTR inserts.

		Eq.	Average deviation [%]	Maximum deviation [%]	Range
Colburn *j*-factors	Laminar	(7.1)	5	15	360 < *Re*(*x*) < 695 R_d = 0.105, 0.216 R_r = 0, 1.25, 2.5, 5 *y* = 5
	Transitional	(7.2)	1	6	580 < *Re*(*x*) < 1 400 R_d = 0.105, 0.216 R_r = 0, 1.25, 2.5, 5 *y* = 5
	Turbulent	(7.3)	1	6	1 000 < *Re*(*x*) < 6 000 R_d = 0.105, 0.216 R_r = 0, 1.25, 2.5, 5 *y* = 5
Friction factors	Laminar	(7.4)	2	8	315 < Re_b < 615 R_d = 0.105, 0.216 R_r = 0, 1.25, 2.5, 5 *y* = 5
	Transitional	(7.5)	1	6	549 < Re_b < 1 275 R_d = 0.105, 0.216 R_r = 0, 1.25, 2.5, 5 *y* = 5
	Turbulent	(7.6)	1	6	1 000 < Re_b < 6 623 R_d = 0.105, 0.216 R_r = 0, 1.25, 2.5, 5 *y* = 5

The following Colburn *j*-factor correlation, as a function of Reynolds number, depth ratio, and ring space ratio for PUCTT inserts in the turbulent flow regime was obtained from the experimental data in Fig. 7.4(c):

$$j_T(x) = 0.019[26[Re(x)]^{-0.45}[R_d]^{0.11}+[R_r]^{-1.1}] \quad 7.3$$

Fig. 7.4(c) and Table 7.2 indicate that Eq. 7.3 performed very well and was able to predict the experimental data within 7%.

7.5.2 Friction factors

Similarly, Eqs. (7.4) – (7.6) were developed to predict the friction factors in tubes with PUCTT and PUCTTR inserts in the laminar, transitional and turbulent flow regimes. Because the method and graphs were similar to the Colburn *j*-factors in Fig. 7.4 the friction factor graphs were not shown in this thesis.

Laminar friction factor correlation for PUCTT and PUCTTR inserts:

$$f_L = 0.3[923[Re_b]^{-1}[R_d]^{0.11}+[R_r]^{-0.74}] \quad 7.4$$

Transitional friction factor correlation for PUCTT and PUCTTR inserts:

$$f_R = 0.3[3.4[Re_b]^{-0.068}[R_d]^{0.34}+[R_r]^{-0.8}] \quad 7.5$$

Turbulent friction factor correlation for PUCTT and PUCTTR inserts:

$$f_T = 0.28[39[Re_b]^{-0.4}[R_d]^{0.36}+[R_r]^{-0.86}] \quad 7.6$$

The ranges and performances of Eqs. (7.4) – (7.6) are summarised in Table 7.2. This table indicates that the friction factor correlations developed in the laminar, transitional and turbulent flow regimes performed very well to predict the experimental data within a maximum deviation of 8%.

7.6 Summary and conclusions

This chapter experimentally investigated the heat transfer and pressure drop characteristics of a smooth tube with PUCTT and PUCTTR inserts in the laminar, transitional and turbulent flow regimes. The focus was on the identification and heat transfer and pressure drop characteristics of the transitional flow regime. The PUCTT inserts were tested at depth ratios of 0.105 and 0.216. Each depth ratio was thereafter tested at ring space ratios of 1.25, 2.5 and 5.

When the Colburn *j*-factor results of the PUCTT insert were compared with the CCCTT and CTT inserts, it was found that no significant heat transfer enhancement occurred in the laminar flow regime. The Colburn *j*-factors of the PUCTT inserts in the transitional and turbulent flow regimes were higher than CTT inserts and lower than CCCTT inserts. The transitional characteristics of the friction factors were the same as those of the Colburn *j*-factors, but the quantitative values of enhancements were different. The friction factors however increased in all the three flow regimes. The start and end of the transitional flow regime were influenced by the modification of the twisted tape, as the transitional flow regime of the PUCTT inserts occurred earlier compared with the CTT inserts and later compared with CCCTT inserts.

The start and end of the transitional flow regime were also influenced by the depth ratio and occurred earlier as the depth ratio was increased. Furthermore, the u-cuts in the PUCTT inserts increased the recirculation close to the tube wall, which enhanced the heat transfer in the transitional flow regime. When the rings were inserted, it also followed that the reduction in the ring space ratios (thus inserting more rings) caused earlier transitions, thus at lower Reynolds numbers, as well as increased Colburn *j*-factors and friction factors. The enhancements were because of the tripping of the boundary layer growth on the tube inner wall and the increased mixing inside the test section.

Correlations were developed to predict the Colburn *j*-factors and friction factors of tubes with PUCTT and PUCTTR inserts in the laminar, transitional and turbulent flow regimes. Where relevant, these correlations were developed as a function of Reynolds number, depth ratio and ring space ratio. In general, the correlations correspond well to the experimental data.

8. Summary, conclusions and recommendations

8.1 Summary

Heat exchangers are found in both domestic-, commercial- and industrial applications in meeting our heat transfer needs. The way in which they are designed and operated could influence heat transfer performance, contribute to energy management and overall efficiency improvement as well as service delivery of all production processes. In general, the two parameters majorly investigated in the design, use and operation of heat exchangers (smooth or enhanced) are the heat transfer and pressure drop. The investigation of these two parameters are mostly limited to the laminar flow regime (low heat transfer and pressure drop) and turbulent flow regime (high heat transfer and pressure drop), while the transitional flow regime, which could be a compromise has in general been avoided. This is because it is associated with unsteadiness, instability uncertainty and there is limited information and methodology to clearly identify the transitional flow regime, particularly in a tube with twisted tape inserts. Heat transfer and pressure drop investigations with the use of twisted tape inserts only focused on heat transfer enhancement and not specifically on the identification of the three flow regimes (laminar, transitional and turbulent). Furthermore, the use of inlet geometry which has been found to influence the transitional flow regime has not been previously reported when twisted tape inserts were investigated.

The purpose of this study was to experimentally investigate the heat transfer and pressure drop characteristics of twisted tape inserts with different modifications in the transitional flow regime, and at different constant heat flux boundary conditions. The experimental set-up used in this study was designed, fabricated, installed and commissioned. The experiments conducted on the set-up were in four categories. The first was experiment in a smooth circular tube with an inner diameter, an outer diameter and a length of 19 mm, 22 mm and 5.27 m, the results of which were compared with literature. The smooth tube was used for the other three categories of experiments which involved the use of twisted pate inserts. Three twisted tape inserts were considered in this study. The first were conventional twisted tape (CTT) inserts with twist ratios of 3, 4 and 5. The second were alternating clockwise and counter clockwise twisted tape (CCCTT) inserts with connection angles of 0°, 30° and 60° at the twist ratio of 5. The third were peripheral u-cut twisted tape (PUCTT) inserts without ring and with ring (PUCTTR) inserts with the twist ratio of 5. The PUCTT and PUCTTR inserts were cut to achieve depth ratios of 0.105 and 0.216. The rings were inserted to form tapes with ring space ratios of 1.25, 2.5 and 5. The sole aim of the study was on the identification of the transitional flow regime with the twisted tape inserts. As the transitional flow regime "connects" the laminar and turbulent flow regimes; the results of these two flow regimes are also given. As the inlet geometry significantly influence transition, a square-edged inlet was used.

8.2 Conclusions

Two independent, yet complementary methods, were used to determine the boundaries where transition started and ended. The first method was the standard deviation method in which the temperature deviations at each measuring station were determined. The second method was to construct three linear curve fits on a log-log scale of Colburn *j*-factors and friction factors as a function of the Reynolds numbers. The curve fits made it possible for correlations to be developed for the non-dimensionalized heat transfer coefficients (Colburn *j*-factors) and friction factors, which took into consideration the twist ratio, heat flux and Reynolds number.

When the CTT inserts were compared at the same heat flux, it was found that the Colburn *j*-factors increased as the twist ratio decreased, and transition started earlier. When the twist ratio was kept constant, and the heat flux were varied, higher heat flux delayed the transition from laminar to transitional flow. Furthermore, the width of the transitional flow regime decreased as the heat flux increased.

For friction factors of the CTT inserts, it was found that friction factors increased as the twist ratio decreased. The width of the transitional flow regime also decreased as the twist ratios increased. When both the twist ratio and the Reynolds number were kept constant, an increase in heat flux was found to decrease the friction factor. Heat transfer and pressure drop correlations were developed for the CTT inserts as a function Reynolds number, twist ratio and heat flux.

The comparison of the Colburn *j*-factor and friction factor results of the CCCTT insert with the CTT and PUCTT inserts showed no enhancement in the laminar flow regime. In the transitional flow regime significant heat transfer enhancements occurred and transition of the CCCTT occurred earlier than with the PUCTT and CTT inserts. In the turbulent flow regime, the heat transfer enhancements of the CCCTT insert were slightly better than that of the CTT insert.

When different connection angles were compared it was found that the increased disturbance created by an increased connection angle enhanced mixing inside the test section, which led to increased heat transfer. Furthermore, it also caused transition to occur at lower Reynolds numbers. However, the connection angle had no significant effect in the laminar and turbulent flow regimes. An increase in heat flux was found to enhance heat transfer in the laminar flow regime and delay transition, however, the turbulent flow regime remained unaffected.

Correlations to predict the start and end of the transitional flow regime, as well as the Colburn *j*-factors and friction factors in the laminar, transitional, and turbulent flow regimes of the CCCTT inserts were developed. These correlations were developed as a function of the Reynolds number, connection angle, and modified Grashof number, to account for different connection angles as well as free convection effects where relevant.

When the Colburn *j*-factor results of the PUCTT insert were compared with the CCCTT and CTT inserts, it was found that no significant heat transfer enhancement occurred in the

laminar flow regime. The Colburn *j*-factors of the PUCTT inserts in the transitional and turbulent flow regimes were higher than CTT inserts and lower than CCCTT inserts. The transitional characteristics of the friction factors were the same as those of the Colburn *j*-factors, but the quantitative values of enhancements were different. The friction factors however increased in all the three flow regimes. The start and end of the transitional flow regime were influenced by the modification of the twisted tape, as the transitional flow regime of the PUCTT inserts occurred earlier compared with the CTT inserts and later compared with CCCTT inserts.

The start and end of the transitional flow regime were also influenced by the depth ratio and occurred earlier as the depth ratio was increased. Furthermore, the u-cuts in the PUCTT inserts increased the recirculation close to the tube wall, which enhanced the heat transfer in the transitional flow regime. When the rings were inserted, it also followed that the reduction in the ring space ratios (thus inserting more rings) caused earlier transitions, thus at lower Reynolds numbers, as well as increased Colburn *j*-factors and friction factors. The enhancements were because of the tripping of the boundary layer growth on the tube inner wall and the increased mixing inside the test section.

Correlations were developed to predict the Colburn *j*-factors and friction factors of tubes with PUCTT and PUCTTR inserts in the laminar, transitional and turbulent flow regimes. Where relevant, these correlations were developed as a function of Reynolds number, depth ratio and ring space ratio. In general, the correlations correspond well to the experimental data.

8.3 Recommendations

Recommendations for future study are stated below:

- When heat transfer and pressure drop experiments are conducted, significant attention should be given to the identification of the transitional flow regime, particularly in enhanced tubes;
- Transitional flow regime should be investigated in:
    - Tubes with perforated twisted tape inserts as well as twisted tape inserts with rod spacing, rather than peripheral twisted tape inserts. This is for the main purpose of reducing pressure drop.
    - Enhanced tubes such as dimpled tubes, tapered tubes, T-section or Y-sections that are generally found in the industries. These tubes could help reduce pressure drop as no partition or tube blockage will be created.
- New inlet geometries (for example a configuration that will incorporate bell-mouth and reentrant together) should be developed and tested with enhanced tubed as well as the other conventional inlet geometries (re-entrant and bellmouth).
- Test fluids other than water and air should be considered and particularly as found being used in industry. For example, nano-fluids, ethylene glycol, propylene glycol, etc.

References

[1] J.P. Meyer, J.A. Olivier, Heat transfer and pressure drop characteristics of smooth horizontal tubes in the transitional flow regime, Heat Transfer Engineering, 35(14-15) (2014) 1246-1253.

[2] S. Rozzi, R. Massini, G. Paciello, G. Pagliarini, S. Rainieri, A. Trifir, Heat treatment of fluid foods in a shell and tube heat exchanger: Comparison between smooth and helically corrugated wall tubes, Journal of Food Engineering, 79(1) (2007) 249-254.

[3] S. Liu, M. Sakr, A comprehensive review on passive heat transfer enhancements in pipe exchangers, Renewable and Sustainable Energy Reviews, 19 (2013) 64-81.

[4] Y. Dong, L. Huixiong, C. Tingkuan, Pressure drop, heat transfer and performance of single-phase turbulent flow in spirally corrugated tubes, Experimental Thermal and Fluid Science, 24(3-4) (2001) 131-138.

[5] L. Liebenberg, J.P. Meyer, In-tube passive heat transfer enhancement in the process industry, Applied Thermal Engineering, 27 (2007) 2713-2726.

[6] L. Wei, L. Zhichun, M. Tingzhen, G. Zengyuan, Physical quantity synergy in laminar flow field and its application in heat transfer enhancement, International Journal of Heat and Mass Transfer, 52(19-20) (2009) 4669-4672.

[7] Z. Zhang, D. Ma, X. Fang, X. Gao, Experimental and numerical heat transfer in a helically baffled heat exchanger combined with one three-dimensional finned tube, Chemical Engineering and Processing: Process Intensification, 47(9-10) (2008) 1738-1743.

[8] T.W. Arment, N.E. Todreas, A.E. Bergles, Critical heat flux and pressure drop for tubes containing multiple short-length twisted-tape swirl promoters, Nuclear Engineering and Design, 257 (2013) 1-11.

[9] A. Mwesigye, T. Bello-Ochende, J.P. Meyer, Heat transfer and entropy generation in a parabolic trough receiver with wall-detached twisted tape inserts, International Journal of Thermal Sciences, 99 (2016) 238-257.

[10] Z. Guo, Z. Sun, N. Zhang, M. Ding, Y. Zhou, Influence of flow guiding conduit on pressure drop and convective heat transfer in packed beds, International Journal of Heat and Mass Transfer, 134 (2019) 489-502.

[11] Z.H. Wang, Z.K. Zhou, External natural convention heat transfer of fluid metal under the influence of magnetic field, International Journal of Heat and Mass Transfer, 134 (2019) 175-184.

[12] C.O. Olsson, B. Sunden, Heat transfer and pressure drop characteristics of ten radiator tubes, International Journal of Heat and Mass Transfer, 39(15) (1996) 3211-3220.

[13] S. Eiamsa-ard, V. Kongkaitpaiboon, K. Nanan, Thermohydraulics of turbulent flow through heat exchanger tubes fitted with circular-rings and twisted tapes, Chinese Journal of Chemical Engineering, 21(6) (2013) 585-593.

[14] A.J. Ghajar, K.F. Madon, Pressure drop measurements in the transition region for a circular tube with three different inlet configurations, Experimental Thermal and Fluid Science, 5(1) (1992) 129-135.

[15] A.J. Ghajar, L.M. Tam, Heat transfer measurements and correlations in the transition region for a circular tube with three different inlet configurations, Experimental Thermal and Fluid Science, 8 (1994) 79-90.

[16] A.J. Ghajar, L.M. Tam, Flow regime map for a horizontal pipe with uniform wall heat flux and three inlet configurations, Experimental Thermal and Fluid Science, 10 (1995) 287-297.

[17] A.J. Ghajar, Y.H. Zurigat, Microcomputer-assisted heat transfer measurements/analysis in a circular tube, International Journal of Applied Engineering Education, 7(2) (1991) 125-134.
[18] H.K. Tam, L.M. Tam, A.J. Ghajar, Effect of inlet geometries and heating on the entrance and fully-developed friction factors in the laminar and transition regions of a horizontal tube, Experimental Thermal and Fluid Science, 44 (2013) 680-696.
[19] L.M. Tam, A.J. Ghajar, Transitional heat transfer in plain horizontal tubes, Heat Transfer Engineering, 27(5) (2006) 23-38.
[20] L.M. Tam, A.J. Ghajar, Effect of inlet geometry and heating on the fully developed friction factor in the transition region of a horizontal tube, Experimental Thermal and Fluid Science, 15 (1997) 52-64.
[21] L.M. Tam, A.J. Ghajar, The unusual behavior of local heat transfer coefficient in a circular tube with a bell-mouth inlet, Experimental Thermal and Fluid Science, 16(3) (1998) 187-194.
[22] J.P. Meyer, T.J. McKrell, K. Grote, The influence of multi-walled carbon nanotubes on single-phase heat transfer and pressure drop characteristics in the transitional flow regime of smooth tubes, International Journal of Heat and Mass Transfer, 58(1-2) (2013) 597-609.
[23] J.P. Meyer, J.A. Olivier, Heat transfer in the transitional flow regime, University of Pretoria, Hatfield, Pretoria, South Africa, (2010).
[24] J.P. Meyer, J.A. Olivier, Transitional flow inside enhanced tubes for fully developed and developing flow with different types of inlet disturbances: Part II-heat transfer, International Journal of Heat and Mass Transfer, 54(7-8) (2011) 1598-1607.
[25] M. Everts, S.R. Ayres, F.A.M. Houwer, C.P. Vanderwagen, N.M. Kotze, J.P. Meyer, The influence of surface roughness on heat transfer in the transitional flow regime, in: Proceedings of the 15th International Heat Transfer Conference, IHTC-15, Kyoto, Japan, 2014, pp. 1626-1637.
[26] J.A. Olivier, J.P. Meyer, Single-phase heat transfer and pressure drop of the cooling of water inside smooth tubes for transitional flow with different inlet geometries (RP-1280), HVAC and Research, 16(4) (2010) 471-496.
[27] S. Osman, M. Sharifpur, J.P. Meyer, Experimental investigation of convection heat transfer in the transition flow regime of aluminium oxide-water nanofluids in a rectangular channel, International Journal of Heat and Mass Transfer, 133 (2019) 895–902.
[28] J. Dirker, J.P. Meyer, D.V. Garach, Inlet flow effects in micro-channels in the laminar and transitional regimes on single-phase heat transfer coefficients and friction factors, International Journal of Heat and Mass Transfer, 77 (2014) 612-626.
[29] M. Everts, J.P. Meyer, Heat transfer of developing and fully developed flow in smooth horizontal tubes in the transitional flow regime, International Journal of Heat and Mass Transfer, 117 (2018) 1331-1351.
[30] M. Everts, J.P. Meyer, Relationship between pressure drop and heat transfer of developing and fully developed flow in smooth horizontal circular tubes in the laminar, transitional, quasi-turbulent and turbulent flow regimes, International Journal of Heat and Mass Transfer, 117 (2018) 1231-1250.
[31] J.P. Meyer, M. Everts, Single-phase mixed convection of developing and fully developed flow in smooth horizontal circular tubes in the laminar and transitional flow regimes, International Journal of Heat and Mass Transfer, 117 (2018) 1251-1273.
[32] J.P. Meyer, M. Everts, A.T.C. Hall, F.A. Mulock-Houwer, M. Joubert, L.M.J. Pallent, E.S. Vause, Inlet tube spacing and protrusion inlet effects on multiple circular tubes in

the laminar, transitional and turbulent flow regimes, International Journal of Heat and Mass Transfer, 118 (2018) 257-274.
[33] J.P. Meyer, Heat transfer in tubes in the transitional flow regime, in: Proceedings of the 15th International Heat Transfer Conference IHTC-15, Kyoto, Japan, 2014, pp. 41-61.
[34] S. Al-Fahed, L.M. Chamra, W. Chakroun, Pressure drop and heat transfer comparison for both microfin tube and twisted-tape inserts in laminar flow, Experimental Thermal and Fluid Science, 18(4) (1999) 323-333.
[35] S.W. Chang, Y.J. Jan, J.S. Liou, Turbulent heat transfer and pressure drop in tube fitted with serrated twisted tape, International Journal of Thermal Sciences, 46(5) (2007) 506-518.
[36] S.W. Chang, T.-M. Liou, J.S. Liou, K.-T. Chen, Turbulent heat transfer in a tube fitted with serrated twist tape under rolling and pitching environments with applications to shipping machineries, Ocean Engineering, 35(16) (2008) 1569-1577.
[37] P. Bharadwaj, A.D. Khondge, A.W. Date, Heat transfer and pressure drop in a spirally grooved tube with twisted tape insert, International Journal of Heat and Mass Transfer, 52(7-8) (2009) 1938-1944.
[38] S.W. Hong, A.E. Bergles, Augmentation of laminar flow heat transfer in tubes by means of twisted-tape inserts, Journal of Heat Transfer, 98(2) (1976) 251-256.
[39] W.J. Marner, A.E. Bergles, Augmentation of highly viscous laminar heat transfer inside tubes with constant wall temperature, Experimental Thermal and Fluid Science, 2(3) (1989) 252-267.
[40] C. Maradiya, J. Vadher, R. Agarwal, The heat transfer enhancement techniques and their thermal performance factor, Beni-Suef University Journal of Basic and Applied Sciences, 7(1) (2017) 1-21.
[41] A. Hasanpour, M. Farhadi, K. Sedighi, Experimental heat transfer and pressure drop study on typical, perforated, v-cut and u-cut twisted tapes in a helically corrugated heat exchanger, International Communications in Heat and Mass Transfer, 71 (2016) 126-136.
[42] A. Hasanpour, M. Farhadi, K. Sedighi, A review study on twisted tape inserts on turbulent flow heat exchangers: The overall enhancement ratio criteria, International Communications in Heat and Mass Transfer, 55 (2014) 53-62.
[43] G.M.O. Varun, H. Nautiyal, S. Khurana, M.K. Shukla, Heat transfer augmentation using twisted tape inserts: A review, Renewable and Sustainable Energy Reviews, 63 (2016) 193-225.
[44] C. Zhang, D. Wang, K. Ren, Y. Han, Y. Zhu, X. Peng, J. Deng, X. Zhang, A comparative review of self-rotating and stationary twisted tape inserts in heat exchanger, Renewable and Sustainable Energy Reviews, 53 (2016) 433-449.
[45] A.W. Date, Prediction of fully-developed flow containing a twisted-tape, International Journal of Heat and Mass Transfer, 17 (1974) 845-859.
[46] K. Hata, Y. Shirai, S. Masuzaki, A. Hamura, Computational study of twisted-tape-induced swirl flow heat transfer and pressure drop in a vertical circular tube under velocities controlled, Nuclear Engineering and Design, 263 (2013) 443-455.
[47] K. Hata, K. Fukuda, K. Hata, Transient critical heat fluxes of subcooled water flow boiling in SUS304-circular tubes with various twisted-tape inserts (influence of twist ratio), Journal of Thermal Science and Engineering Applications, 6(3) (2014).
[48] J.P. Du Plessis, D.G. Kröger, Heat transfer correlation for thermally developing laminar flow in a smooth tube with a twisted-tape insert, International Journal of Heat and Mass Transfer, 30(3) (1987) 509-515.

[49] J.P. Meyer, S.M. Abolarin, Heat transfer and pressure drop in the transitional flow regime for a smooth circular tube with twisted tape inserts and a square-edged inlet, International Journal of Heat and Mass Transfer, 117 (2018) 11-29.
[50] S.M. Abolarin, M. Everts, J.P. Meyer, Heat transfer and pressure drop characteristics of alternating clockwise and counter clockwise twisted tape inserts in the transitional flow regime, International Journal of Heat and Mass Transfer, 133 (2019) 203-217.
[51] S.M. Abolarin, M. Everts, J.P. Meyer, The influence of peripheral u-cut twisted tapes and ring inserts on the heat transfer and pressure drop characteristics in the transitional flow regime, International Journal of Heat and Mass Transfer, 132 (2019) 970-984.
[52] J. Li, C. Dang, E. Hihara, Heat transfer enhancement in a parallel, finless heat exchanger using a longitudinal vortex generator, Part B: Experimental investigation on the performance of finless and fin-tube heat exchangers, International Journal of Heat and Mass Transfer, 128 (2019) 66-75.
[53] J. Li, C. Dang, E. Hihara, Heat transfer enhancement in a parallel, finless heat exchanger using a longitudinal vortex generator, Part A: Numerical investigation, International Journal of Heat and Mass Transfer, 128 (2019) 87-97.
[54] H. Han, F. Song, G. Zhang, L. Yang, Y. Li, Analysis on compound heat transfer enhancement performance in outward convex corrugated tube with twisted insert, Huagong Xuebao/CIESC Journal, 67(S1) (2016) 195-202.
[55] K. Sivakumar, K. Rajan, S. Murali, S. Prakash, V. Thanigaivel, T. Suryakumar, Augmentation of heat transfer performance with aluminium and copper twisted tape inserts, International Journal of Chemical Sciences, 14 (2016) 439-445.
[56] P. Eiamsa-ard, N. Piriyarungroj, C. Thianpong, S. Eiamsa-ard, A case study on thermal performance assessment of a heat exchanger tube equipped with regularly-spaced twisted tapes as swirl generators, Case Studies in Thermal Engineering, 3 (2014) 86-102.
[57] A. Kumar, M. Kumar, S. Chamoli, Comparative study for thermal-hydraulic performance of circular tube with inserts, Alexandria Engineering Journal, 55(1) (2016) 343-349.
[58] M.T. Naik, S.S. Fahad, L.S. Sundar, M.K. Singh, Comparative study on thermal performance of twisted tape and wire coil inserts in turbulent flow using CuO/water nanofluid, Experimental Thermal and Fluid Science, 57 (2014) 65-76.
[59] S. Rainieri, F. Bozzoli, L. Cattani, G. Pagliarini, Compound convective heat transfer enhancement in helically coiled wall corrugated tubes, International Journal of Heat and Mass Transfer, 59(1) (2013) 353-362.
[60] R.K. Ali, M.A. Sharafeldeen, N.S. Berbish, M.A. Moawed, Convective heat transfer enhancement inside tubes using inserted helical coils, Thermal Engineering, 63(1) (2016) 42-50.
[61] F. Jiao, X. Deng, P. Song, Effect of inserts on heat transfer performance of new heat exchanger, Shiyou Xuebao, Shiyou Jiagong/Acta Petrolei Sinica (Petroleum Processing Section), 31(3) (2015) 796-802.
[62] V. Zimparov, Enhancement of heat transfer by a combination of a single-start spirally corrugated tubes with a twisted tape, Experimental Thermal and Fluid Science, 25(7) (2002) 535-546.
[63] V. Zimparov, Enhancement of heat transfer by a combination of three-start spirally corrugated tubes with a twisted tape, International Journal of Heat and Mass Transfer, 44(3) (2001) 551-574.
[64] X. Tang, X. Dai, D. Zhu, Experimental and numerical investigation of convective heat transfer and fluid flow in twisted spiral tube, International Journal of Heat and Mass Transfer, 90 (2015) 523-541.

[65] S. Wang, J. Wen, H. Yang, Y. Xue, H. Tuo, Experimental investigation on heat transfer enhancement of a heat exchanger with helical baffles through blockage of triangle leakage zones, Applied Thermal Engineering, 67(1-2) (2014) 122-130.
[66] K.R. Aharwal, B.K. Gandhi, J.S. Saini, Experimental investigation on heat-transfer enhancement due to a gap in an inclined continuous rib arrangement in a rectangular duct of solar air heater, Renewable Energy, 33(4) (2008) 585-596.
[67] X.-H. Tan, D.-S. Zhu, G.-Y. Zhou, L.-D. Zeng, Heat transfer and pressure drop performance of twisted oval tube heat exchanger, Applied Thermal Engineering, 50(1) (2013) 374-383.
[68] K. Watanabe, T. Taira, Y. Mori, Heat transfer augementation in tubular flow by twisted tapes at high temperatures and optimum performance, Heat Transfer - Japanese Research, 12(3) (1983) 1-31.
[69] P. Promvonge, S. Pethkool, M. Pimsarn, C. Thianpong, Heat transfer augmentation in a helical-ribbed tube with double twisted tape inserts, International Communications in Heat and Mass Transfer, 39(7) (2012) 953-959.
[70] C. Chang, C. Xu, Z.Y. Wu, X. Li, Q.Q. Zhang, Z.F. Wang, Heat transfer enhancement and performance of solar thermal absorber tubes with circumferentially non-uniform heat flux, in: Energy Procedia, 2015, pp. 320-327.
[71] V. Ozceyhan, S. Gunes, O. Buyukalaca, N. Altuntop, Heat transfer enhancement in a tube using circular cross sectional rings separated from wall, Applied Energy, 85(10) (2008) 988-1001.
[72] T.C. Carnavos, Heat transfer performance of internally finned tubes in turbulent flow, Heat Transfer Engineering, 1(4) (1980) 32-37.
[73] W.T. Ji, A.M. Jacobi, Y.L. He, W.Q. Tao, Summary and evaluation on single-phase heat transfer enhancement techniques of liquid laminar and turbulent pipe flow, International Journal of Heat and Mass Transfer, 88 (2015) 735-754.
[74] M. Pan, I. Bulatov, R. Smith, Novel MILP-based optimization method for retrofitting heat exchanger networks, Computer Aided Chemical Engineering, 30 (2012) 567-571.
[75] P.S. Bandyopadhyay, U.N. Gaitonde, S.P. Sukhatme, Influence of free convection on heat transfer during laminar flow in tubes with twisted tapes, Experimental Thermal and Fluid Science, 4(5) (1991) 577-586.
[76] H. Safikhani, F. Abbasi, Numerical study of nanofluid flow in flat tubes fitted with multiple twisted tapes, Advanced Powder Technology, 26(6) (2015) 1609-1617.
[77] A.E. Bergeles, H.L. Morton, Survey and evaluation of techniques to augement convection heat transfer, Cambrige, MA, Massachusetts Institute of Technology, 1965.
[78] R.M. Manglik, A.E. Bergles, Heat transfer and pressure drop correlations for twisted-tape inserts in isothermal tubes: Part II - transition and turbulent flows, Journal of Heat Transfer, 115(4) (1993) 890-896.
[79] A. Bartwal, A. Gautam, M. Kumar, C.K. Mangrulkar, S. Chamoli, Thermal performance intensification of a circular heat exchanger tube integrated with compound circular ring–metal wire net inserts, Chemical Engineering and Processing - Process Intensification, 124 (2018) 50-70.
[80] M. Everts, The influence of surface roughness in the transitional flow regime, University of Pretoria, South Africa, 2012.
[81] R. Koch, Pressure loss and heat transfer for turbulent flow, Atomic Energy Commission Translation Ser. 3875, 1960.
[82] S.W. Chang, J.Y. Gao, H.L. Shih, Thermal performances of turbulent tubular flows enhanced by ribbed and grooved wire coils, International Journal of Heat and Mass Transfer, 90 (2015) 1109-1124.

[83] S. Rainieri, G. Pagliarini, Convective heat transfer to temperature dependent property fluids in the entry region of corrugated tubes, International Journal of Heat and Mass Transfer, 45(22) (2002) 4525-4536.
[84] Q. Xiao, W.Q. Tao, Effect of fin spacing on heat transfer and pressure drop of two-row corrugated-fin and tube heat exchangers, International Communications in Heat and Mass Transfer, 17(5) (1990) 577-586.
[85] S. Rainieri, F. Bozzoli, L. Cattani, G. Pagliarini, Experimental investigation on the convective heat transfer enhancement for highly viscous fluids in helical coiled corrugated tubes, Journal of Physics: Conference Series, 395 (2012) 012032-012032.
[86] A. García, J.P. Solano, P.G. Vicente, A. Viedma, The influence of artificial roughness shape on heat transfer enhancement: corrugated tubes, dimpled tubes and wire coils, Applied Thermal Engineering, 35 (2012) 196-201.
[87] F. Illan, A. Viedma, Prediction of ice slurry performance in a corrugated tube heat exchanger, International Journal of Refrigeration, 32(6) (2009) 1302-1309.
[88] S.K. Saha, Thermohydraulics of turbulent flow through rectangular and square ducts with axial corrugation roughness and twisted-tapes with and without oblique teeth, Experimental Thermal and Fluid Science, 34(6) (2010) 744-752.
[89] S. Pethkool, S. Eiamsa-ard, S. Kwankaomeng, P. Promvonge, Turbulent heat transfer enhancement in a heat exchanger using helically corrugated tube, International Communications in Heat and Mass Transfer, 38(3) (2011) 340-347.
[90] S. Mei, C. Qi, T. Luo, X. Zhai, Y. Yan, Effects of magnetic field on thermo-hydraulic performance of Fe_3O_4-water nanofluids in a corrugated tube, International Journal of Heat and Mass Transfer, 128 (2019) 24-45.
[91] K. Navickaitė, L. Cattani, C.R.H. Bahl, K. Engelbrecht, Elliptical double corrugated tubes for enhanced heat transfer, International Journal of Heat and Mass Transfer, 128 (2019) 363-377.
[92] Y. Liu, Y. Rao, B. Weigand, Heat transfer and pressure loss characteristics in a swirl cooling tube with dimples on the tube inner surface, International Journal of Heat and Mass Transfer, 128 (2019) 54-65.
[93] S. Xie, Z. Liang, J. Zhang, L. Zhang, Y. Wang, H. Ding, Numerical investigation on flow and heat transfer in dimpled tube with teardrop dimples, International Journal of Heat and Mass Transfer, 131 (2019) 713-723.
[94] V. Kongkaitpaiboon, K. Nanan, S. Eiamsa-ard, Experimental investigation of convective heat transfer and pressure loss in a round tube fitted with circular-ring turbulators, International Communications in Heat and Mass Transfer, 37(5) (2010) 568-574.
[95] M.S. Hossain, B. Shabani, Experimental study on confined metal foam flow passage as compact heat exchanger surface, International Communications in Heat and Mass Transfer, 98 (2018) 286-296.
[96] A.A. Mohammed, A.A. Hussein, The effect of inclination angle on the convective heat transfer in tube fitted with conical ring and swirl generator inserts, International Journal of Mechanical and Mechatronics Engineering, 15(6) (2015) 51-58.
[97] P. Promvonge, S. Eiamsa-ard, Heat transfer behaviors in a tube with combined conical-ring and twisted-tape insert, International Communications in Heat and Mass Transfer, 34(7) (2007) 849-859.
[98] Y. Huang, J.R. Chen, X.X. Liu, Numerical simulation on heat transfer enhancement in tube with conical twisted-tape insert, Huaxue Gongcheng/Chemical Engineering (China), 43(4) (2015) 11-14 and 20.
[99] A.R. Anvari, R. Lotfi, A.M. Rashidi, S. Sattari, Experimental research on heat transfer of water in tubes with conical ring inserts in transient regime, International Communications in Heat and Mass Transfer, 38(5) (2011) 668-671.

[100] V. Kongkaitpaiboon, K. Nanan, S. Eiamsa-ard, Experimental investigation of heat transfer and turbulent flow friction in a tube fitted with perforated conical-rings, International Communications in Heat and Mass Transfer, 37(5) (2010) 560-567.
[101] M.E. Nakhchi, J.A. Esfahani, Entropy generation of turbulent Cu–water nanofluid flow in a heat exchanger tube fitted with perforated conical rings, Journal of Thermal Analysis and Calorimetry, (2019) 1-14.
[102] A. Garcia, J.P. Solano, P.G. Vicente, A. Viedma, Enhancement of laminar and transitional flow heat transfer in tubes by means of wire coil inserts, International Journal of Heat and Mass Transfer, 50(15-16) (2007) 3176-3189.
[103] S. Gunes, V. Ozceyhan, O. Buyukalaca, The experimental investigation of heat transfer and pressure drop in a tube with coiled wire inserts placed separately from the tube wall, Applied Thermal Engineering, 30(13) (2010) 1719-1725.
[104] S. Gunes, V. Ozceyhan, O. Buyukalaca, Heat transfer enhancement in a tube with equilateral triangle cross sectioned coiled wire inserts, Experimental Thermal and Fluid Science, 34(6) (2010) 684-691.
[105] D.S. Martínez, A. García, J.P. Solano, Heat transfer enhancement of laminar and transitional Newtonian and non-Newtonian flows in tubes with wire coil inserts, International Journal of Heat and Mass Transfer, 76 (2014) 540-548.
[106] P. Kumar, R.L. Judd, Heat transfer with coiled wire turbulence promoters, The Canadian Journal of Chemical Engineering, 48 (1970) 378-386.
[107] S. Eiamsa-ard, P. Nivesrangsan, S. Chokphoemphun, P. Promvonge, Influence of combined non-uniform wire coil and twisted tape inserts on thermal performance characteristics, International Communications in Heat and Mass Transfer, 37(7) (2010) 850-856.
[108] P. Naphon, P. Sriromruln, Single-phase heat transfer and pressure drop in the micro-fin tubes with coiled wire insert, International Communications in Heat and Mass Transfer, 33(2) (2006) 176-183.
[109] R. Sethumadhavan, M. Raja Rao, Turbulent flow heat transfer and fluid friction in helical-wire-coil-inserted tubes, International Journal of Heat and Mass Transfer, 26(12) (1983) 1833-1845.
[110] Y. Hong, J. Du, S. Wang, W.-B. Ye, S.-M. Huang, Turbulent thermal-hydraulic and thermodynamic characteristics in a traverse corrugated tube fitted with twin and triple wire coils, International Journal of Heat and Mass Transfer, 130 (2019) 483-495.
[111] S. Chamoli, R. Lu, J. Xie, P. Yu, Numerical study on flow structure and heat transfer in a circular tube integrated with novel anchor shaped inserts, Applied Thermal Engineering, 135 (2018) 304-324.
[112] S. Chamoli, R. Lu, D. Xu, P. Yu, Thermal performance improvement of a solar air heater fitted with winglet vortex generators, Solar Energy, 159 (2018) 966-983.
[113] Y.-X. Li, X. Wang, J. Zhang, L. Zhang, J.-H. Wu, Comparison and analysis of the arrangement of delta winglet pair vortex generators in a half coiled jacket for heat transfer enhancement, International Journal of Heat and Mass Transfer, 129 (2019) 287-298.
[114] J.S. Sawhney, R. Maithani, S. Chamoli, Experimental investigation of heat transfer and friction factor characteristics of solar air heater using wavy delta winglets, Applied Thermal Engineering, 117 (2017) 740-751.
[115] S.K. Singh, M. Kumar, A. Kumar, A. Gautam, S. Chamoli, Thermal and friction characteristics of a circular tube fitted with perforated hollow circular cylinder inserts, Applied Thermal Engineering, 130 (2018) 230-241.

[116] S. Chamoli, R. Lu, P. Yu, Thermal characteristic of a turbulent flow through a circular tube fitted with perforated vortex generator inserts, Applied Thermal Engineering, 121 (2017) 1117-1134.
[117] A. Nouri-Borujerdi, M.E. Nakhchi, Heat transfer enhancement in annular flow with outer grooved cylinder and rotating inner cylinder: Review and experiments, Applied Thermal Engineering, 120 (2017) 257-268.
[118] A. Nouri-Borujerdi, M.E. Nakhchi, Optimization of the heat transfer coefficient and pressure drop of Taylor-Couette-Poiseuille flows between an inner rotating cylinder and an outer grooved stationary cylinder, International Journal of Heat and Mass Transfer, 108 (2017) 1449-1459.
[119] S.S. Chougule, S.K. Sahu, Heat transfer and friction characteristics of Al_2O_3/water and CNT/water nanofluids in transition flow using helical screw tape inserts – a comparative study, Chemical Engineering and Processing: Process Intensification, 88 (2015) 78-88.
[120] N.M. Zade, S. Akar, S. Rashidi, J.A. Esfahani, Thermo-hydraulic analysis for a novel eccentric helical screw tape insert in a three dimensional tube, Applied Thermal Engineering, 124 (2017) 413-421.
[121] S. Rashidi, N.M. Zade, J.A. Esfahani, Thermo-fluid performance and entropy generation analysis for a new eccentric helical screw tape insert in a 3D tube, Chemical Engineering and Processing: Process Intensification, 117 (2017) 27-37.
[122] N. Moghaddaszadeh, J.A. Esfahani, O. Mahian, Performance enhancement of heat exchangers using eccentric tape inserts and nanofluids, Journal of Thermal Analysis and Calorimetry, (2019).
[123] H. Meng, M. Song, Y. Yu, F. Wang, J. Wu, Chaotic mixing characteristics in static mixers with different axial twisted-tape inserts, Canadian Journal of Chemical Engineering, 93(10) (2015) 1849-1859.
[124] M. Hong, X. Deng, K. Huang, Z. Li, Compound heat transfer enhancement of a converging-diverging tube with evenly spaced twisted-tapes, Chinese Journal of Chemical Engineering, 15(6) (2007) 814-820.
[125] S.B. Bhajankar, U.S. Wankhede, A comprehensive review of heat transfer enhancement by passive inserts, International Journal of Applied Engineering Research, 10(6) (2015) 13863-13876.
[126] M.K. Jensen, A correlation for predicting the critical heat flux condition with twisted-tape swirl generators, International Journal of Heat and Mass Transfer, 27(11) (1984) 2171-2173.
[127] Y.T. Kang, R. Stout, R.N. Christensen, The effects of inclination angle on flooding in helically fluted tube with twisted insert, International Journal of Multiphase Flow, 23(6) (1997) 1111-1129.
[128] S.N. Sarada, A. Raju, Enhancement of heat transfer using varying width twisted tape inserts, International Journal of Engineering Science and Technology, 2(6) (2010) 107-118.
[129] A. Saysroy, S. Eiamsa-ard, Enhancing convective heat transfer in laminar and turbulent flow regions using multi-channel twisted tape inserts, International Journal of Thermal Sciences, 121 (2017) 55-74.
[130] M.T. Naik, G.R. Janardana, L.S. Sundar, Experimental investigation of heat transfer and friction factor with water–propylene glycol based CuO nanofluid in a tube with twisted tape inserts, International Communications in Heat and Mass Transfer, 46 (2013) 13-21.

[131] V. Hejazi, M.A. Akhavan-Behabadi, A. Afshari, Experimental investigation of twisted tape inserts performance on condensation heat transfer enhancement and pressure drop, International Communications in Heat and Mass Transfer, 37(9) (2010) 1376-1387.
[132] K. Wongcharee, S. Eiamsa-ard, Friction and heat transfer characteristics of laminar swirl flow through the round tubes inserted with alternate clockwise and counter-clockwise twisted-tapes, International Communications in Heat and Mass Transfer, 38(3) (2011) 348-352.
[133] J.P. Du Plessis, D.G. Kroger, Friction factor prediction for fully developed laminar twisted-tape flow, International Journal of Heat and Mass Transfer, 27(1) (1984) 2095-2100.
[134] P. Murugesan, K. Mayilsamy, S. Suresh, P.S.S. Srinivasan, Heat transfer and pressure drop characteristics in a circular tube fitted with and without V-cut twisted tape insert, International Communications in Heat and Mass Transfer, 38(3) (2011) 329-334.
[135] R.M. Manglik, A.E. Bergles, Heat transfer and pressure drop correlations for twisted-tape inserts in isothermal tubes: Part I-laminar flows, Journal of Heat Transfer, 115(4) (1993) 881-889.
[136] S.K. Agarwal, M. Raja Rao, Heat transfer augmentation for the flow of a viscous liquid in circular tubes using twisted tape inserts, International Journal of Heat and Mass Transfer, 39(17) (1996) 3547-3557.
[137] M.M.K. Bhuiya, A.K. Azad, M.S.U. Chowdhury, M. Saha, Heat transfer augmentation in a circular tube with perforated double counter twisted tape inserts, International Communications in Heat and Mass Transfer, 74 (2016) 18-26.
[138] V. Pavendan, K. Muthukumar, N. Arivazhagan, K. Srithar, Heat transfer augmentation in a solar water heater using cross and twisted tape inserts, International Journal of Applied Engineering Research, 10(6) (2015) 14739-14754.
[139] N.T. Ravi Kumar, P. Bhramara, A. Kirubeil, L. Syam Sundar, M.K. Singh, A.C.M. Sousa, Effect of twisted tape inserts on heat transfer, friction factor of Fe_3O_4 nanofluids flow in a douple pipe u-bend heat exchanger, International Communications in Heat and Mass Transfer, 95 (2018) 53-62.
[140] M.E. Nakhchi, J.A. Esfahani, Numerical investigation of rectangular-cut twisted tape insert on performance improvement of heat exchangers, International Journal of Thermal Sciences, 138 (2019) 75-83.
[141] M.E. Nakhchi, J.A. Esfahani, Cu-water nanofluid flow and heat transfer in a heat exchanger tube equipped with cross-cut twisted tape, Powder Technology, 339 (2018) 985-994.
[142] M.E. Nakhchi, J. Esfahani, Sensitivity analysis of a heat exchanger tube fitted with cross-cut twisted tape with alternate axis, Journal of Heat Transfer, 141(4) (2019) 41902-41901-41908.
[143] P. Seemawute, S. Eiamsa-ard, Thermohydraulics of turbulent flow through a round tube by a peripherally-cut twisted tape with an alternate axis, International Communications in Heat and Mass Transfer, 37(6) (2010) 652-659.
[144] J. Guo, A. Fan, X. Zhang, W. Liu, A numerical study on heat transfer and friction factor characteristics of laminar flow in a circular tube fitted with center-cleared twisted tape, International Journal of Thermal Sciences, 50(7) (2011) 1263-1270.
[145] H. Bas, V. Ozceyhan, Heat transfer enhancement in a tube with twisted tape inserts placed separately from the tube wall, Experimental Thermal and Fluid Science, 41 (2012) 51-58.
[146] S.W. Chang, W.L. Cai, R.S. Syu, Heat transfer and pressure drop measurements for tubes fitted with twin and four twisted fins on rod, Experimental Thermal and Fluid Science, 74 (2016) 220-234.

[147] P.V. Durga Prasad, A.V.S.S.K.S. Gupta, Experimental investigation on enhancement of heat transfer using Al_2O_3/water nanofluid in a u-tube with twisted tape inserts, International Communications in Heat and Mass Transfer, 75 (2016) 154-161.
[148] Z.H. Ayub, S.F. Al-Fahed, The effect of gap width between horizontal tube and twisted tape on the pressure drop in turbulent water flow, International Journal of Heat and Fluid Flow, 14(1) (1993) 64-67.
[149] R.M. Manglik, A.E. Bergles, Characterization of twisted-tape-induced helical swirl flows for enhancement of forced convective heat transfer in single-phase and two-phase flows, Journal of Thermal Science and Engineering Applications, 5 (2013) 1-12.
[150] S. Eiamsa-ard, K. Wongcharee, S. Sripattanapipat, 3-D Numerical simulation of swirling flow and convective heat transfer in a circular tube induced by means of loose-fit twisted tapes, International Communications in Heat and Mass Transfer, 36(9) (2009) 947-955.
[151] S. Gunes, E. Karakaya, Thermal characteristics in a tube with loose-fit perforated twisted tapes, Heat Transfer Engineering, 36(18) (2015) 1504-1517.
[152] N. Piriyarungrod, S. Eiamsa-ard, C. Thianpong, M. Pimsarn, K. Nanan, Heat transfer enhancement by tapered twisted tape inserts, Chemical Engineering and Processing: Process Intensification, 96 (2015) 62-71.
[153] B.V.N. Ramakumar, J.D. Arsha, P. Tayal, Tapered twisted tape inserts for enhanced heat transfer, Journal of Heat Transfer, 138(1) (2016).
[154] S.R. Shabanian, S. Lashgari, T. Hatami, Application of intelligent methods for the prediction and optimization of thermal characteristics in a tube equipped with perforated twisted tape, Numerical Heat Transfer; Part A: Applications, (2016) 1-18.
[155] E. Kannan, C. Balasuthagar, S. Ponsankar, M. Sivashankar, Experimental investigation on convective heat transfer characteristics in a circular tube fitted with perforated twisted tape and wire coil, Journal of Chemical and Pharmaceutical Sciences, 9(4) (2016) 2767-2769.
[156] I. Yaningsih, T. Istanto, A.T. Wijayanta, Experimental study of heat transfer enhancement in a concentric double pipe heat exchanger with different axial pitch ratio of perforated twisted tape inserts, in: AIP Conference Proceedings, 2016.
[157] M.M.K. Bhuiya, M.S.U. Chowdhury, M. Saha, M.T. Islam, Heat transfer and friction factor characteristics in turbulent flow through a tube fitted with perforated twisted tape inserts, International Communications in Heat and Mass Transfer, 46 (2013) 49-57.
[158] K. Nanan, C. Thianpong, P. Promvonge, S. Eiamsa-ard, Investigation of heat transfer enhancement by perforated helical twisted-tapes, International Communications in Heat and Mass Transfer, 52 (2014) 106-112.
[159] A.K. Khatua, P. Kumar, H.N. Singh, R. Kumar, Measurement of enhanced heat transfer coefficient with perforated twisted tape inserts during condensation of R-245fa, Heat and Mass Transfer/Waerme- und Stoffuebertragung, 52(4) (2016) 683-691.
[160] S.W. Chang, K.W. Yu, M.H. Lu, Heat transfer in tubes fitted with single, twin and tripple twisted tapes, Journal of Experimental Heat Transfer, 18 (2005) 279-294.
[161] M.M.K. Bhuiya, A.S.M. Sayem, M. Islam, M.S.U. Chowdhury, M. Shahabuddin, Performance assessment in a heat exchanger tube fitted with double counter twisted tape inserts, International Communications in Heat and Mass Transfer, 50 (2014) 25-33.
[162] A. Boonloi, W. Jedsadaratanachai, Turbulent forced convection and heat transfer characteristic in a circular tube with modified-twisted tapes, Journal of Thermodynamics, 2016 (2016) 1-16.
[163] S. Al-Fahed, L. Chamra, W. Chakroun, Pressure drop and heat transfer comparison for both microfin tube and twisted-tape inserts in laminar flow, Experimental Thermal Fluid Science, 18(4) (1998) 323-333.

[164] M.K. Abdolbaqi, W.H. Azmi, R. Mamat, N.M.Z.N. Mohamed, G. Najafi, Experimental investigation of turbulent heat transfer by counter and co-swirling flow in a flat tube fitted with twin twisted tapes, International Communications in Heat and Mass Transfer, 75 (2016) 295-302.
[165] G.J. Kidd, Heat transfer and pressure drop for nitrogen flowing in tubes containing twisted tapes, AIChE Journal, 15(4) (1969) 581-585.
[166] O. Klepper, Heat transfer performance of short twisted tapes, National Lab, Tennesse, Oak Ridge, 1972.
[167] S.K. Saha, A. Dutta, Thermohydraulic study of laminar swirl flow through a circular tube fitted with twisted tapes, Journal of Heat Transfer, 123(3) (2001) 417-427.
[168] R. Royds, Heat transmission by radiation, conduction and convection, Constable & Co., London, 1921.
[169] E. Smithberg, F. Landis, Friction and forced convection heat-transfer characteristics in tubes with twisted tape swirl generators, Journal of Heat Transfer, 86(1) (1964) 39-48.
[170] S.M. Abolarin, J.P. Meyer, Area goodness factor of flow in a plain circular tube with twisted tape insert and square-edged entry in the transitional flow regime, in: 13th International Conference on Heat Transfer, Fluid Mechanics and Thermodynamics, HEFAT, Portorož, Slovenia, 2017, pp. 978-983.
[171] W.J. Marner, A.E. Bergles, Augementation of tubeside laminar flow heat transfer by means of twisted-tape inserts, static-mixer inserts and internally finned tubes, Heat Transfer, 2 (1978) 583-588.
[172] W.G. Osley, P. Droegemueller, P. Ellerby, CFD investigation of heat transfer and flow patterns in tube side laminar flow and the potential for enhancement, Chemical Engineering Transactions, 35(1936) (2013) 997-1002.
[173] S.D. Salman, A.A.H. Kadhum, M.S. Takriff, A.B. Mohamad, CFD simulation of heat transfer augmentation in a circular tube fitted with alternative axis twisted tape in laminar flow under a constant heat flux, Heat Transfer - Asian Research, 43(4) (2014) 384-396.
[174] S.K. Saha, A. Dutta, S.K. Dhal, Friction and heat transfer characteristics of laminar swirl flow through a circular tube fitted with regularly spaced twisted-tape elements, International Journal of Heat and Mass Transfer, 44 (2001) 4211-4223.
[175] S.K. Saha, U.N. Gaitonde, A.W. Date, Heat transfer and pressure drop characteristics of laminar flow in circular tube fitted with regularly spaced twisted-tape elements, Experimental Thermal and Fluid Science, 2 (1989) 310-322.
[176] Q.S. Mahdi, N.A.M. Mohammed, Heat transfer augmentation of laminar nanofluid flow in horizontal tube inserted with twisted tapes, International Journal of Mechanical Engineering and Technology, 7(3) (2016) 225-239.
[177] Y. Aldali, I. Elbaba, K. Morad, Heat transfer enhancement for laminar flow in circular tubes with twisted-tape inserts, Journal of Thermophysics and Heat Transfer, 29(4) (2015) 805-811.
[178] S.D. Salman, A.A.H. Kadhum, M.S. Takriff, A.B. Mohamad, Heat transfer enhancement of laminar nanofluids flow in a circular tube fitted with parabolic-cut twisted tape inserts, The Scientific World Journal, 2014(1-7) (2014).
[179] P.K. Sarma, T. Subramanyam, P.S. Kishore, V.D. Rao, S. Kakac, Laminar convective heat transfer with twisted tape inserts in a tube, International Journal of Thermal Sciences, 42(9) (2003) 821-828.
[180] S. Pal, S.K. Saha, Laminar flow and heat transfer through a circular tube having integral transverse corrugations and fitted with centre-cleared twisted-tape, Experimental Thermal and Fluid Science, 57 (2014) 388-395.

[181] S. Ray, A.W. Date, Laminar flow and heat transfer through square duct with twisted tape insert, International Journal of Heat and Fluid Flow, 22 (2001) 460-472.
[182] Z. Wang, J. Zhu, R. Tian, S. Wang, Laminar flow characteristics in a circular tube fitted with an eccentric twisted tape, Beijing Huagong Daxue Xuebao (Ziran Kexueban)/Journal of Beijing University of Chemical Technology (Natural Science Edition), 42(1) (2015) 50-56.
[183] A.G. Patil, Laminar flow heat transfer and pressure drop characteristics of power law fluids inside tubes with varying width twisted tape inserts, Transaction of ASME, Journal of Heat Transfer, 22 (2000) 143-149.
[184] M. Tiwari, S.K. Saha, Laminar flow through a circular tube having transverse ribs and twisted tapes, Journal of Thermal Science and Engineering Applications, 7(4) (2015).
[185] S. Pal, S.K. Saha, Laminar fluid flow and heat transfer through a circular tube having spiral ribs and twisted tapes, Experimental Thermal and Fluid Science, 60 (2015) 173-181.
[186] T. Wang, F. Wang, A. Fan, W. Liu, Laminar heat transfer characteristics in circular tubes with twisted tapes of alternate axes, Huagong Xuebao/CIESC Journal, 65 (2014) 316-322.
[187] K.Y. Lim, Y.M. Hung, B.T. Tan, Performance evaluation of twisted-tape insert induced swirl flow in a laminar thermally developing heat exchanger, Applied Thermal Engineering, 121 (2017) 652-661.
[188] S.K. Saha, S. Bhattacharyya, P.K. Pal, Thermohydraulics of laminar flow of viscous oil through a circular tube having integral axial rib roughness and fitted with center-cleared twisted-tape, Experimental Thermal and Fluid Science, 41 (2012) 121-129.
[189] S. Bhattacharyya, S.K. Saha, Thermohydraulics of laminar flow through a circular tube having integral helical rib roughness and fitted with centre-cleared twisted-tape, Experimental Thermal and Fluid Science, 42 (2012) 154-162.
[190] S. Eiamsa-ard, P. Seemawute, K. Wongcharee, Influences of peripherally-cut twisted tape insert on heat transfer and thermal performance characteristics in laminar and turbulent tube flows, Experimental Thermal and Fluid Science, 34(6) (2010) 711-719.
[191] S. Ghadirijafarbeigloo, A.H. Zamzamian, M. Yaghoubi, 3D numerical simulation of heat transfer and turbulent flow in a receiver tube of solar parabolic trough concentrator with louvered twisted-tape inserts, Energy Procedia, 49 (2014) 373-380.
[192] R.K. Nair, Performance of twisted-tape inserts in laminar and turbulent, Iowa State University, Ames, IA, 1986.
[193] A. Saysroy, S. Eiamsa-ard, Periodically fully-developed heat and fluid flow behaviors in a turbulent tube flow with square-cut twisted tape inserts, Applied Thermal Engineering, 112 (2017) 895-910.
[194] V. Zimparov, Prediction of friction factors and heat transfer coefficients for turbulent flow in corrugated tubes combined with twisted tape inserts. Part 1: friction factors, International Journal of Heat and Mass Transfer, 47(3) (2004) 589-599.
[195] S. Eiamsa-ard, Study on thermal and fluid flow characteristics in turbulent channel flows with multiple twisted tape vortex generators, International Communications in Heat and Mass Transfer, 37(6) (2010) 644-651.
[196] S.W. Chang, M.H. Guo, Thermal performances of enhanced smooth and spiky twisted tapes for laminar and turbulent tubular flows, International Journal of Heat and Mass Transfer, 55(25-26) (2012) 7651-7667.
[197] W.H. Azmi, K.V. Sharma, R. Mamat, S. Anuar, Turbulent forced convection heat transfer of nanofluids with twisted tape insert in a plain tube, in: Energy Procedia, 2014, pp. 296-307.

[198] W. Changcharoen, P. Samruaisin, P. Eiamsa-ard, S. Eiamsa-ard, Heat transfer characteristics of decaying swirl flow through a circular tube with co/counter dual twisted-tape swirl generators, Thermophysics and Aeromechanics, 23(4) (2016) 523-536.
[199] W. Changcharoen, P. Somravysin, S. Eiamsa-ard, Thermal and fluid flow characteristics in a tube equipped with peripherally-cut dual twisted tapes, Open Engineering, 5(1) (2015) 89-98.
[200] A. Klaczak, Heat transfer and pressure drop in tubes with short turbulators, Heat and Mass Transfer, 31(6) (1996) 399-401.
[201] M.S. Lokanath, Performance evaluation of full-length and half-length twisted tape inserts on laminar flow heat transfer in tubes, in: Proceedings of the 14th National Heat and Mass Transfer Conference and Third ISHMT ASME Joint Heat and Mass Transfer Conference, IIT Kanpur, India, Paper No. HMT-97-031, 1997, pp. 319-324.
[202] A.W. Date, U.N. Gaitonde, Development of correlations for predicting characteristics of laminar flow in a tube fitted with regularly spaced twisted-tape elements, Experimental Thermal and Fluid Science, 3 (1990) 373-382.
[203] S. Eiamsa-ard, C. Thianpong, P. Eiamsa-ard, P. Promvonge, Thermal characteristics in a heat exchanger tube fitted with dual twisted tape elements in tandem, International Communications in Heat and Mass Transfer, 37(1) (2010) 39-46.
[204] P. Promvonge, Thermal augmentation in circular tube with twisted tape and wire coil turbulators, Energy Conversion and Management, 49(11) (2008) 2949-2955.
[205] S. Eiamsa-ard, P. Promvonge, Performance assessment in a heat exchanger tube with alternate clockwise and counter-clockwise twisted-tape inserts, International Journal of Heat and Mass Transfer, 53(7-8) (2010) 1364-1372.
[206] S. Eiamsa-ard, K. Wongcharee, P. Eiamsa-ard, C. Thianpong, Heat transfer enhancement in a tube using delta-winglet twisted tape inserts, Applied Thermal Engineering, 30(4) (2010) 310-318.
[207] S.W. Chang, B.J. Huang, Thermal performances of tubular flows enhanced by ribbed spiky twist tapes with and without edge notches, International Journal of Heat and Mass Transfer, 73 (2014) 645-663.
[208] S.W. Chang, T.L. Yang, J.S. Liou, Heat transfer and pressure drop in tube with broken twisted tape insert, Experimental Thermal and Fluid Science, 32(2) (2007) 489-501.
[209] S. Eiamsa-ard, C. Nuntadusit, P. Promvonge, Effect of twin delta-winged twisted-tape on thermal performance of heat exchanger tube, Heat Transfer Engineering, 34(15) (2013) 1278-1288.
[210] N. Piriyarungrod, M. Kumar, C. Thianpong, M. Pimsarn, V. Chuwattanakul, S. Eiamsa-ard, Intensification of thermo-hydraulic performance in heat exchanger tube inserted with multiple twisted-tapes, Applied Thermal Engineering, 136 (2018) 516-530.
[211] S. Eiamsa-ard, P. Promvonge, Thermal characteristics in round tube fitted with serrated twisted tape, Applied Thermal Engineering, 30(13) (2010) 1673-1682.
[212] P. Murugesan, K. Mayilsamy, S. Suresh, Turbulent heat transfer and pressure drop in tube fitted with square-cut twisted tape, Chinese Journal of Chemical Engineering, 18(4) (2010) 609-617.
[213] ASHRAE, ASHRAE Handbook - Fundamentals, American Society of Heating, Refrigerating and Air-Conditioning Engineers, Inc., Atlanta, 2009.
[214] N.T. Obot, E.B. Esen, T.J. Rabas, The role of transition in determining friction and heat transfer in smooth and rough passages, International Journal of Heat and Mass Transfer, 33(1) (1990) 2133-2143.

[215] Z. Duan, Fully developed turbulent flow pressure drop in circular and noncircular ducts, Journal of Fluids Engineering, 134 (2012) 1-10.
[216] Y.S. Muzychka, Z.P. Duan, M.M. Yovanovich, Fluid friction and heat transfer in microchannels, microfluidics and nanofluidics handbook: Chemistry physics and life science principles, Taylor and Francis, (2011) 477-610.
[217] Z. Duan, New correlative models for fully developed turbulent heat and mass transfer in circular and noncircular ducts, Transaction of ASME, Journal of Heat Transfer, 134 (2012) 1-6.
[218] A.J. Ghajar, L.M. Tam, Laminar-transition-turbulent forced and mixed convective heat transfer correlations for pipe flows with different inlet configurations, in: Winter Annual Meeting of the American Society of Mechanical Engineers, ASME, New York, NY, United States, 1991, pp. 15-23.
[219] M. Everts, Heat transfer and pressure drop of developing flow in the transitional flow regime, MEng Dissertation, University of Pretoria, South Africa, 2014.
[220] H.K. Tam, L.M. Tam, A.J. Ghajar, C. Sun, H.Y. Leung, Experimental investigation of single-phase friction factor and heat transfer inside the horizontal internally micro-fin tubes in transition region, in: ASME-JSME-KSME Joint Fluids Engineering Conference, ASME, Hamamatsu, Shizuoka, Japan, 2011, pp. AJK2011-16026.
[221] H.K. Tam, L.M. Tam, A.J. Ghajar, C. Sun, W.K. Lai, Experimental investigation of single-phase heat transfer in a horizontal internally micro-fin tube with three different inlet configurations, in: ASME 2012 Summer Heat Transfer Conference, ASME, Rio Grande, Puerto Rico, 2012, pp. HT2012-58125.
[222] J.A. Olivier, Single-phase heat transfer and pressure drop of water cooled at a constant wall temperature inside horizontal circular smooth and enhanced tubes with different inlet configurations in the transitional flow regime, PhD Thesis, University of Pretoria, South Africa, 2009.
[223] J.P. Meyer, J.A. Olivier, Transitional flow inside enhanced tbes for fully developed and developing flow with different types of inlet disturbances: Part I - Adiabatic pressure drops, International Journal of Heat & Mass Transfer, 54 (2011) 1587-1597.
[224] F. Durst, S. Ray, B. Unsal, O.A. Bayoumi, The development lengths of laminar pipe and channel flows, Journal of Fluids Engineering, 127 (2005) 1154–1160.
[225] B. Donevski, J. Kulesza, Resistance coefficients of laminar and turbulent flow in swirling ducts, Archiwum Termodynamiki i Spalania [in Polish], 9(3) (1978) 497-506.
[226] A.W. Date, P.I. Jagad, Prediction of f and Nu during laminar-turbulent transition: case of flow in a tube containing a twisted tape, in: Proceedings of the ASME 2013 Summer Heat Transfer Conference & HT 2013, ASME, Minneapolis, USA, 2013, pp. 1-10.
[227] R. Bhadouriya, A. Agrawal, S.V. Prabhu, Experimental and numerical study of fluid flow and heat transfer in a twisted square duct, International Journal of Heat and Mass Transfer, 82 (2015) 143-158.
[228] A. Garcia, P.G. Vicente, A. Viedma, Experimental study of heat transfer enhancement with wire coil inserts in laminar-transition-turbulent regimes at different Prandtl numbers, International Journal of Heat and Mass Transfer, 48(21-22) (2005) 4640-4651.
[229] M. Everts, J.P. Meyer, Heat transfer of developing flow in the transitional flow regime, in: Proceedings of the 1st Thermal and Fluid Engineering Summer Conference, TFESC ASTFE, New York City, USA, 2015, pp. 1-13.
[230] R.E. Rayle, Influence of Orifice Geometry on Static Pressure Measurements, ASME Paper No. 59-A-234, (1959).

[231] M. Everts, Single-phase mixed convection of developing and fully developed flow in smooth horizontal tubes in the laminar, transitional, quasi-turbulent and turbulent flow regimes, PhD Thesis, University of Pretoria, South Africa, 2017.
[232] M. Everts, J.P. Meyer, Flow regime maps for smooth horizontal tubes at a constant heat flux, International Journal of Heat and Mass Transfer, 117 (2018) 1274-1290.
[233] J.P. Meyer, L. Liebenberg, J.A. Olivier, Measurement and evaluation of single-phase heat transfer and pressure drop inside enhanced tubes for transition flow, ASHRAE (American Society of Heating, Refrigerating and Air-Conditioning Engineers, Report nr: 1280-RP, (2008) 204.
[234] C.O. Popiel, J. Wojtkowiak, Simple formulas for thermophysical properties of liquid water for heat transfer calculations (from 0°C to 150°C), Heat Transfer Engineering, 19(3) (1998) 87-101.
[235] P.F. Dunn, Measurement and data analysis for engineering and science, 2nd ed., CRC Press, Taylor and Francis Group, Boca Raton, New York, USA, 2010.
[236] S.M. Morcos, A.E. Bergles, Experimental investigation of combined forced and free laminar convection in horizontal tubes, Journal of Heat Transfer, 97 (1975) 212-219.
[237] Y.A. Cengel, A.J. Ghajar, Heat and mass transfer: fundamentals & applications, 5th ed. in SI units. ed., Mcgraw Hill Education, New York, 2015.
[238] H. Schlichting, K. Gersten, Boundary-layer theory, Springer-Verlag Berlin Heidelberg, Germany, 2017.
[239] V. Gnielinski, On heat transfer in tubes, International Journal of Heat and Mass Transfer, 63 (2013) 134-140.
[240] S.W. Chang, Y. Zhen, Enhanced heat transfer with swirl duct under rolling and pitching environment, Journal of Ship Research, 46(3) (2002) 149-166.
[241] F.L. Test, Laminar flow heat transfer for fluids and liquids with temperature-dependent viscosity, Journal of Heat Transfer, 90 (1968) 385-393.
[242] P.R.H. Blasius, The law of similarity of frictional processes in fluids. Originally in German: das aehnlichkeitsgesetz bei reibungsvorgangen in flüs sigk eiten, ForschArbeitIngenieur-Wesen, (131) (1913) 1-4.
[243] R.W. Allen, E.R.G. Eckert, Friction and heat-transfer measurements to turbulent pipe flow of water (Pr=7 and 8) at uniform wall heat flux, Journal of Heat Transfer, 86(3) (1964) 301-310.
[244] A. Pantokratoras, Steady laminar flow in a 90^{o} bend, Advances in Mechanical Engineering, 8(9) (2016) 1-9.
[245] W.M. Chakroun, S.F. Al-Fahed, The effect of twisted-tape width on heat transfer and pressure drop for fully developed laminar flow, Journal of Engineering for Gas Turbines and Power, 118(3) (1996) 584-589.
[246] F. Bishara, M.A. Jog, R.M. Manglik, Heat transfer and pressure drop of periodically fully developed swirling laminar flows in twisted tubes with elliptical cross sections, ASME International Mechanical Engineering Congress and Exposition, Heat Transfer, Fluid Flows, and Thermal Systems, Parts A, B and C, 9 (2009) 1131-1137.